UNIVERSITY OF CALIFORNIA, SAN DIEGO

Primordial Nucleosynthesis and Neutrino Physics

A dissertation submitted in partial satisfaction of the
requirements for the degree
Doctor of Philosophy

in

Physics

by

Christel Johanna Smith

Committee in charge:

Professor George M. Fuller, Chair
Professor Kurt Marti
Professor Michael Norman
Professor David Tytler
Professor Nolan Wallach

2009

The dissertation of Christel Johanna Smith is approved, and it is acceptable in quality and form for publication on microfilm:

_____

_____

_____

_____

_____

Chair

University of California, San Diego

2009

DEDICATION

To my mother,

for daring to be one of the few female engineers of her generation,

and to my father,

for always pointing out the simple beauties in nature and physics.

TABLE OF CONTENTS

LIST OF FIGURES

LIST OF TABLES

ACKNOWLEDGEMENTS

I am incredibly lucky to be in this difficult position of attempting to thank so many people in my life who made this dissertation possible.

Thank you George for not only training me to be a contributing scientist in an extremely challenging field, but for sharing your deep intuition for understanding the basic underlying physics of complex situations. I am extremely grateful to be a part of your wide spread network of past graduate students, associates, and colleagues and I feel honored to have learned from and worked with you these last six years. Thank you for taking a chance on a clueless first year and producing a somewhat less clueless physicist.

My parents - not only have you always told me I could achieve anything I wanted, but you supported me in every way possible to help make that happen. From helping me out financially to letting me take over your dining room table and feeding and watering me while I studied for my qualifying exam, your support has made this possible and I will always be indebted to you. Like my dedication says, thank you for instilling a love of nature and science in me from an early age and for being exemplary people. You always said, "you are not here for yourself," and I hope with this degree I can make a contribution in some positive way. Thank you for putting up with your "demonio" child all these years.

The process of graduate school has not been easy for me and the two people who understand this most are my other two-thirds, Ginger and Catherine. What can I say, we got through this together and we will get through so much more together as well. I almost dedicated this whole damn thing to the both of you, but then I knew you would understand when I dedicated it to Mommy and Daddy. Ginger - you have always looked out for me and took care of me, even when I was not the most pleasant to deal with. You have always walked with me through my most difficult times and helped me make hard decisions. You always just seem to know when I'm struggling and call me everyday to make sure I'm OK. Among so many things you have done for me Catherine, I will always remember how you

took care of me, were right by my side all summer, and kept me sane as I studied for the qualifying exam. You still keep me sane when I vent to you on g-chat or we online shop together. You make me laugh every time we chat by your weirdo sense of humor and talking to you is a bright spot in every day. When the three of us are together I feel like we can do anything! Thank you for being my crazy amazing sisters.

Kyle - you came into my life at a crucial turning point and your love and belief in me was like a breath of fresh air. Your excitement for life and big dreams are infectious. I'm excited for all of the adventures we will go on together. Thank you for believing in me when I needed it most and thank you for dealing with me and loving me everyday. I know we will make it back to the ocean together. Mahal kita.

Lola - your strength and courage has always been a source of inspiration. Thank you for being my lola , I'm sorry I threw eggs at you and hid frogs in drawers, I love you!

Beth and Maryam - Thank you for being my best friends and supporting me through all 24 years of education (yes, we've known each other that long!!). I couldn't have asked for more amazing, genuine, kind, intelligent, fun ladies to be my lifelong friends.

I'd also like to thank my crazy Titas and Titos who were so much fun to be around growing up and who basically helped raise us. Alexis, you've grown up into a beautiful person and I am proud to be your friend. Thank you for your love and understanding. Tita Anne, I love you, write your books!

I've been fortunate to have made great friendships during my time here. Regina - my women in physics partner in crime! I feel so lucky that we got to spend most of our time at UCSD together. You've become one of my best friends and I hope we can have many more hawaii reunions (or anywhere in the world actually)! Casey - you have listened to endless whining and complaining from me, given me support, and been there when I have been down in the dumps and needed a drinking buddy, thank you for being a great friend. Hannah - Thank you for being a great roommate

and friend. Tommy - Thank you for helping me get started in research (showing me how to search for papers on ADS and helping me learn how to program) and for helping me learn and grow as a person. Chad - you are probably one of the most intelligent people I've ever met, yet also one of the most humble. Thank you for answering all of my stupid questions, it has been a pleasure to work with you and I hope we can continue working together when we both "leave" SD. Alison - thank you for showing me that not only can women succeed in physics, they can flourish. I would also like to acknowledge extremely helpful discussions with Professor David Tytler. Thank you for providing me lots of helpful advice all along way.

Although this degree is in physics, I don't think I could have gotten through it all without my favorite sport – water polo and the people associated with it. Coach Stoll, I will always be grateful to you for your belief in me. Thank you for instilling a love of the sport in me, for taking a chance on a goalie that couldn't swim, and for helping me play at the best WP school, UCLA! Coach Grosse, my first physics teacher and water polo coach, thank you for explaining water polo in terms of physics (ball trajectories and conservation of momentum) and physics in terms of water polo! My UCLA WP girls, Janelle, Julie, Robyn, Erin, Liz, Carly, Bina: I feel honored to be a part of such a talented, smart, strong group of women...going to nationals in 2001 will always be one of my favorite memories...."break the bread!" My UCSD club team, playing with you literally helped keep me sane these last six years, our tie-dye oddball team and hot pink day-glo suits have been glorious, thank you!

As an undergrad, I was lucky to have made many important friendships. Mike - I am sure that if I didn't meet you as an undergrad, I would not be getting my graduate degree right now. I can't express enough thanks for helping me realize I could be a physicist and for helping all along the way. From tutoring me when I was struggling in a subject, getting me a job in your plasma lab, to helping me apply to grad school, I owe you a lot. Thank you. Cindy and Hooman - you have been so supportive of me all along, thank you! Johan - thank you for always

believing in me. Thank you to my crazy friends - Simone. Matt, and Alex.

Chapter 2, in full, is a reprint of the material as it appears in Physical Review D 2006. Smith, Christel J.; Fuller, George M.; Kishimoto, Chad T.;Abazajian, Kevork N.; Phys. Rev. D, 2006. The dissertation author was the primary investigator and author of this paper. We would like to acknowledge discussions with Huaiyu Duan, David Kirkman, Max Pettini, Michael Smith, Nao Suzuki, and David Tytler. The work of G.M.F., C.T.K., and C.J.S. was supported in part by NSF grant PHY-04-00359 and a UC/LANL CARE grant at UCSD; C.T.K. acknowledges financial support from the ARCS Foundation, Inc.; K.N.A. was supported by Los Alamos National Laboratory (under DOE contract W-7405-ENG-36) and also acknowledges the UC/LANL CARE grant.

Chapter 3, in full, is a reprint of the material as it appears in Physical Review D 2009. Smith, Christel J.; Fuller, George M.; Smith, Michael S., Phys. Rev. D, 2009. The dissertation author was the primary investigator and author of this paper. We would like to acknowledge discussions with Chad Kishimoto and Kevork Abazajian. ORNL is managed by UT-Battelle, LLC, for the U.S. DOE under Contract No. DE-AC05-00OR22725. The work of G.M.F and C.J.S. was supported in part by NSF Grant No. PHY-06-53626 and a UC/LANL CARE grant at UCSD.

Chapter 4, in full, is in preparation for submission to Physical Review D. Smith, Christel J.; Fuller, George M.; Phys. Rev. D, 2009. The dissertation author was the primary investigator and author of this paper. We would like to acknowledge discussions with Chad Kishimoto and Kevork Abazajian. The work of G.M.F and C.J.S. was supported in part by NSF Grant No. PHY-06-53626 and a UC/LANL CARE grant at UCSD.

Appendix B, in full, is a reprint of the material as it appears in Physical Review Letters 2006. Kishimoto, Chad T.; Fuller, George M.; Smith, Christel J., Phys. Rev. Lett. 2006. The dissertation author was a contributing author and investigator. We would like to thank K. Abazajian, N. Bell, M. Smith, and especially M. Patel for insightful discussions. This work was supported in part by NSF Grant

PHY-04-00359 at UCSD. C.T.K. would like to acknowledge a fellowship from the ARCS Foundation, Inc.

VITA

Education

2009	Ph.D. Physics, University of California, San Diego
2007	C.Phil., Physics, University of California, San Diego
2005	M.S., Physics, University of California, San Diego
2003	B.S., Astrophysics, University of California, Los Angeles

PUBLICATIONS

Christel J. Smith, George M. Fuller, Michael S. Smith, "Big Bang Nucleosynthesis with Independent Neutrino Distribution Functions ", *Phys.Rev.D79*, 105001, 2009.

Christel J. Smith, George M. Fuller, Chad T. Kishimoto, Kevork N. Abazajian, "Light Element Signatures of Sterile Neutrinos and Cosmological Lepton Numbers ", *Phys.Rev.D74*, 085008, 2006.

Chad T. Kishimoto, George M. Fuller, Christel J. Smith, "Coherent Active-Sterile Neutrino Flavor Transformation in the Early Universe ", *Phys.Rev.Lett 97*, 141301, 2006

ABSTRACT OF THE DISSERTATION

Primordial Nucleosynthesis and Neutrino Physics

by

Christel Johanna Smith
Doctor of Philosophy in Physics

University of California San Diego, 2009

Professor George M. Fuller, Chair

We study primordial nucleosynthesis abundance yields for assumed ranges of cosmological lepton numbers, sterile neutrino mass-squared differences and active-sterile vacuum mixing angles. We fix the baryon-to-photon ratio at the value derived from the cosmic microwave background (CMB) data and then calculate the deviation of the ^{2}H, ^{4}He, and ^{7}Li abundance yields from those expected in the zero lepton number(s), no-new-neutrino-physics case. We conclude that high precision ($< 5\%$ error) measurements of the primordial ^{2}H abundance from, *e.g.*, QSO absorption line observations coupled with high precision ($< 1\%$ error) baryon density measurements from the CMB could have the power to either: (1) reveal or rule out the existence of a light sterile neutrino if the sign of the cosmological lepton number is known; or (2) place strong constraints on lepton numbers, sterile neutrino mixing properties and resonance sweep physics. Similar conclusions would hold if the primordial ^{4}He abundance could be determined to better than 10%.

We have performed new Big Bang Nucleosynthesis calculations which employ arbitrarily-specified, time-dependent neutrino and antineutrino distribution functions for each of up to four neutrino flavors. We self-consistently couple these distributions to the thermodynamics, the expansion rate and scale factor-time/temperature relationship, as well as to all relevant weak, electromagnetic, and strong nuclear reaction processes in the early universe. With this approach,

we can treat any scenario in which neutrino or antineutrino spectral distortion might arise. These scenarios might include, for example, decaying particles, active-sterile neutrino oscillations, and active-active neutrino oscillations in the presence of significant lepton numbers. Our calculations allow lepton numbers and sterile neutrinos to be constrained with observationally-determined primordial helium and deuterium abundances. We have modified a standard BBN code to perform these calculations and have made it available to the community.

We have applied a fully relativistic Coulomb wave correction to the weak reactions in the full Kawano/Wagoner Big Bang Nucleosynthesis (BBN) code. We have also added the zero temperature radiative correction. We find that using this higher accuracy Coulomb correction results in good agreement with previous work, giving only a modest $\sim 0.04\%$ increase in helium mass fraction over correction prescriptions applied previously in BBN calculations. We have calculated the effect of these corrections on other light element abundance yields in BBN and we have studied these yields as functions of electron neutrino lepton number. This has allowed insights into the role of the Coulomb correction in the setting of the neutron-to-proton ratio during the BBN epoch. We find that the lepton capture processes' contributions to this ratio are only second order in the Coulomb correction.

Chapter 1

Introduction

The main theme of this dissertation is to use the study of primordial nucleosynthesis to probe unknown fundamental physics - physics beyond the standard model. The methodology consists of use of improved big bang nucleosynthesis (BBN) simulation tools that were developed for this purpose to discover and/or constrain new weak interaction physics based on continually improving precision of light element abundance and cosmic microwave background observations. This introduction will provide a brief review of relevant information in these fields and illustrate the connection between them in order to understand the following chapters.

1.1 Nucleosynthesis of the Primordial Elements

1.1.1 Setting the Stage: The Moments Before Big Bang Nucleosynthesis

Before the conditions of the early universe become appropriate for nucleosynthesis, there are several events that set the stage for this epoch.

The quark-hadron transition occurs when the universe is $\sim 10^{-6}$ seconds old and at a temperature of ~ 1 GeV. At times before this transition and at hotter

temperatures, the universe consisted of a plasma of quarks, gauge bosons, and leptons. It is during this phase change that quarks become confined into baryons, creating the baryon asymmetry (the lack of anti-baryons) and the baryon number seen today. After this transition, there are nucleons with which to build nuclei and the universe consists of a plasma of neutrinos (and antineutrinos), electrons (and positrons), photons, and baryons.

For the purpose of this study, the rest of the history of the early universe can be looked at in first approximation as a series of equilibrium-breaking phase changes resulting from the expanding and cooling evolution of the hot big bang. These changes happen when processes whose rates, mediated by temperature-dependent interaction strengths, are initially fast compared to the expansion rate of the universe, allowing the constituents to be in thermal and chemical equilibrium. Eventually as the universe cools and expands, the rates of these reactions become slow compared to the expansion rate of the universe and the conditions for equilibrium can no longer be maintained. The time at which this occurs can be seen by comparing the expansion rate of the universe, given from the Freidmann equation below, to the reaction rate in question. The Freidmann equation is

$$H^2 = \frac{8\pi}{3} G\left(\rho_{\text{total}}\right), \tag{1.1}$$

where $\rho_{\text{total}} = \rho_\gamma + (\rho_{e^-} + \rho_{e^+}) + \rho_\nu + \rho_b$ is the total energy density. These critical equilibrium breaking moments give the universe many of the characteristics we see today.

After the quark-hadron transition, the next important transition in the universe is the period of weak decoupling. This is when the weak reactions rates that couple neutrinos to the plasma of the universe, such electron-neutrino scattering, become slow. At this point the neutrinos cease to efficiently exchange energy with the plasma and they decouple. This occurs when the universe is slightly less than one minute old and around a temperature of ~ 3 MeV. The decoupled neutrinos continue to adiabatically expand with the universe, retaining the thermal Fermi-Dirac distribution function shape, but with a temperature parameter that decreases

inversely with scale factor. The neutrino spectra keeps a thermal shape unless a process such as particle decay or neutrino oscillation alters the neutrino spectra. This is an interesting feature of this epoch because any events that occur in the weak sector prior to weak decoupling will have been thermalized and ultimately erased, but those events happening after weak decoupling will be frozen into the neutrino spectra with the potential to affect later epochs.

Although the neutrinos decouple at temperatures of ~ 3 MeV, they continue to interact with the baryons of the universe through the following reactions, collectively referred to as the weak reactions:

$$\nu_e + n \rightleftharpoons p + e^-, \tag{1.2}$$

$$\bar{\nu}_e + p \rightleftharpoons n + e^+, \tag{1.3}$$

$$n \rightleftharpoons p + e^- + \bar{\nu}_e. \tag{1.4}$$

These interactions have a negligible effect on the neutrino energy distributions because of the small relative abundance of baryons. The baryon-to-photon ratio is defined as

$$\eta \equiv \frac{n_{\text{baryons}} - n_{\text{anti-baryons}}}{n_\gamma}, \tag{1.5}$$

the best measure of which is currently obtained by anisotropies in the cosmic microwave background (CMB). The current value taken from the Wilkinson Microwave Anisotropy Probe (WMAP) is $\eta \sim 6 \times 10^{-10}$[1, 2].

The rates for the weak reactions are denoted by $\lambda_{\nu_e n}$ and $\lambda_{e^- p}$, $\lambda_{\bar{\nu}_e p}$ and $\lambda_{e^+ n}$, $\lambda_{n_{\text{decay}}}$ and $\lambda_{p e^- \bar{\nu}_e}$ for the forward and reverse reactions in Eq. (1.2), Eq. (1.3), and Eq. (1.4), respectively.

At high enough temperatures, $T \sim 1$ MeV, these rates are fast enough to maintain chemical equilibrium. In chemical equilibrium the neutrino, neutron, electron, and proton chemical potentials μ_{ν_e}, μ_n, μ_{e^-}, and μ_p, respectively, satisfy the Saha equation, $\mu_{\nu_e} + \mu_n = \mu_{e^-} + \mu_p$. The neutron-to-proton ratio is then given by its equilibrium value

$$\frac{n}{p} \approx e^{(\mu_e - \mu_{\nu_e} - \delta m_{np})/T}. \tag{1.6}$$

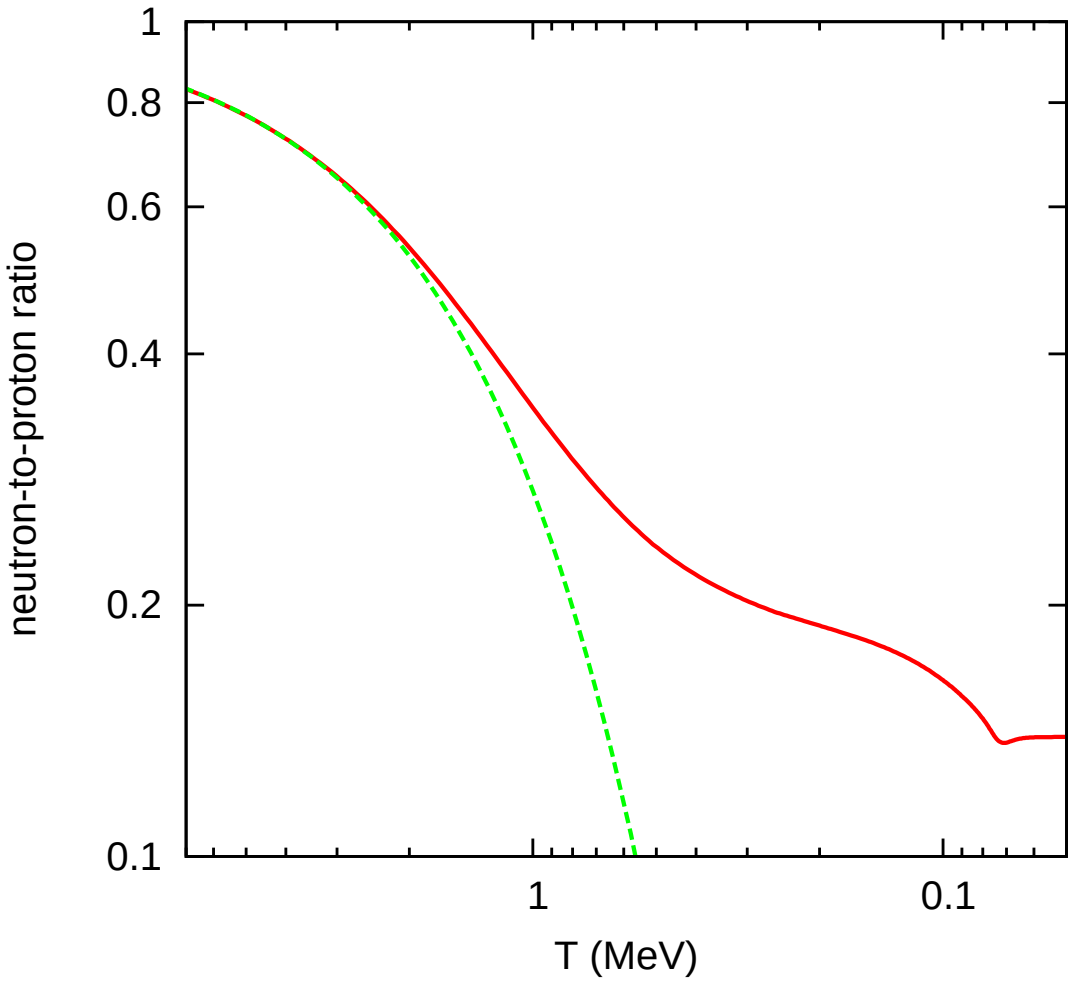

Figure 1.1: The dashed line is the equilibrium value of the neutron-to-proton ratio. The solid line is the actual neutron-to-proton ratio calculated as a function of temperature. The point at which the actual neutron-to-proton ratio deviates from the equilibrium value is called the "weak freeze out."

This can be seen as the dashed green line in Fig. 1.1. Like weak decoupling, eventually these rates become slow compared to the expansion rate of the universe. Chemical equilibrium can no longer be maintained and the value of the neutron-to-proton ratio pulls off of its equilibrium value. This is known as the "weak freeze out" and occurs at temperatures $\sim$ 0.8 MeV. Although the weak reactions are comparatively slow after the weak freeze out, they still have a hand in altering the neutron-to-proton ratio.

Eventually, all the weak reactions except free neutron decay cease to have an effect on the value of the neutron-to-proton ratio. This is shown in Fig. 1.1, where the neutron-to-proton ratio is dominated by free neutron decay from temperatures $\sim$0.3 MeV to $\sim$0.01 MeV. Finally nucleosynthesis occurs, binding all the neutrons into nuclei and the neutron-to-proton ratio abruptly plateaus. This leads to the next important phase in the history of the universe, primordial nucleosynthesis.

The calculation of the weak reaction rates and consequently the evolution of the neutron-to-proton ratio is of crucial importance to the outcome of big bang nucleosynthesis. Not only does it effectively determine the primordial element abundances, but it could provide clues to unknown physics in the early universe. It is a main theme of this work to accurately handle the calculations of these rates, and to use these calculational tools to model the effects of hypothesized new and unknown neutrino physics.

1.1.2 Big Bang Nucleosynthesis

Nucleosynthesis can be understood analogously to the previous freeze out events. Instead of following the departure from chemical equilibrium, nucleosynthesis can be understood by following departures from nuclear statistical equilibrium (NSE).

NSE occurs when the nuclear reaction rates that destroy and create a particular nuclide are fast enough to keep that nuclide's abundance in equilibrium. In NSE

the mass fraction of a particular nuclide is given by

$$X_A = \xi(3)^{A-1}\pi^{(1-A)/2}2^{(3A-5)/2}A^{5/2}(T/m_N)^{3(A-1)/2}\eta^{A-1}X_p^Z X_n^{A-Z}\exp(B_A/T). \tag{1.7}$$

Here η is the baryon-to-photon ratio, A is the mass number, Z is the charge, and B_A is the binding energy of nuclear species $A(Z)$ defined as $B_A \equiv Zm_p + (A - Z)m_n - m_A$. The mass fraction of each element is given by the NSE value for as long as the nuclear reaction processes are fast. In BBN this equilibrium usually gets broken because the nuclides which build up a particular nucleus are not numerous enough to maintain the forward reactions.

The high entropy of the universe, or in other words - the very low value of η, delays the production of any element heavier than hydrogen until relatively low temperatures. This can be seen by noting the mass fraction dependence on η^{A-1} in Eq. (1.7). Once it finally becomes energetically favorable to build nuclei, the abundances start to accumulate relatively fast along their own equilibrium abundance contours. NSE gets broken first for the heavier elements (because they require substantial abundances of other heavy elements to remain in NSE) and then sequentially down to the lightest elements.

For example as the mass fraction of ^{4}He builds with decreasing temperature, it is forced to pull away from its NSE value because it reaches a point where there are not enough mass-3 nuclides to produce it. Afterwards, the mass fraction of ^{4}He trails along with ^{3}He and ^{3}H abundances. These mass-3 nuclides build according to their own NSE contours until they too are forced to fall off of NSE because there is not enough deuterium. Now ^{4}He, ^{3}He, and ^{3}H trail along with the slowly increasing NSE value of deuterium. This is what is referred to as the "deuterium bottleneck."

Eventually deuterium too is forced to freeze out of NSE because all of the neutrons have either decayed or been placed into nuclei. Deuterium and the mass-three nuclides reach their maximum value at this point. They continue to participate in nuclear reactions which build heavier elements, mainly ^{4}He and trace amounts of

mass-7 nuclides. In order to bridge the mass gaps between helium and any heavier elements, the temperatures must be high to overcome these coulomb barriers. By the time ^{4}He is made, the universe is already too cool to build anything heavier. The temperature continues to decrease with the expansion of the universe and nucleosynthesis ceases.

At the outset of nucleosynthesis, essentially all the neutrons in the universe are sequestered into alpha particles, or ^{4}He nuclei. The neutron-to-proton ratio thus determines the presently observed ratios of $\sim 25\%$ helium, $\sim 75\%$ hydrogen, and trace amounts of deuterium, ^{3}He, and ^{7}Li.

In summary, the key pieces of physics in BBN, which are discussed in subsequent chapters, are:

1)Weak freeze out. This is the time/temperature when the weak reaction rates are of the same order as the expansion rate of the universe. This fine balance has a large role in setting the value of the neutron-to-proton ratio and consequently the ^{4}He abundance. One can imagine adding in more sources of energy density to the universe, which in turn creates a faster expansion rate by Eq. (1.1). This would make weak freeze out happen sooner, leading to a higher value of the neutron-to-proton ratio, thus resulting in an increase in helium. Alternatively, one could imagine a scenario with faster weak reaction rates so that the freeze out happens later. This leads to a lower neutron-to-proton ratio and therefore less ^{4}He.

2)Neutrinos and the weak reactions rates. The actual values of the weak reaction rates are closely coupled to the neutrino physics in the early universe. The number density, or flux, of the neutrinos can enhance the neutrino capture rates or inhibit the rates with a neutrino in the final state by phase space blocking. Not only is the density important, but the shape of the neutrino energy distributions are also a determining factor in the calculation of the weak reaction rates. This is because the rates are integrated over four factors of neutrino energy and the neutrino distribution functions. In order to properly track the neutron-to-proton ratio through the calculation of the weak reaction rates, one must properly track the evolution of the neutrino distribution functions.

3) The baryon-to-photon ratio. This is essentially a measure of the entropy of the universe. The largest effect it has is to determine when nucleosynthesis occurs. Deuterium is particularly sensitive to the timing of BBN because it has a very slowly increasing NSE mass fraction. This is because of its low binding energy. For high η, BBN happens sooner and less deuterium gets made.

4)The nuclear reaction rates. The actual laboratory measurements of the nuclear reaction cross-sections allow us to simulate nucleosynthesis. The accuracy of predictions made is dependent on the accuracy of the precision of the nuclear reaction rates.

BBN is a intricate balance of many factors in the early universe, such as the particle physics, the thermodynamics, the nuclear physics, and the physics of the hot big bang. Understanding this epoch by comparing predictions to observations can give not only a window to the very early universe, but a new tool to probe physics beyond the standard model. The following section will describe how the predictions are calculated and the current status of the observations.

1.1.3 Nucleosynthesis Predictions and Comparison to Observation

The ideas which led to modern primordial nucleosynthesis calculations were first suggested by G. Gamow. He was the first to realize that in the model for the hot big bang, there would be a time where nuclear reactions could proceed rapidly. He used this idea to try to explain all of the observed abundances in the universe. In a physical review letter to the editor in 1946, he pointed out that there is a period in the expansion history of the universe where the density would drop an order of magnitude in less than a second. This would mean the conditions required for fast nuclear reactions would only last for a short amount of time[3]. Because of this short nucleosynthesis window and the high entropy of the universe, he was not able to create heavy elements in the big bang.

Since then, various codes have evolved to calculate the primordial element

abundances. In 1967, R. Wagoner, W. Fowler, and F. Hoyle wrote a nuclear reaction network that calculated the synthesis of elements in the early universe and in exploding and imploding supermassive stars [4]. Given the high entropy of the universe from the CMB, they found that only significant quantities of light elements could be produced in the big bang. The heavy elements could be synthesized in the death of massive stars, bridging the mass gaps between ^{4}He to ^{12}C.

In 1969, Wagoner converted the Wagoner, Fowler, Hoyle reaction network into what has become the standard BBN[5, 6] code. In 1988 L. Kawano modernized this code, added a user interface, and provided documentation [7, 8, 9]. A modified version of the Kawano/Wagoner code was used in this work. The specific details of the modification are discussed in Chapter 3.

Before the launch of WMAP, the main goal of the study of BBN was to predict the baryon-to-photon ratio, η. This was done by comparing the predicted abundances from a calculation with a tool such as the Kawano/Wagoner BBN code to the observed primordial abundances. To constrain η, the light element abundances ^{4}He, D/H, ^{3}He/H, and ^{7}Li/H, were calculated as a function of η. The observed primordial abundance error bars were overlaid on these contours to provide an allowed range of η.

The baryon-to-photon ratio is now derived independently from the baryon-acoustic oscillations in the CMB to an accuracy of $< 5\%$. This presents an opportunity to use BBN considerations to probe other unknowns of the universe, namely the lepton numbers of the universe and the weak-sector physics which mediate them. The neutrino lepton numbers are defined analogously to the baryon-to-photon ratio as

$$L_{\nu_\alpha} = \frac{n_{\nu_\alpha} - n_{\bar{\nu}_\alpha}}{n_\gamma}, \tag{1.8}$$

where n_{ν_α} and $n_{\bar{\nu}_\alpha}$ are the number densities of the neutrinos and antineutrinos respectively. The electron lepton number is known by assuming charge neutrality of the universe, meaning the number of electrons are equal to the number of protons, so that $L_e \sim \eta$.

In order to use BBN calculations in combination with the observations of the primordial element abundances, it is useful to review the current status of these observations.

The measurement of primordial ^{4}He is inherently challenging because ^{4}He is synthesized in stars. The ^{4}He mass fraction, Y_p, is measured by looking at the relative flux of helium and hydrogen emission lines in metal poor objects such as HII regions and compact blue galaxies. HII regions are clouds of gas, which are ionized by the radiation from hot young stars within. Since stars also synthesize metals, the usual routine is to extrapolate Y_p to zero metallicity in order to determine the primordial value. The main sources of uncertainty in these measurements include collisions of neutral hydrogen with electrons, the temperature structure of HII regions, the assumptions made in extrapolating Y_p to zero metallicity, and the uncertainty of the recombination coefficients of the helium lines[10, 11].

Current measurements of primordial helium cover a wide range of values and uncertainties. In 2007, Ref. [10] found a value of $Y_p = 0.2477$ with a statistical error of ± 0.0018 and a systematic error of ± 0.0023. In 2004, Ref. [12] documented the systematic uncertainties in previous measurements and concluded that the allowable range of helium should be considered $0.232 \leq Y_p \leq 0.258$. We have used this allowed range of helium for comparison in our calculations.

^{3}He is also observed in HII regions by its signature ^{3}He$^+$ hyperfine line at 3.46 cm. This is analogous to the 21 centimeter spin-flip transition line in neutral hydrogen. Unfortunately, this line is very hard to detect and can only be seen in a handful of these HII regions. Like ^{4}He, ^{3}He is also made in stars. This would suggest that the abundance would follow a similar trend as the metallicity in the galaxy (metallicity increasing towards the center of the galaxy)[13]. This is trend is not seen, which has led Ref. [14] to argue that there is a fine balance between post-BBN production and destruction of ^{3}He. Although this argument could mean that the galactic abundance of ^{3}He is a valid estimate of the primordial abundance, Ref. [14] takes the measurements from distant HII regions in combination with recent theoretical understandings of stellar light-element synthesis and destruction

to place an upper limit of $^3\mathrm{He/H} \leq 1.1 \pm 0.2 \times 10^{-5}$.

Unlike helium, deuterium is easily destroyed by photo-disassociation and is never synthesized in lasting amounts after BBN. In addition to this, deuterium is extremely sensitive to the baryon-to-photon ratio, making it an ideal barometer for primordial nucleosynthesis considerations.

In order to probe the primordial D/H value, deuterium must be observed in low metallicity, high redshift objects. This is done by looking at the absorption spectra from Quasi Stellar Objects or QSOs. Light from a distant QSO passes through an absorption system, a cloud of neutral gas, where deuterium and hydrogen absorb radiation and imprint their characteristic spectra. By comparing the isotope shifted lines of deuterium to the much larger absorption lines of hydrogen, a primordial value of D/H can be inferred. This is problematic, however, because hydrogen and deuterium have an identical absorption spectra with a slight ~ 82 km/s offset due to the mass difference of the isotope. Any hydrogen with a relative velocity (an HI interloper) could look like the isotope shifted deuterium line. This means that only QSOs with well understood velocity structures can be used for this measurement.

The best current measurement of primordial D/H is $2.78^{+0.44}_{-0.38} \times 10^{-5}$, from D/H values toward five QSOs[15, 16]. In 2007, Ref. [13] argued that the mean log of the individual abundances used in Ref. [16] is not the best estimator of primordial deuterium. Instead, Ref. [13] states that minimizing the χ^2 for the individual log(D/H) determinations will provide a better estimate for primordial deuterium. This yields $\mathrm{D/H} = 2.68^{+0.27}_{-0.25} \times 10^{-5}$. Both estimates agree well with the WMAP value of the baryon-to-photon ratio.

The lithium isotopes are the problem children of the primordial elements. Currently, ^{7}Li is predicted to be ~ 3 to 4 factors more that what has been observed. If the observations are correct, ^{6}Li is observed as ~ 4 orders of magnitude more than BBN predictions.

^{7}Li is measured in the absorption spectra of old metal-poor stars in the galactic halo. The first convincing measurement of primordial lithium was done in 1982 by

Spite and Spite[17]. They found that ^{7}Li/H increased with the mass of the star and then would plateau. For the highest mass stars, they found a constant abundance of ^{7}Li/H. This plateau is known as the "Spite Plateau." The plateau is believed to be caused by the lack of convection or mixing with the surface layers of the heavier stars. ^{7}Li is easily burned into helium in the interior of stars. It is argued that the lithium plateau is the primordial abundance because of the lack of mixing and consequently lack of lithium destruction. Since the Spite measurement, many observations have been done to check this trend, especially since the plateau infers a primordial value of lithium much lower than the BBN prediction. Most of the recent measurements have seen that there is little dependence on metallicity[18, 19], except Ref. [20] which found a slight trend of decreasing lithium with decreasing metallicity. All of these observations see a value of lithium that is still significantly lower than the BBN prediction.

Many possible solutions have been posed to understand this disparity such as systematic errors in the abundance analysis, destruction of lithium by cosmic ray spallation or rotational effects, dilution of lithium during the lifetime of these old stars, or incorrect BBN predictions from uncertainties in the nuclear reaction rates[13]. Thus far, most of these posed solutions have been unsuccessful in bridging the gap between observation and prediction. In 2006, Ref. [21] conducted a study looking at stars only in the globular cluster NGC 6397 because they have arguably similar stellar age and metallicity. They combined their observation with simulations of stellar evolution and backtracked to derive a primordial abundance of lithium that agrees with BBN.

Recently, there has been evidence for a plateau not only in ^{7}Li, but in ^{6}Li as well at about 1/3rd the value of ^{7}Li/H [20]. This corresponds to $^6\mathrm{Li/H} \sim 10^{-12}$ which is about 4 orders of magnitude higher than the BBN prediction. BBN does not make much ^{6}Li because it is easily destroyed by $^6\mathrm{Li}(p,\alpha)^3\mathrm{He}$.

Ref. [22] points out the difficulty in observing ^{6}Li. The ^{6}Li resonance line is shifted only 0.16 Å to the red of the matching ^{7}Li line. These lines are weak doublets and can be hard to resolve due to thermal broadening and turbulence.

Ref. [22] concludes that 7 or 8 of the 9 detections of ^{6}Li in Ref. [20] can be explained by ^{7}Li alone by considering the effects of intrinsic line symmetry. Intrinsic line symmetry is the symmetry between upward and downward flows in the convective profile of the absorbing material.

Both of the discrepancies in the lithium abundances present an interesting problem. It could be a sign of a lack of understanding of what the measurements mean, or it could be a signature of new physics.

As measurements of the primordial elements become more accurate with the advent of 30 meter class telescopes and the general evolution of technology, it is possible that signatures of new physics can be resolved. The following work describes signatures of neutrino physics beyond the standard model on BBN. The next chapter will provide a brief review of the current status of neutrino physics.

1.2 A Brief History of and Introduction to Neutrino Physics

The creator of the neutrino is testing and teasing us.

-Moshe Gai

Ever since Wolfgang Pauli first postulated neutrinos were neutral carriers of missing energy in neutron decay, they have continued to be a source of confusion and contradiction. Named by Enrico Fermi as the "little neutral one", they were originally thought to have no mass and travel at the speed of light.

However, for almost thirty years, earth based detectors failed to detect the calculated flux of neutrinos created from the hydrogen burning nuclear reactions in the sun. This was known as the "solar neutrino problem." The realization that neutrinos have mass solved this problem because mass allows them to have flavor oscillations. The presence of a neutrino mass allows the neutrino energy eigenstates to be independent representations of the flavor eigenstates. In other-words, the

neutrino energy eigenstates can be written as a superposition of flavor eigenstates and vice-versa.

In solar neutrino oscillation, a neutrino produced at the center of the sun is created in the electron flavor eigenstate by specific nuclear reactions in the hydrogen burning chain such as:

$$p + p \rightarrow {}^2H + e^+ + \nu_e \tag{1.9}$$

$$p + e^- + p \rightarrow {}^2H + \nu_e \tag{1.10}$$

$${}^7Be + e^- \rightarrow {}^7Li + \nu_e \tag{1.11}$$

$${}^8B \rightarrow {}^8Be + e^+ + \nu_e. \tag{1.12}$$

Due to the high densities of electrons and protons in the core of the sun, the neutrino that is created in the electron flavor eigenstate is more closely associated with the high energy eigenstate. This is because the electron flavor neutrino is coupled to the stellar medium through forward scattering on electrons, whereas the other neutrino flavors are not. As the neutrino travels outward, going from high to low densities, it remains associated to the high energy eigenstate in adiabatic conditions. When the neutrino finally exits the sun in the high energy eigenstate, it "looks" more like a tau or mu flavor neutrino. This is because a mu or tau flavor neutrino is associated closest with the high energy eigenstate in vacuum. For this reason, only $\sim 1/3$ of the expected electron flavor neutrinos were detected from the sun. The rest "looked" more like tau or mu flavor neutrinos.

This mechanism of neutrino transformation was derived by Mikheyev, Smirnov, and Wolfenstein and is described as the Mikheyev-Smirnov-Wolfenstein effect or MSW effect. Not only is the effect important in understanding the behavior of neutrinos in the sun, but it can describe neutrinos oscillating in the early universe.

In addition to evidence for neutrino oscillation (and therefore neutrino mass) from solar neutrinos, neutrino oscillation has been detected from atmospheric neutrinos as well. High energy neutrinos are produced from cosmic rays colliding with the earth's atmosphere, creating high energy pions. These pions decay into muons,

which themselves decay, producing mu and electron flavor neutrinos at a ratio of 2/1. This can be seen by the atmospheric neutrino producing reactions

$$\begin{aligned} \pi^+ &\rightarrow \mu^+ + \nu_\mu \\ &\quad \searrow e^+ + \nu_e + \bar{\nu}_\mu \end{aligned} \tag{1.13}$$

$$\begin{aligned} \pi^- &\rightarrow \mu^- + \bar{\nu}_\mu \\ &\quad \searrow e^- + \bar{\nu}_e + \nu_\mu. \end{aligned} \tag{1.14}$$

Underground detectors noticed a deficit of mu neutrinos, which can be explained easiest by transformation of a mu flavor neutrino to a tau flavor.

These two independent measurements of neutrino oscillation not only confirm the existence of the neutrino mass, but also give two different mass-squared differences $\delta m^2 = m_1^2 - m_2^2$. The two mass-squared differences imply the existence of three active neutrino flavors. The mass-squared differences from solar and atmospheric neutrino oscillation are

$$\delta m^2_{\text{solar}} \sim 8 \times 10^{-5}\,\text{eV}^2 \tag{1.15}$$

$$\delta m^2_{\text{atmos}} \sim 3 \times 10^{-3}\,\text{eV}^2. \tag{1.16}$$

These give the difference between the neutrino masses, but the absolute value of the neutrino masses are still unknown.

This leads to the question of mass hierarchy. There are two mass hierarchy schemes. The normal hierarchy is where the solar doublet is the difference between the lightest and second lightest mass eigenstate and the atmospheric difference is between the second lightest and heaviest. The inverted hierarchy is the reverse of the normal, where the atmospheric difference is between the lightest and second lightest and the solar doublet now is between the heaviest and 2nd lightest.

Although two mass-squared differences have been inferred to relatively high accuracy, it does not rule out the possibility for other neutrinos to exist. The lifetime of the weak interaction boson, Z^0, provides limits of three active neutrino flavors because the amount of available neutrino channels or phase space for the

boson to decay into is proportional to the lifetime of the boson. If other neutrinos exist, they must be sub-weak interacting or "sterile". They would only interact through the neutrino mass-mixing mechanism.

The Liquid Scintillator Neutrino Detector (LSND) [23] found an excess of $\bar{\nu}_e$ events which was interpreted as oscillation from $\bar{\nu}_\mu \rightarrow \bar{\nu}_e$. This implied a third mass-squared difference which meant the existence of a fourth neutrino flavor. This was recently reinvestigated by the MiniBoone experiment [24, 25]. Due to the lack of electron neutrino appearance events at high energies, the experiment was able to rule out the two-neutrino oscillation explanation of the LSND detection. However, they did see an excess of events at low energies, which is still unexplained.

Although these ongoing experiments are trying to place constraints on neutrino oscillation, the number of neutrino flavors and the mass-mixing parameters of which are still unknown. As we will show, we can use BBN to probe regions or parameter space that cannot be probed by terrestrial experiments. This will be discussed in detail in the following chapters.

Bibliography

[1] D. N. Spergel *et al.*, astro-ph/0603449.

[2] SDSS Collaboration, M. Tegmark *et al.*, Phys. Rev. D **69**, 103501 (2004).

[3] G. Gamow, Phys. Rev. **70**, 572 (1946).

[4] R. V. Wagoner, W. A. Fowler and F. Hoyle, Astrophys. J. **148**, 3 (1967).

[5] R. V. Wagoner, Astrophys. J. **179**, 343 (1973).

[6] R. V. Wagoner, Ann. Rev. Astron. Astrophys. **7**, 553 (1969).

[7] L. Kawano, NASA STI/Recon Technical Report N **92**, 25163 (1992).

[8] L. Kawano, FERMILAB-PUB-88/34-A.

[9] M. S. Smith, L. H. Kawano and R. A. Malaney, Astrophys. J. Suppl. **85**, 219 (1993).

[10] M. Peimbert, V. Luridiana and A. Peimbert, **666**, 636 (2007), [arXiv:astro-ph/0701580].

[11] M. Peimbert, ArXiv e-prints (2008), [0811.2980].

[12] K. A. Olive and E. D. Skillman, Astrophys. J. **617**, 29 (2004).

[13] G. Steigman, Annual Review of Nuclear and Particle Science **57**, 463 (2007), [0712.1100].

[14] T. M. Bania, R. T. Rood and D. S. Balser, **415**, 54 (2002).

[15] D. Kirkman, D. Tytler, N. Suzuki, J. M. O'Meara, and D. Lubin, Astrophys. J. Suppl. **149**, 1 (2003).

[16] J. M. O'Meara, D. Tytler, D. Kirkman, N. Suzuki, J. X. Prochaska, D. Lubin and A. M. Wolfe, Astrophys. J. **552**, 718 (2001).

[17] F. Spite and M. Spite, Astron. Astrophys. **115**, 357 (1982).

[18] J. Meléndez and I. Ramírez, **615**, L33 (2004), [arXiv:astro-ph/0409383].

[19] C. Charbonnel and F. Primas, **442**, 961 (2005), [arXiv:astro-ph/0505247].

[20] M. Asplund, D. L. Lambert, P. E. Nissen, F. Primas and V. V. Smith, **644**, 229 (2006), [arXiv:astro-ph/0510636].

[21] A. J. Korn, F. Grundahl, O. Richard, P. S. Barklem, L. Mashonkina, R. Collet, N. Piskunov and B. Gustafsson, **442**, 657 (2006), [arXiv:astro-ph/0608201].

[22] R. Cayrel, M. Steffen, P. Bonifacio, H.-G. Ludwig and E. Caffau, ArXiv e-prints (2008), [0810.4290].

[23] K. Eitel, New J. Phys. **2**, 1 (2000).

[24] MiniBooNE, Z. Djurcic, 0901.1648.

[25] MiniBooNE Collaboration, G. McGregor, in *Particle Physics and Cosmology: Third Tropical Workshop on Particle Physics and Cosmology - Neutrinos, Branes, and Cosmology*, edited by J. F. Nieves and C. N. Leung, AIP Conf. Proc. No. 655, p. 58, New York, 2003, AIP.

Chapter 2

Light Element Signatures of Sterile Neutrinos and Cosmological Lepton Numbers

2.1 Introduction

Recent developments in observational cosmology may allow the primordial abundances of the light elements, including deuterium, to become novel probes of the mass and mixing properties of light sterile neutrinos. The high precision inference of the baryon-to-photon ratio η from the observed relative acoustic peak amplitudes in the cosmic microwave background (CMB) [1, 2, 3] suggests a new way to employ Big Bang Nucleosynthesis (BBN) considerations.

Historically, the comparison of the observationally-inferred light element abundances with calculated BBN abundance yields has been carried out with the intent of obtaining the baryon density. Indeed, on account of the near-exponential dependence of the deuterium yield on η in BBN, the observations of isotope-shifted hydrogen absorption lines in Lyman limit systems along lines of sight to high redshift QSO's provide another, independent high precision measure of the baryon content of the universe [4, 5]. This value of η currently is in good agreement,

within errors, with the CMB-derived value [6, 7].

However, these two independent determinations of the baryon density depend on new neutrino physics in different ways. In particular, the BBN deuterium yield depends, albeit weakly, on the neutron-to-proton ratio and the expansion rate at the BBN epoch [8] and these quantities, in turn, can depend on the mass/mixing properties of sterile neutrinos.

It has been shown recently that the ^{4}He abundance yield in Big Bang Nucleosynthesis (BBN) can be dramatically sensitive to medium-enhanced active-sterile neutrino flavor transformation in the presence of a significant lepton number [9, 10]. This sensitivity comes about through (post-neutrino-decoupling) neutrino flavor mixing-induced alterations in the ν_e and $\bar{\nu}_e$ energy spectra. These alterations cause changes in the weak interaction rates governing the inter-conversion of neutrons and protons, and so ultimately they cause changes in the neutron-to-proton ratio in BBN. We show here that active-sterile neutrino mixing likewise can induce modest changes in the deuterium and ^{7}Li abundance yields.

This sets up a potentially new avenue for probing or constraining the active-sterile neutrino mixing parameter space: comparison of the value of η derived from observationally-inferred deuterium on the one hand and the CMB-derived value on the other. Though the ^{4}He BBN yield is far more sensitive to alterations of the neutron-to-proton ratio than is the ^{2}H yield, at present the prospects for reliable and precise determination of the primordial deuterium abundance might be better than for helium.

The primordial helium abundance is likely between 23% and 26% by mass [11, 12, 13]. It may be possible to do much better than this by adroit attention to issues of radiative transfer and compact blue galaxy morphology [14, 15, 16]. However, as more QSO lines of sight become available, the statistics for deuterium abundance determinations in quasar absorption line systems will improve. Arguably, we may already know the primordial deuterium abundance at least as well as we know helium[4, 5, 17]. In any case, it is worth exploring how much leverage deuterium measurements have in constraining the parameter space of sterile

neutrino mass/mixing values and lepton number(s).

The LSND anomaly is being re-investigated in the mini-BooNE experiment [18, 19]. A positive signal in that experiment would indicate active neutrino coherent flavor transformation at a mass-squared scale significantly different from the atmospheric and solar neutrino mass-squared differences, $\delta m^2_{\rm atm} \approx 3 \times 10^{-3}\,{\rm eV}^2$ and $\delta m^2_{\odot} \approx 8 \times 10^{-5}\,{\rm eV}^2$, respectively. Given the Z^0-width limit, this would immediately imply the existence of a light sterile neutrino.

If this light sterile neutrino (and its helicity-flipped partner, or "sterile antineutrino") were to completely thermalize in the early universe, there could be both an increased ^{4}He yield, which is possibly unwelcome, and trouble with CMB- and large scale structure-derived bounds on the sterile neutrino rest mass closure contribution [1, 2, 9, 20, 21, 22, 23, 24, 25, 26, 27, 28]. Invocation of a significant net lepton number can suppress the production of sterile neutrinos in the epoch when neutrinos scatter frequently (*i.e.,* prior to weak decoupling), thereby easing these constraints [29, 30, 31]. However, this lepton number will drive active-sterile resonant production of the sterile neutrino (or sterile antineutrino) after weak decoupling [9]. Post-weak-decoupling resonant sterile neutrino production would leave the active neutrinos and the sterile neutrino with distorted, non-thermal energy spectra which can have a significant impact on the neutron-to-proton ratio and the ^{4}He yield [9].

To investigate the effects of these spectral distortions and resonant transformation scenarios on the ^{4}He, ^{2}H and ^{7}Li BBN yields, we follow the evolution of the neutrino distribution functions in various resonance sweep scenarios and self-consistently couple this with a calculation of the light element abundances performed with the full BBN nuclear reaction network code. (We employ a modified version of the Kawano/Wagoner code described in Ref. [32].) In Section II we briefly outline the physics of active-sterile resonance sweep in the early universe. We describe our nucleosynthesis calculations in Section III. Results are given in Section IV. Discussion and conclusions are given in Section V.

2.2 Resonant Active-Sterile Neutrino Flavor Transformation in the Early Universe

Invocation of a significant lepton number as a dodge to full population of both helicity states of a sterile neutrino in the early universe [29, 30, 9, 31] will imply at least some resonant, medium-enhanced destruction of this lepton number and the concomitant production of sterile neutrinos [9, 31]. In Ref. [9] this general picture of post-weak-decoupling active-sterile resonance sweep in the presence of a net lepton number was laid out in detail. The single channel active-sterile neutrino conversion problem posed in Ref. [9] has recently been solved [10].

The weak decoupling epoch is where active neutrinos cease to scatter rapidly enough to exchange energy effectively with the background plasma. This takes place when the temperature is $T \approx 3\,\mathrm{MeV}$. Any neutrino energy spectral distortions which develop after this epoch will not be entirely erased by scattering and emission/absorption processes.

A pre-existing net lepton number in any of the neutrino flavors can drive medium-enhanced active-sterile neutrino flavor transformation in the early universe, both in the coherent regime after weak decoupling, and in the high temperature regime where de-coherence in the neutrino field becomes significant [33]. The lepton number residing in the neutrino sector associated with flavor $\alpha = \mathrm{e}, \mu, \tau$ is defined to be (in analogy to the baryon-to-photon ratio η)

$$L_{\nu_\alpha} \equiv \frac{n_{\nu_\alpha} - n_{\bar{\nu}_\alpha}}{n_\gamma}, \tag{2.1}$$

where n_{ν_α}, $n_{\bar{\nu}_\alpha}$, and n_γ are the neutrino, antineutrino, and photon number densities at some epoch. The potential lepton number corresponding to active neutrino flavor is

$$\mathcal{L}_\alpha \equiv 2L_{\nu_\alpha} + \sum_{\beta \neq \alpha} L_{\nu_\beta}, \tag{2.2}$$

where also $\beta = \mathrm{e}, \mu, \tau$. (Note that neither L_{ν_α} or $\mathcal{L}_\alpha$ are comoving invariants; we quote values of these assuming no dilution from $e^\pm$ annihilation, *i.e.,* at epoch

$T \approx 3\,\mathrm{MeV}$.)

It is convenient to cast the neutrino transformation problem in terms of the scaled-energy $\epsilon \equiv E_\nu/T$, instead of the neutrino energy E_ν, because the former quantity is a co-moving invariant. A Mikheyev-Smirnov-Wolfenstein (MSW) [34, 35] resonance, or neutrino mass level crossing, will occur between sterile and active neutrinos for electron neutrinos or antineutrinos for scaled-energy

$$\epsilon_{\mathrm{res}} \approx \frac{\pi^2 \delta m^2 \cos 2\theta}{4\sqrt{2}\,\zeta\,(3)\; G_{\mathrm{F}} T^4} \left| \frac{1}{\mathcal{L}_e + \eta \left(\frac{3}{2} Y_e - \frac{1}{2} \right)} \right|, \tag{2.3}$$

and for mu and tau neutrinos or antineutrinos for scaled-energy

$$\epsilon_{\mathrm{res}} \approx \frac{\pi^2 \delta m^2 \cos 2\theta}{4\sqrt{2}\,\zeta\,(3)\; G_{\mathrm{F}} T^4} \left| \frac{1}{\mathcal{L}_{\mu,\tau} + \eta \left(\frac{1}{2} Y_e - \frac{1}{2} \right)} \right|, \tag{2.4}$$

where δm^2 is the mass-squared difference appropriate for the active-sterile mixing channel, $\zeta\,(3) \approx 1.20206$ is the Riemann-Zeta function of argument 3, G_{F} is the Fermi constant, and $Y_e = (n_{e^-} - n_{e^+})\, n_\gamma^{-1} \eta^{-1}$ is the net electron number per baryon. Neutrinos transform at resonance if the terms inside the absolute value symbols in Eqs. (2.3) and (2.4) are positive; antineutrinos transform if these terms are negative. In practice, for the rather large lepton numbers we employ, we can neglect the neutrino-electron scattering term (second term in the denominator within the absolute value) since $\eta \approx 6 \times 10^{-10}$ is so small.

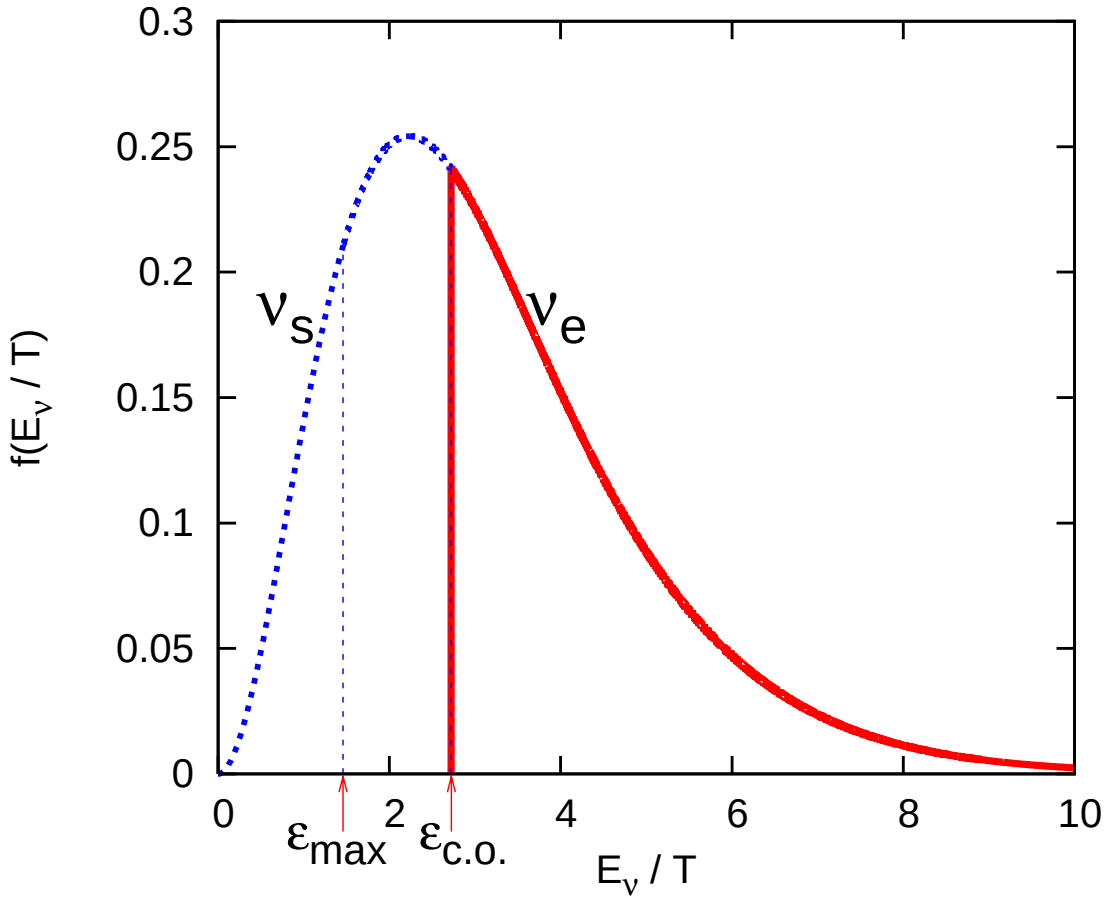

Figure 2.1: Example active neutrino distribution function for a forced, adiabatic resonance sweep scenario.

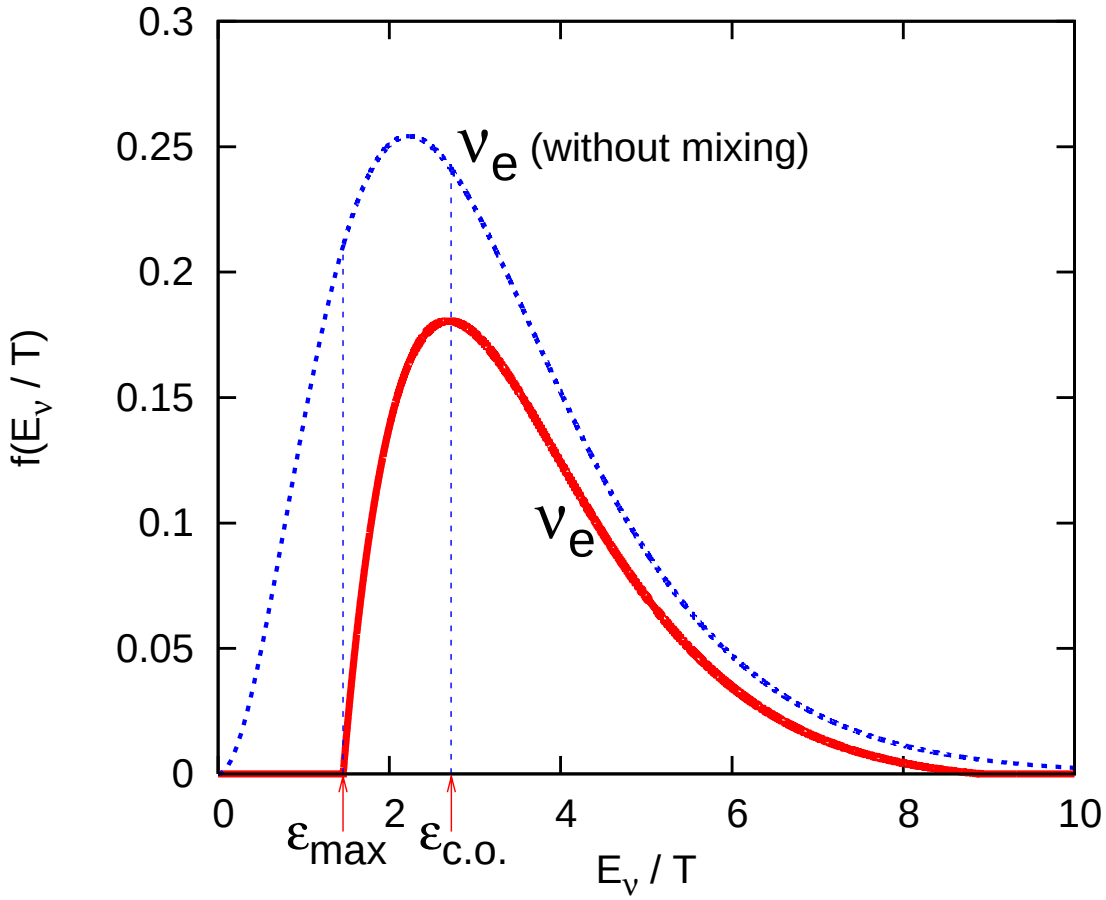

Figure 2.2: Active neutrino distribution function obtained from the active-sterile transformation solution in Ref. [10].

The general picture of MSW resonance sweep (*i.e.*, how the resonance scaled-energy $\epsilon_{\rm res}$ depends on time/temperature) in the early universe is evident from Eqs. (2.3) and (2.4). As the universe expands and the temperature drops, $\epsilon_{\rm res}$ will increase from zero. If ν_α neutrinos propagate through the MSW resonance coherently and adiabatically, they will be converted to sterile neutrinos with 100% efficiency and, consequently, the lepton number will be depleted ($\mathcal{L}_\alpha$ will decrease) [33, 9]. Ref. [9] showed that the resonance can sweep smoothly, continuously, and (most importantly) adiabatically only from $\epsilon_{\rm res} = 0$ to $\epsilon_{\rm res} = \epsilon_{\rm max}$. Here $\epsilon_{\rm max}$ is the value of the scaled energy where the product $\epsilon\mathcal{L}_\alpha$ is a maximum, $\epsilon_{\rm max}^3 \approx 2\zeta\left(3\right)\,\left(e^{\epsilon_{\rm max}-\eta_{\nu_\alpha}}+1\right)\mathcal{L}_\alpha\left(\epsilon_{\rm max}\right)$ [9]. Ref. [9] showed that the MSW resonance cannot sweep smoothly and adiabatically beyond this point, $\epsilon_{\rm res} = \epsilon_{\rm max}$.

If we force the resonance to continue to sweep adiabatically and continuously past $\epsilon_{\rm max}$, completely converting ν_α neutrinos in the portion of the ν_α distribution with scaled energy $E_\nu/{\rm T} \leq \epsilon_{\rm res}$, we would completely deplete the lepton number ($\mathcal{L}_\alpha = 0$) when the resonance reaches $\epsilon_{\rm res} = \epsilon_{\rm c.o.}$ (where "c.o." stands for cut-off). As an example, the initial and final distribution functions for a Fermi-Dirac ν_e energy spectrum with degeneracy parameter (chemical potential divided by temperature) $\eta_{\nu_e} = 0.05$ and potential lepton number $\mathcal{L} = 0.368$ for this forced adiabatic sweep scenario is shown in Figure 4.2. The resulting active neutrino spectrum in this case would have a low energy "cut". That is, the distribution function would be zero for $E_\nu/{\rm T} \leq \epsilon_{\rm c.o.}$. The sterile neutrino produced in this scenario $\nu_\alpha \rightarrow \nu_{\rm s}$ would have a distribution function identical to the original ν_e-spectrum for $E_\nu/{\rm T} \leq \epsilon_{\rm c.o.}$ but zero for larger values of scaled energy.

Recently the active-sterile resonance sweep problem for $\epsilon_{\rm res} > \epsilon_{\rm max}$ has been solved [10]. The resonance does sweep continuously past $\epsilon_{\rm max}$ to (near) lepton number depletion, but it does so non-adiabatically. That is, for $\epsilon_{\rm res} > \epsilon_{\rm max}$, $\nu_\alpha \rightarrow \nu_{\rm s}$ is not 100% efficient. The net result is that the resonance must sweep to higher energy to significantly deplete the lepton number. The resonance will sweep adiabatically as before to $\epsilon_{\rm max}$, but there will be non-adiabatic, incomplete conversion in the $\nu_\alpha \rightarrow \nu_{\rm s}$ channel as $\epsilon_{\rm res}$ sweeps to higher scaled energy, and then a return

to complete, adiabatic conversion at large values of $\epsilon_{\rm res}$. This scenario is depicted in Figure 4.3 for the case of ν_e's with an initial Fermi-Dirac spectrum and lepton numbers $L_{\nu_e} = 0.0343$, and $L_{\nu_\mu} = L_{\nu_\tau} = 0.15$.

A distorted, non-thermal ν_e (or $\overline{\nu}_e$) spectrum will change the neutron-to-proton ratio in BBN and hence, the light element abundance yields over the case with thermal, Fermi-Dirac energy spectra [9]. This is because the ν_e and/or $\overline{\nu}_e$ energy spectra determine the rates of the neutron and proton inter-conversion processes,

$$\nu_e + n \rightleftharpoons p + e^-, \tag{2.5}$$

$$\bar{\nu}_e + p \rightleftharpoons n + e^+, \tag{2.6}$$

$$n \rightleftharpoons p + e^- + \bar{\nu}_e. \tag{2.7}$$

For a given initial potential lepton number, removing neutrino population at higher scaled energy in the spectrum results in a larger effect on the neutron-to-proton ratio. This is because of the significant neutrino energy dependence in the cross sections and dsitribution functions which factor into the rates of the processes in Eqs. (3.2), (3.3), and (3.4). However, another factor in this behavior is that more neutrino population lies in the portion of the ν_e or $\overline{\nu}_e$ spectrum for $E_\nu/{\rm T} \geq \epsilon_{\rm c.o.}$ for the values of potential lepton number of most interest here.

For a given initial potential lepton number, the actual (full solution) resonance sweep scenario will give bigger BBN alteration effects than will the artificial forced continuous, adiabatic sweep model [10]. This is shown in Figure 2.3, where we plot the fractional change (in percent) in the helium and deuterium abundance yields from their standard BBN values for the CMB-determined baryon density as a function of the mass-squared difference δm^2, characterizing the $\nu_e \rightarrow \nu_{\rm s}$ oscillation channel. We give this for both the adiabatic sweep to $\epsilon_{\rm c.o.}$ scenario and the full resonance sweep solution. In these calculations we have taken the initial lepton numbers to be $L_{\nu_e} = 0.0343$ and $L_{\nu_\mu} = L_{\nu_\tau} = 0.15$.

In reality we could expect active-active neutrino conversion simultaneous with active-sterile transformation. This could leave complicated distortion features in the energy spectra of all neutrino species [9]. It is the spectral distortions of

ν_e and $\overline{\nu}_e$ neutrinos which are most important for BBN. Active-active neutrino mixing could tend to partially fill in the $E_\nu/\mathrm{T} < \epsilon_{\mathrm{max}}$ portion of the ν_e or $\overline{\nu}_e$ spectrum, though this could be offset by continued sweep to even higher E_ν/T. In any case, to be conservative in our BBN abundance yield estimates we will in what follows assume a smooth, adiabatic resonance sweep to $\epsilon_{\mathrm{c.o.}}$ for a given potential lepton number. Therefore, our calculated abundance yield changes for given lepton numbers and sterile neutrino mass/mixing data will be (usually) underestimates.

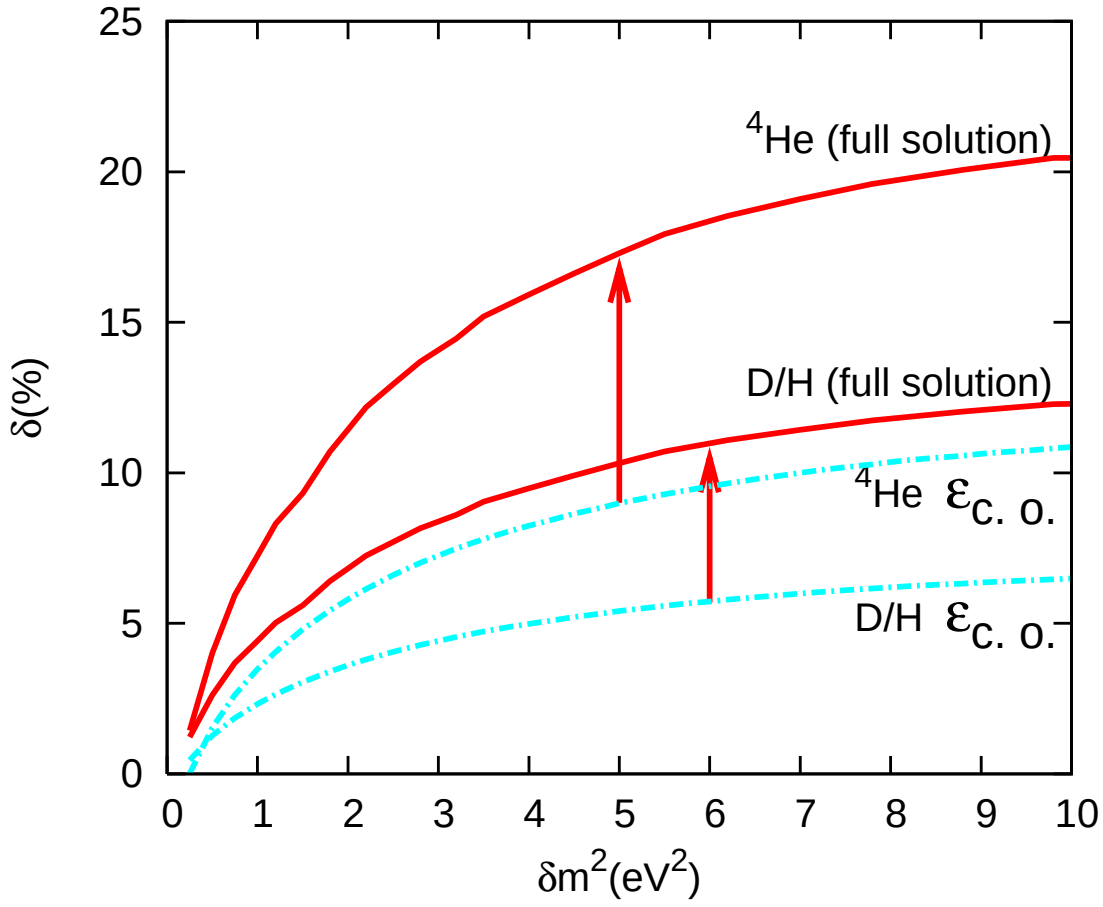

Figure 2.3: The two cases are forced adiabatic resonance sweep to $\epsilon_{\text{c.o.}}$ (Figure 4.2) and the full solution (Figure 4.3).

2.3 Primordial Nucleosynthesis Calculations with Neutrino Spectral Distortions

In general, active-sterile resonance sweep will go on simultaneously with the charged current weak interactions that set the neutron-to-proton ratio (n/p), as well as the strong and electromagnetic nuclear reactions associated with BBN. We will have distorted neutrino ν_e and $\bar{\nu}_e$ energy spectra with distortions that change in time as the active-sterile resonance sweeps and active-active neutrino flavor transformation proceeds. These new features necessitate handling the weak interactions differently than in the standard BBN case.

The standard BBN code, originally written by R. Wagoner [36] and later revised by L. Kawano [37, 38], calculates the processes in Eqs. (3.2), (3.3), and (3.4) by adding the three $n \rightarrow p$ rates; likewise, the three $p \rightarrow n$ rates:

$$\lambda_n = \lambda_{\nu_e + n \rightarrow p + e^-} + \lambda_{n + e^+ \rightarrow p + \bar{\nu}_e} + \lambda_{n \rightarrow p + e^- + \bar{\nu}_e} \tag{2.8}$$

$$\lambda_p = \lambda_{p + e^- \rightarrow \nu_e + n} + \lambda_{\bar{\nu}_e + p \rightarrow n + e^+} + \lambda_{p + e^- + \bar{\nu}_e \rightarrow n}. \tag{2.9}$$

In the standard calculations, the integrands in λ_n and λ_p are manipulated and condensed into a shorter, two-part integral to save computation time. This requires the neutrino and antineutrino distribution functions (as well as the electron and positron) be of Fermi-Dirac form. If the neutrino degeneracy parameters are zero, the code calculates λ_n and λ_p with a series approximation to further cut down computation time. This can lead to an erroneous $\approx 0.5\%$ increase in the neutron-to-proton ratio [37, 38].

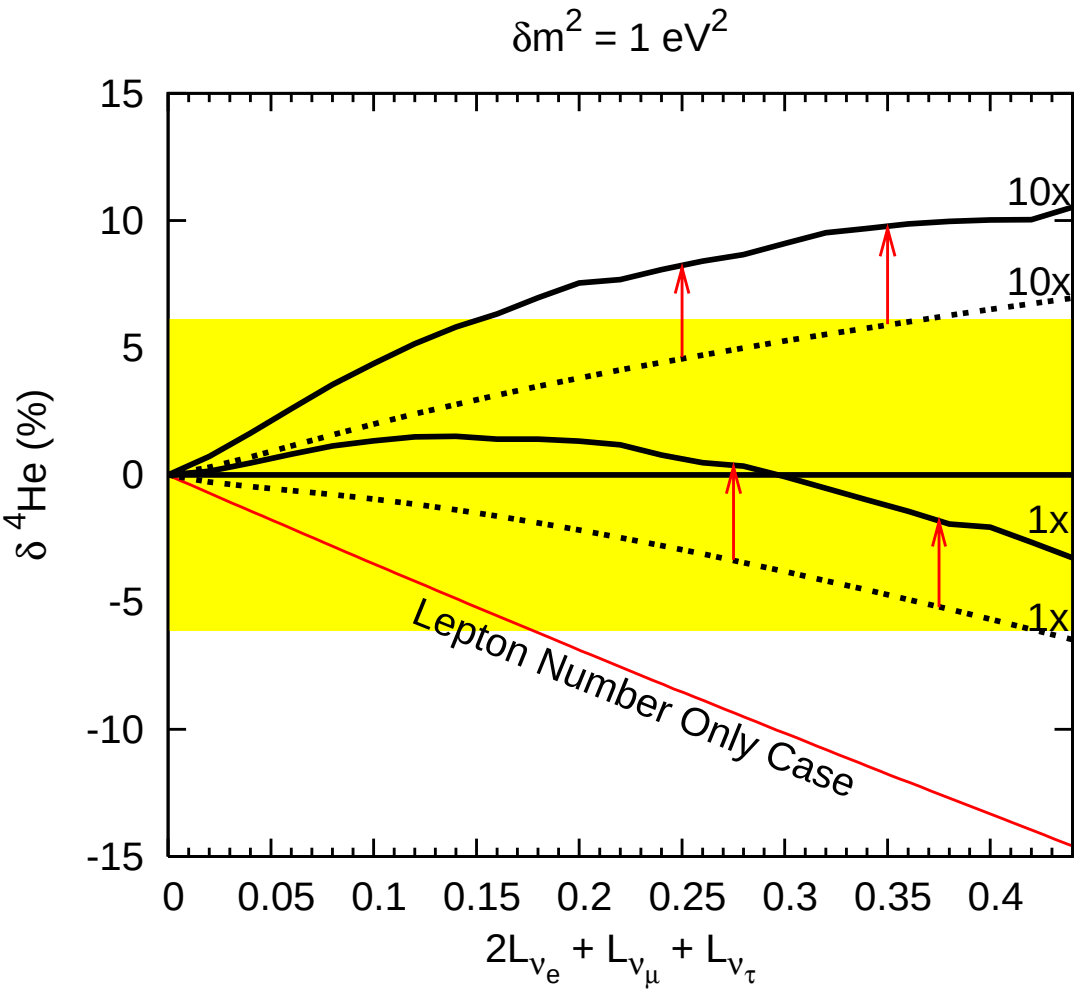

Figure 2.4: In all cases the baryon-to-photon ratio is fixed at the CMB-derived value $\eta = 6.11 \times 10^{-10}$. The central horizontal line is the standard BBN case. The light solid line is the case with lepton numbers but with no active-sterile neutrino mixing. In this case we set all individual lepton numbers to be equal. The lower dashed line is the case with active-sterile neutrino mixing in the forced, adiabatic resonance sweep scenario with lepton number distribution factor $= (L_{\nu_\mu} + L_{\nu_\tau})/2L_{\nu_e} = 1$. The lower heavy solid line is the same case but in the full resonance sweep scenario. The upper dashed line similarly corresponds to the adiabatic resonance sweep scenario but with lepton number distribution factor 10, while the upper solid line is the same case in the full resonance sweep scenario. All active-sterile mixing cases here have $\delta m^2 = 1\,\mathrm{eV}^2$. The light horizontal band gives the $23\% - 26\%$ range for Y_p allowed by observational bounds.

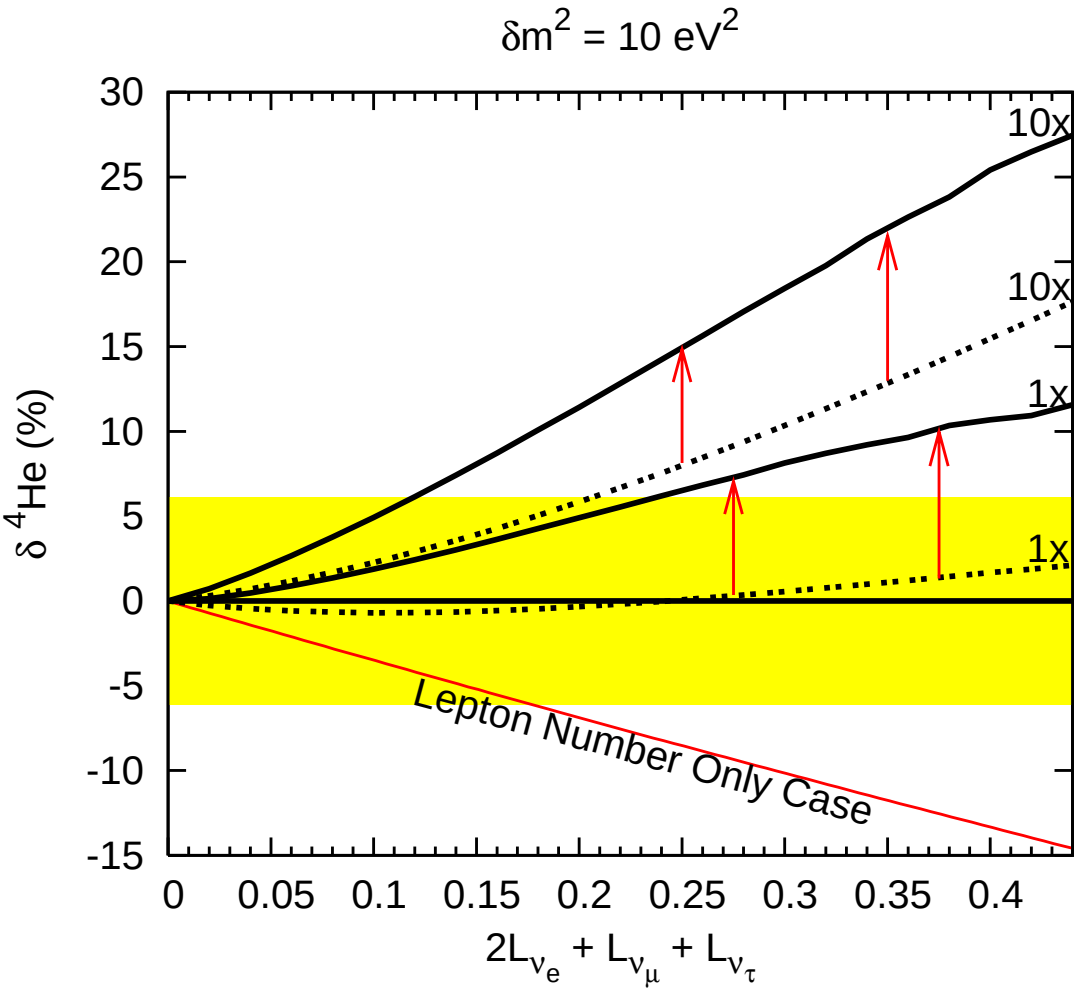

Figure 2.5: Same as for Fig. 2.4 but now with $\delta m^2 = 10\,\mathrm{eV}^2$.

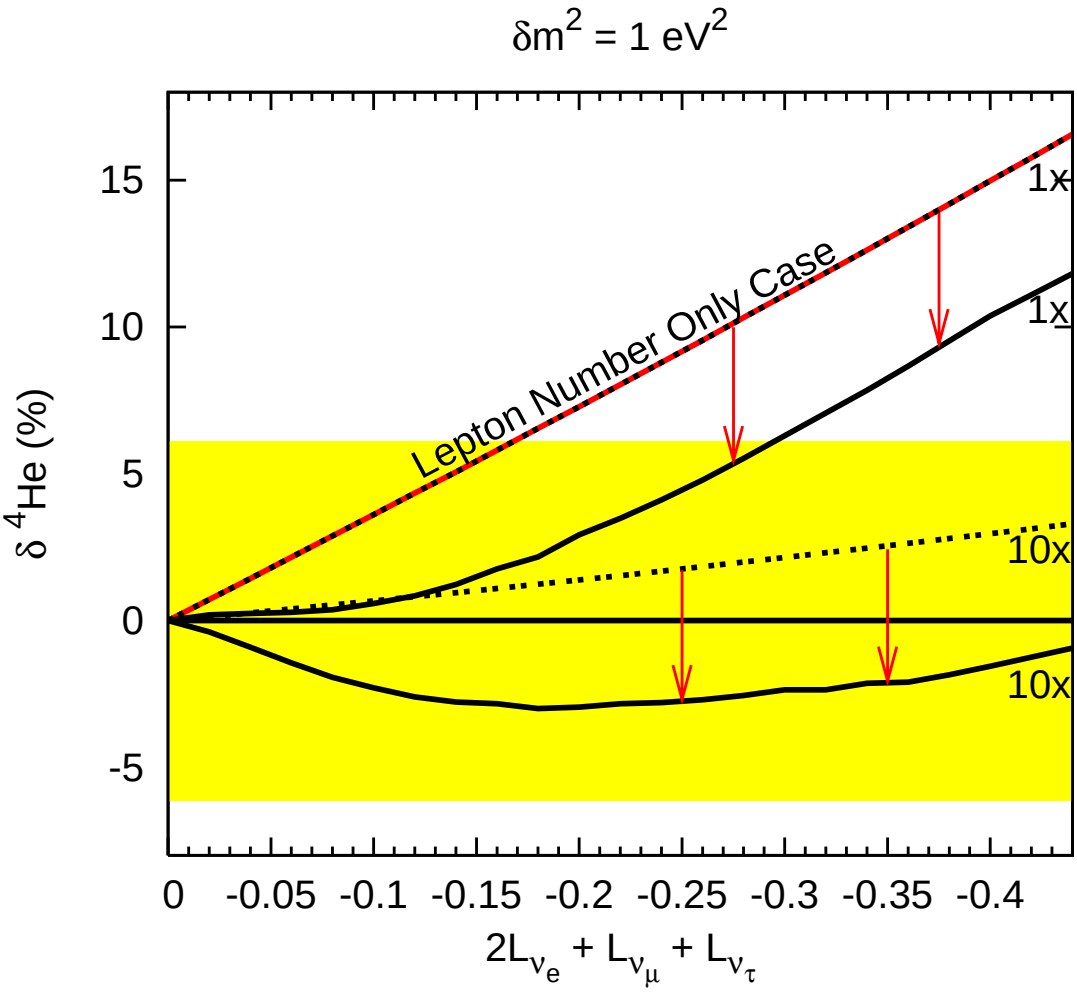

Figure 2.6: Same as for Fig. 2.4 but now with negative lepton numbers.

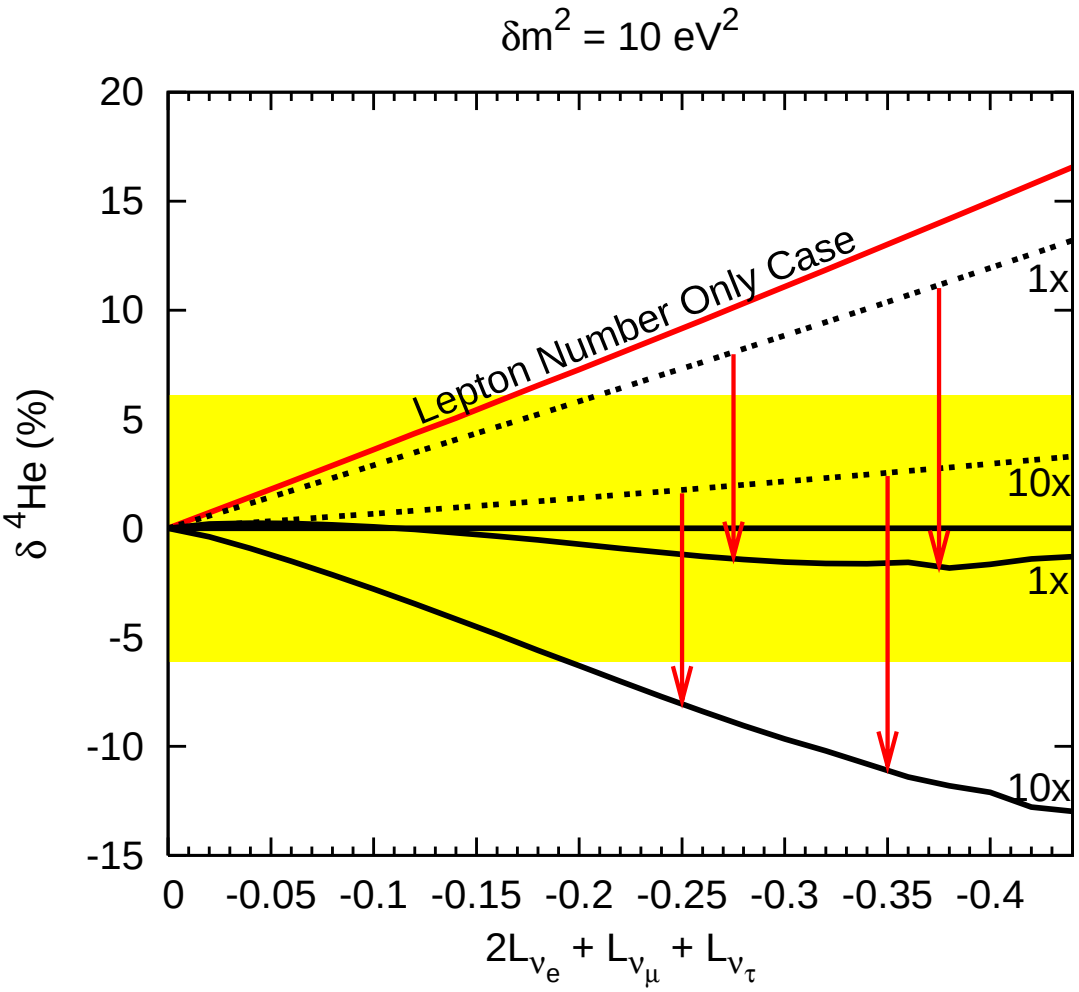

Figure 2.7: Same as for Fig. 2.5 but now with negative lepton numbers.

In order to implement time-dependent neutrino and antineutrino spectral distortions, we rewrote the BBN code to calculate each weak rate in Eqs. (3.2), (3.3), and (3.4) independently, with no series approximations, and changed the integration variable to neutrino/antineutrino energy instead of electron/positron energy. We then modularized the weak rate calculations so that any neutrino or antineutrino distribution function could be entered. Likewise, our modifications allow us to implement any desired time dependence in these distribution functions and they also allow us to calculate consistently the energy density in (and spectra of) any sterile neutrinos which are produced. These modifications are implemented in four modules. One module contains the matrix elements and phase space integrands for the weak rates. The phase space integrands call a second module which contains the ν_e and $\bar{\nu}_e$ distribution functions. The third module defines the limits of integration. Finally, the fourth module calculates the resonance energy for active-sterile transformation and calls the integrator, which in turn calls the other modules for the integrands and integration limits. In addition, the expansion rate of the universe at any temperature is calculated self-consistently with all active and sterile neutrino distribution functions.

In all of our BBN calculations, we set the baryon-to-photon ratio to $\eta = 6.11 \times 10^{-10}$. This corresponds to the central value of the CMB acoustic peak amplitude-determined WMAP Three Year Mean result, $\eta = (6.11 \pm .22) \times 10^{-10}$, which, in turn, corresponds to a baryon rest mass closure fraction $\Omega_{\rm b}h^2 = 0.0223 \pm 0.0008$ [3], where h is the Hubble parameter in units of 100 km s^{-1} Mpc^{-1}.

In our calculations, for illustrative purposes, we adopt neutron lifetime $\tau_n = 887.8\,{\rm s}$. The current world average [39] for this lifetime is $\tau_n = 885.7 \pm 0.8\,{\rm s}$, but a recent measurement [40] suggests it could be as small as $\tau_n = 878.5 \pm 0.7 \pm 0.3\,{\rm s}$. Our adopted τ_n is larger than all of these and this has the effect of making our distorted-neutrino-spectrum calculations *underestimates* of the actual change in the n/p-ratio and, hence, nucleosynthesis yield deviations. Though these differences are small, it must be kept in mind that τ_n remains uncertain to a degree.

With these choices of η and τ_n, our modified version of the BBN code calculates

the ^{4}He mass fraction to be $Y_p = 0.2429$ and the deuterium abundance relative to hydrogen to be D/H $= 2.543 \times 10^{-5}$. Although the current uncertainty in the WMAP-derived baryon density is relatively small ($\sim \pm 3.6\%$), it nevertheless translates into a $\sim \pm 5.5\%$ uncertainty in the predicted primordial value of D/H. This is because the BBN deuterium yield is a very sensitive function of η. As we discuss below, the error in D/H stemming from the current error in the CMB-determined η precludes using the observationally-determined deuterium abundance to constrain the sterile neutrino physics discussed in this paper. However, the higher precision determinations of η in the projected Four Year WMAP results lead to an uncertainty of ± 0.00047 in $\Omega_{\rm b}h^2$, corresponding to ± 0.117 in η, while the forthcoming Planck mission forecasts ± 0.00017 in $\Omega_{\rm b}h^2$, or ± 0.045 in η [41]. These more precise determinations of η will translate into commensurately better precision in the calculated D/H values. As we discuss below, these could allow for new neutrino physics and/or lepton number constraints.

Corrections to the code, such as time-step corrections and Coulomb and radiative corrections, have been discussed extensively (*e.g.*, Ref. [42]; Ref. [43]). Most corrections are a small additive factor to the final helium abundance Y_p and are functions of the chosen time-step, η, and τ_n. Since this work uses set values for these parameters and presents the results in terms of percent change, the additive corrections do not contribute to the final results.

It is beyond the scope of this work to present precision element abundance predictions. Our goal here is to illustrate the global trends in element production resulting from adding in the active-sterile transformation physics. Eventually corrections, such as the coulomb correction, should be calculated autonomously in the weak rates in order to give the $< 1\%$ accuracy desired.

2.4 BBN Abundance Yields with Lepton Numbers and Sterile Neutrinos

Here we describe the results of our calculations of light element primordial nucleosynthesis in the presence of significant lepton numbers and active-sterile neutrino flavor mixing. The properties of light sterile neutrinos and the lepton numbers of the universe could be related [33, 29], but here we shall vary them independently to gauge effects on BBN abundance yields. We therefore have five quantities to vary.

The first of these parameters is the rest mass of the sterile neutrino m_s or, equivalently, the mass-squared difference $\delta m^2 \approx m_s^2$ characteristic of active-sterile neutrino flavor mixing. The second quantity is the effective 2×2 vacuum mixing angle θ characterizing the unitary transformation between an active neutrino, which we will take to be electron flavor $|\nu_e\rangle$, and a sterile state $|\nu_s\rangle$ and mass/energy eigenstates $|\nu_1\rangle$ and $|\nu_2\rangle$,

$$\begin{aligned} |\nu_e\rangle &= \cos\theta|\nu_1\rangle + \sin\theta|\nu_2\rangle, \\ |\nu_s\rangle &= -\sin\theta|\nu_1\rangle + \cos\theta|\nu_2\rangle, \end{aligned} \tag{2.10}$$

with corresponding rest-mass eigenvalues m_1 and m_2, respectively, such that $\delta m^2 \equiv |m_2^2 - m_1^2|$. Here we set $\sin^2 2\theta = 10^{-3}$ to conform with the LSND results. Because the expansion rate of the universe is so slow at the epoch of medium-enhanced coherent MSW sterile neutrino production, flavor evolution is likely adiabatic, at least for scaled resonance energy $\epsilon_{\rm res} \leq \epsilon_{\rm max}$ [9, 10]. As a consequence, our nucleosynthesis results will change little with variation in θ so long as $\sin^2 2\theta > 10^{-5}$.

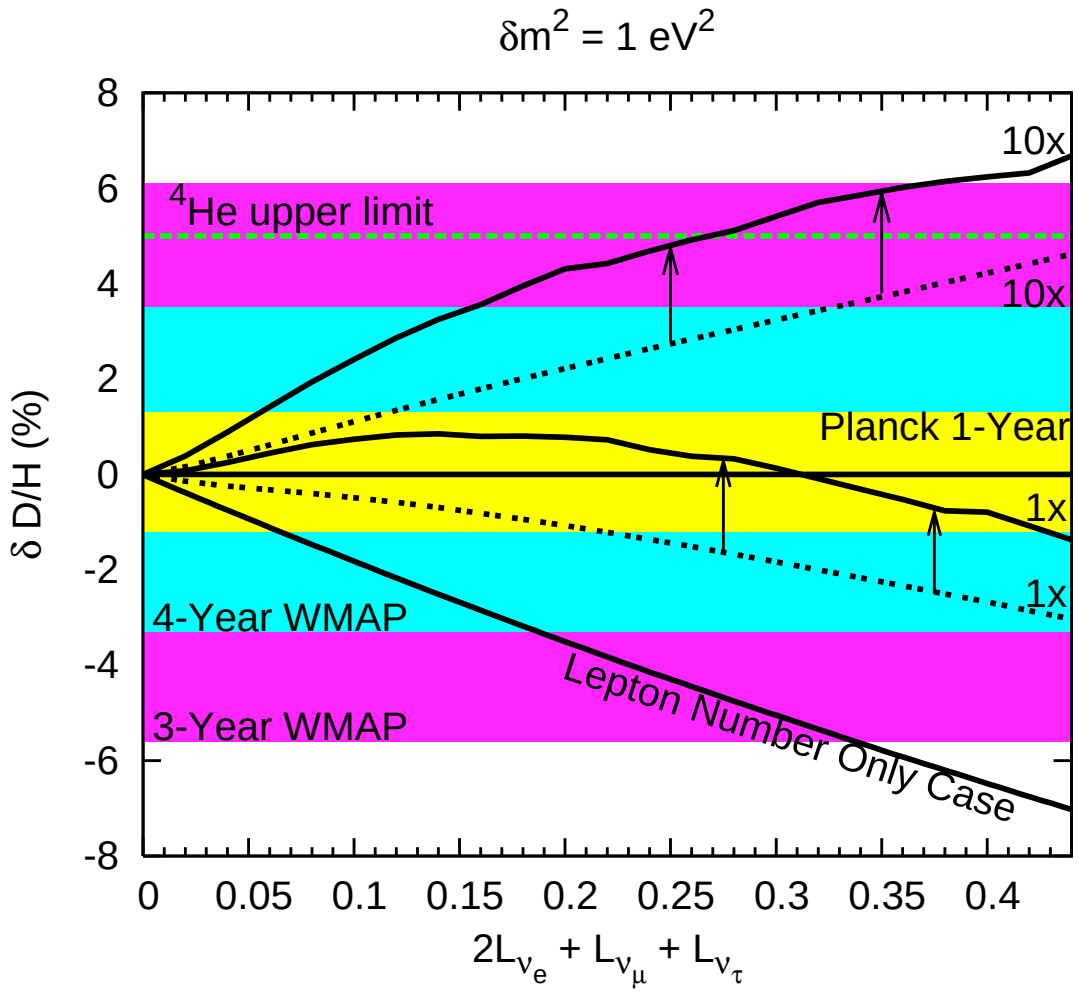

Figure 2.8: Here the outer horizontal band gives the standard BBN range in D/H corresponding to the uncertainty in baryon-to-photon ratio η for the Three Year WMAP data, while the middle and inner bands give the D/H range for the uncertainty in η for the Four Year WMAP and the projected one year Planck result, respectively. The horizontal dashed line shows where neutrino spectral distortion plus lepton number will give a ^{4}He yield exceeding 26%. Here $\delta m^2 = 1\,\mathrm{eV}^2$.

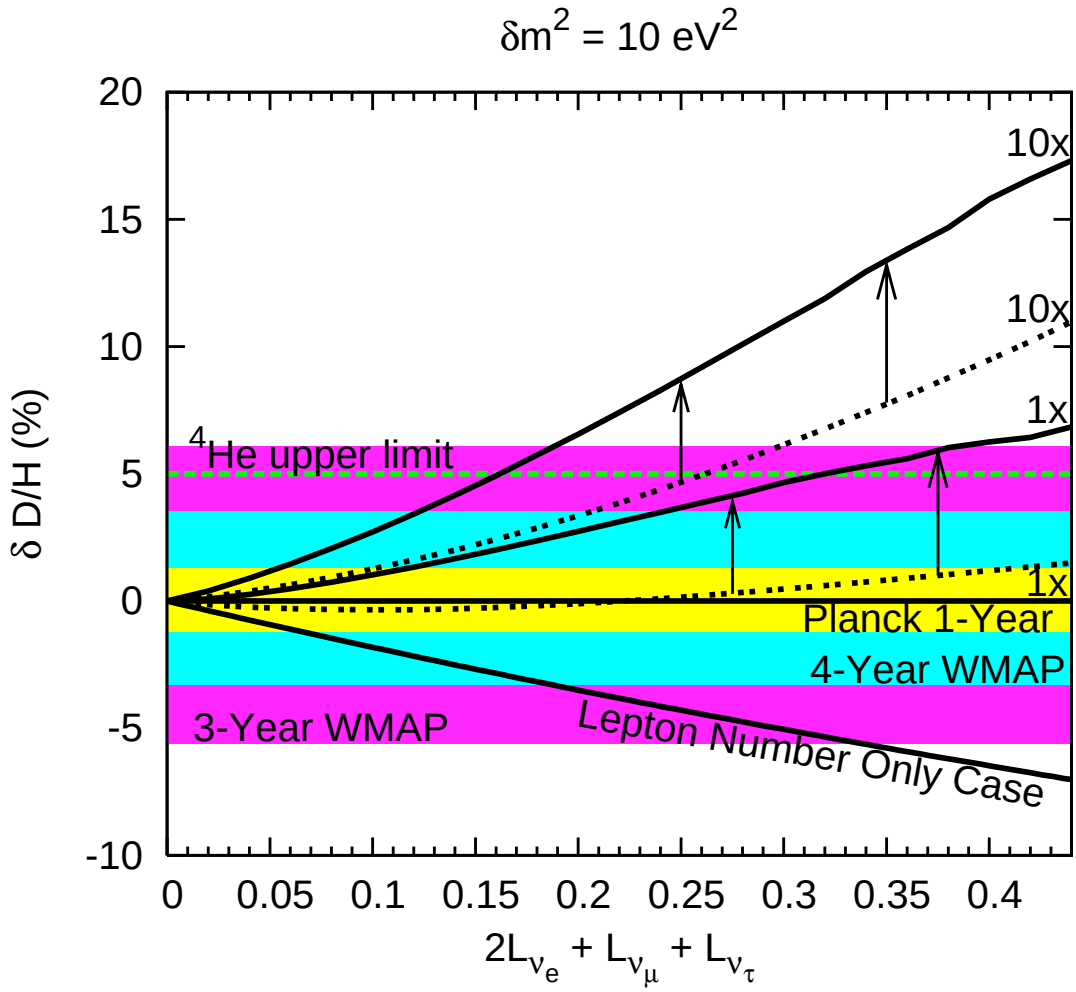

Figure 2.9: Same as for Fig. 2.8 but now with $\delta m^2 = 10\,\mathrm{eV}^2$.

As outlined above and in Ref. [9], instead of treating the complete 4×4 mass/mixing matrix with its many unknown mixing parameters, we shall consider the effective 2×2 conversion channels $\nu_e \rightleftharpoons \nu_s$ or $\bar{\nu}_e \rightleftharpoons \bar{\nu}_s$ and adopt two different resonance sweep schemes in an attempt to bracket the BBN effects of the active-active plus active-sterile mixing-induced spectral distortions. To follow resonance sweep we use: (1) continuous, adiabatic sweep to lepton depletion at $\epsilon_{\rm c.o.}$, and (2) the full solution of Ref. [10]. The latter resonance sweep scheme gives the most dramatic alterations in ν_e or $\bar{\nu}_e$ energy distribution for a given lepton number, but in reality active-active mixing $\nu_e \rightleftharpoons \nu_{\mu,\tau}$ or $\bar{\nu}_e \rightleftharpoons \bar{\nu}_{\mu,\tau}$, as well as $\nu_{\mu,\tau} \rightleftharpoons \nu_s$ or $\bar{\nu}_{\mu,\tau} \rightleftharpoons \bar{\nu}_s$, will likely fill in some of the spectral deficits in ν_e or $\bar{\nu}_e$, as will post-decoupling inelastic neutrino and antineutrino scattering. By contrast, the continuous, adiabatic sweep to $\epsilon_{\rm c.o.}$ scenario gives conservative underestimates of BBN effects [9].

The remaining three parameters in our BBN calculations are the actual lepton numbers. For $\alpha = e, \mu, \tau$ we have

$$L_{\nu_\alpha} = \left(\frac{\pi^2}{12\zeta(3)}\right)\left(\frac{T_\nu}{T_\gamma}\right)^3 \left[\eta_{\nu_\alpha} + \eta_{\nu_\alpha}^3/\pi^2\right], \tag{2.11}$$

where $\zeta(3) \approx 1.20206$, T_ν and T_γ are the neutrino and plasma temperature, respectively, and the ratio of neutrino chemical potential to neutrino temperature is the neutrino degeneracy parameter η_{ν_α}. While η_{ν_α} is a co-moving invariant, L_{ν_α} is not because the ratio T_ν/T_γ varies as temperature drops and the entropy initially in the seas of electrons and positrons is transferred to photons. (After all $e^\pm$-pairs have disappeared, $(T_\nu/T_\gamma)^3 = 4/11$.) The lepton numbers given in our figures are for $T_\nu/T_\gamma = 1$. We assume that all neutrinos and antineutrinos initially have Fermi-Dirac equilibrium energy spectra (*e.g.*, the heavy dashed line in Fig. 4.3), so that $\eta_{\bar{\nu}_\alpha} = -\eta_{\nu_\alpha}$.

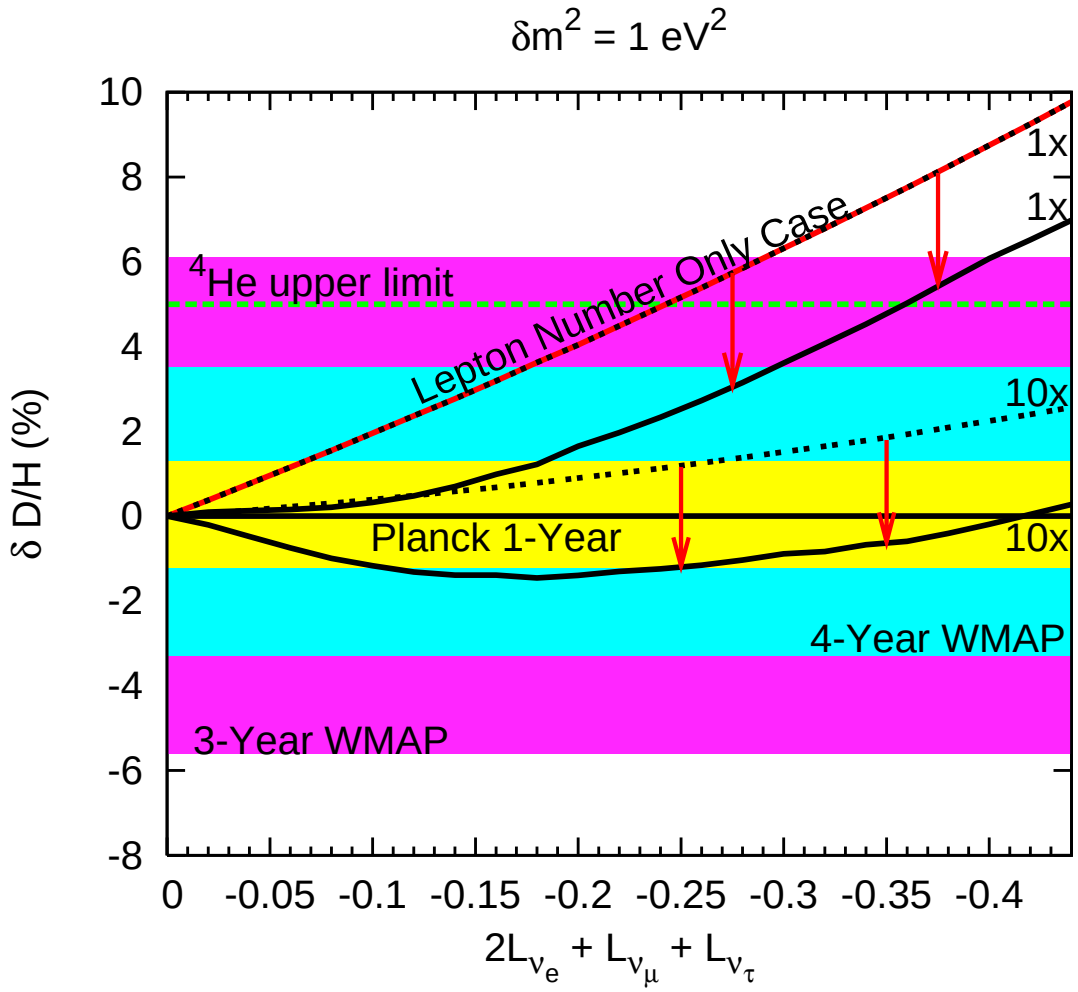

Figure 2.10: Same as for Fig. 2.8 but now with negative lepton numbers.

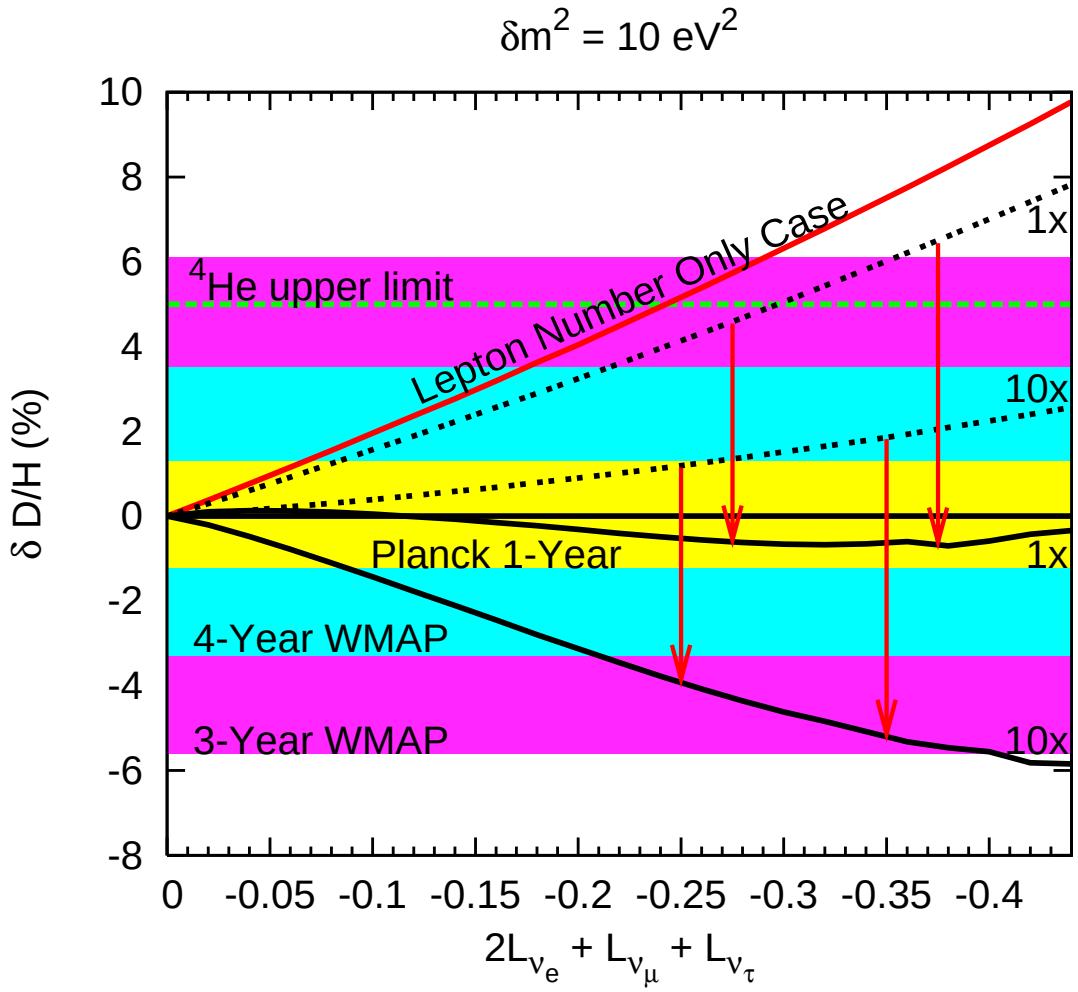

Figure 2.11: Same as for Fig. 2.9 but now with negative lepton numbers.

Active-active 3×3 neutrino mixing with the solar and atmospheric mass-squared differences has been shown to "even up" the lepton numbers of each neutrino flavor to within a factor of $\sim$10 [44, 45, 46, 47]. This also may be true in the 4×4 mixing case. Since we consider $\nu_e \rightleftharpoons \nu_s$ or $\bar{\nu}_e \rightleftharpoons \bar{\nu}_s$, the relevant potential lepton number is $\mathcal{L}_e = 2L_{\nu_e} + L_{\nu_\mu} + L_{\nu_\tau}$. The lepton number distribution factor

$$\text{factor} = \frac{L_{\nu_\mu} + L_{\nu_\tau}}{2L_{\nu_e}} \tag{2.12}$$

is an important determinant of spectral distortion. We consider values of this factor between 1 and 10. The bigger the value of this factor, the larger will be the spectral distortion for a given value of η_{ν_e} or $\eta_{\bar{\nu}_e}$ [9]. This is because the larger the potential lepton number, the larger will be, *e.g.*, $\epsilon_{\max}$ and $\epsilon_{\text{c.o.}}$, quantities which set the scale for spectral distortion.

A positive ν_e degeneracy parameter η_{ν_e} reflects an excess of ν_e's over $\bar{\nu}_e$'s, which will have the effect of driving the reaction in Eq. (3.2) to the right, thereby lowering n/p and the ^{4}He yield. However, $\nu_e \rightarrow \nu_s$ flavor conversion can effectively distort the ν_e spectrum so as to lower the overall ν_e number density and thereby shift the reaction in Eq. (3.2) back to the left, in effect counteracting the ν_e degeneracy and, possibly, leading to an *increase* in the ^{4}He yield over the standard BBN, $\eta_{\nu_e} = 0$ result. This argument can be reproduced in analogous fashion for a $\bar{\nu}_e$ excess ($\eta_{\nu_e} < 0$) and $\bar{\nu}_e \rightleftharpoons \bar{\nu}_s$ flavor conversion.

Figures 2.4 and 2.5 show the percent change in the ^{4}He primordial nucleosynthesis yield relative to the standard BBN model with no lepton numbers and no new neutrino physics as a function of (positive) potential lepton number. In all cases the baryon-to-photon ratio is set to the central CMB-derived value $\eta = 6.11 \times 10^{-10}$. With lepton numbers alone, but without sterile neutrino mixing and spectral distortion, the neutron-to-proton ratio is suppressed and the ^{4}He yield is decreased relative to the standard model. This trend is weakened or even completely reversed when $\nu_e \rightleftharpoons \nu_s$ generated spectral distortion is included in the calculations. In general, the spectral distortions generated in the full resonance sweep scenario produce bigger increases in abundance yield over the lepton-number-only case than

does the forced adiabatic resonance sweep scenario. As discussed above, this stems from the tendency in the full resonance sweep mechanism to deplete ν_e population at higher energy in the distribution function. From Figures 2.4 and 2.5 it is clear that the existence of a sterile neutrino could alter significantly the relationship between predicted ^{4}He abundance and lepton numbers. It is also clear from these figures that improvement in the precision of the observationally-inferred value of Y_p could make for stringent new constraints on the sterile neutrino parameters and lepton numbers. Even with the (likely overly) generous range of $23\% - 26\%$ for Y_p we see that larger sterile neutrino masses together with larger positive lepton numbers tend to produce too much ^{4}He.

Figures 2.6 and 2.7 likewise show the deviation in the ^{4}He yield from the standard model value but now for negative lepton numbers. These figures are not simply mirror images of Figures 2.4 and 2.5. This is because negative lepton numbers will produce distortions in the $\bar{\nu}_e$ energy spectrum. There is a threshold in the $\bar{\nu}_e$ capture process in Eq. (3.3), while there is no threshold in the ν_e capture process in Eq. (3.2). The result is that we must have a distortion extending to higher energy in the $\bar{\nu}_e$ distribution than in the ν_e distribution to produce the same magnitude change in ^{4}He yield. This trend is obvious in Fig. 2.4 where there is no discernible difference between the case with lepton number alone and the case with $\bar{\nu}_e \rightleftharpoons \bar{\nu}_s$ mixing in the forced adiabatic sweep scenario with lepton number distribution factor 1. However, in Fig. 2.7 we see that with large enough δm^2, negative potential lepton number, and lepton number distribution factor it is possible that the ^{4}He yield would fall below 23% by mass fraction, at least for the full resonance sweep scenario.

Similar trends are evident in the deuterium yield as shown in Figures 2.8, 2.9, 2.10, and 2.11. These figures are essentially similar in overall structure to those for ^{4}He. However, because the deuterium yield is so sensitive to baryon-to-photon ratio η, in these figures we show bands of ranges of calculated D/H corresponding to the quoted uncertainty ranges in η for the Three Year WMAP data and for the expected η uncertainties in the Four Year WMAP and the Planck results.

The general change in D/H relative to standard BBN is similar to that for ^{4}He. In the lepton number only cases with no sterile neutrinos a positive potential lepton number with its accompanying suppression in n/p results in a decrease in the deuterium abundance yield. Again, this trend is reversed for large enough spectral distortion. In general, bigger increases in D/H are created by larger δm^2 and larger positive lepton numbers plus $\nu_e \rightleftharpoons \nu_s$ conversion in the full resonance sweep solution.

However, given the current uncertainty in η it is evident from these figures that no meaningful constraints on lepton numbers alone or on combinations of lepton numbers and sterile neutrino properties can be obtained from measurements of D/H. The δD/H produced, for example, at $\delta m^2 = 10\,\mathrm{eV}^2$ for $\mathcal{L}_e > 0.15$ could exceed the uncertainty range in deuterium yield stemming from the Three Year WMAP uncertainty in η, but the ν_e spectral distortions accompanying this scenario would produce ^{4}He in excess of 26% by mass fraction, *i.e.*, exceeding the observational bound (horizontal dashed line).

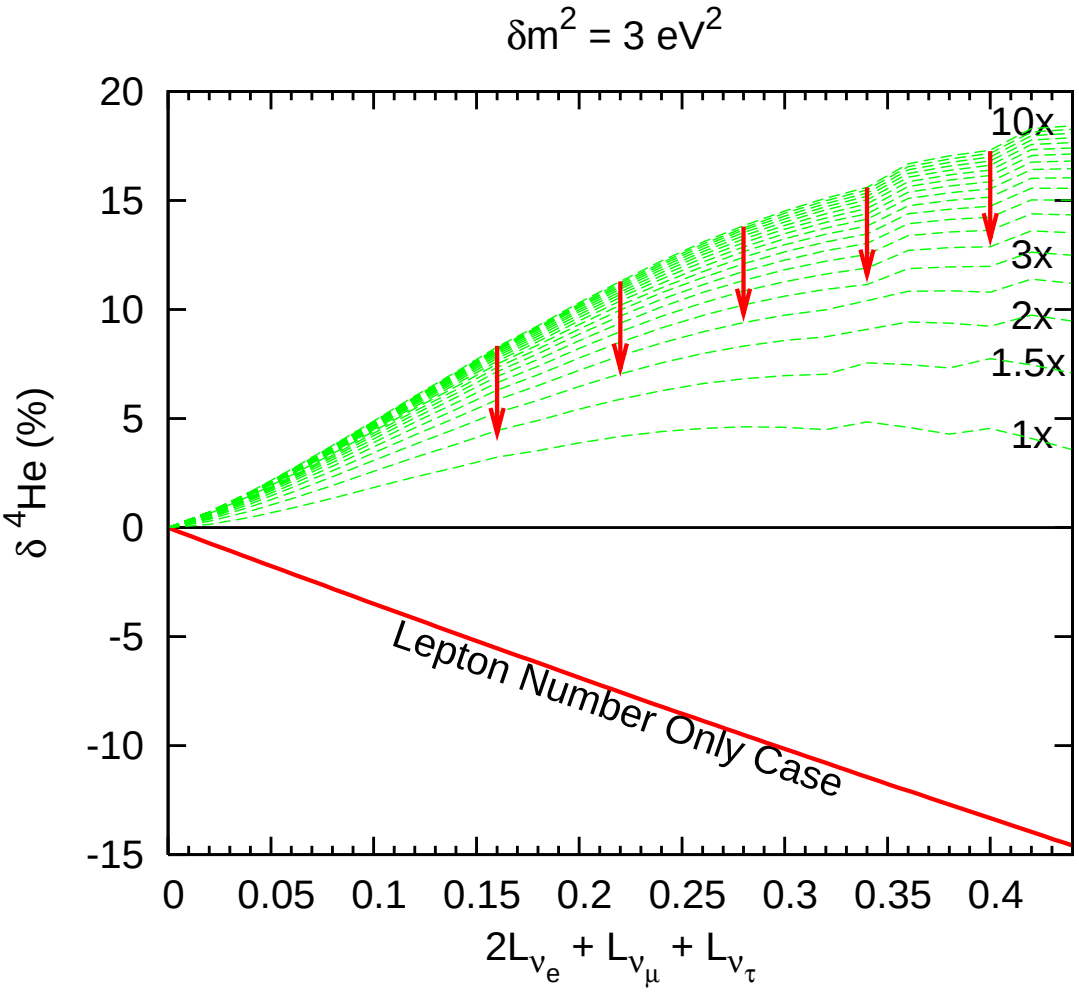

Figure 2.12: Same as for Fig. 2.4 but now with $\delta m^2 = 3\,\mathrm{eV}^2$ and where the dashed curves are for lepton number distribution factors as labeled, up to 10. Here the full resonance sweep solution is employed.

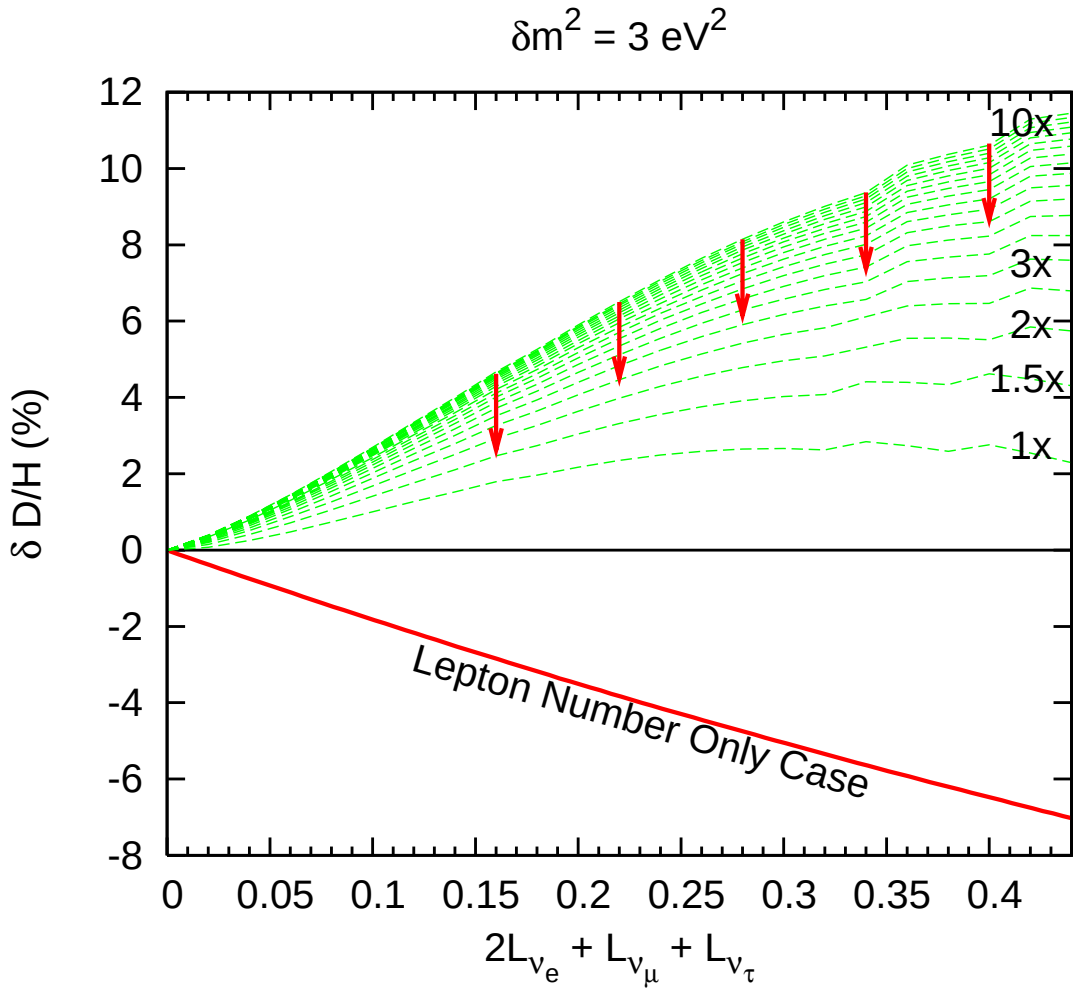

Figure 2.13: Same as Fig. 2.12 but now for deuterium.

By contrast, the considerably smaller uncertainty expected in, *e.g.*, the Planck CMB-determined baryon-to-photon ratio could allow for rather stringent constraints on (or signatures of) either lepton numbers alone or combinations of lepton numbers and sterile and active neutrino mixing parameters. However, as is evident in Fig. 2.9, realizing statistically significant constraints or signatures would require that the observationally-derived primordial deuterium abundance be known to better than 5% accuracy. This is problematic as currently there is likely a 15% to 30% error in observationally-determined primordial D/H. Prospects for bettering these errors will be discussed in the next section.

Negative lepton numbers produce alterations in D/H yield which are qualitatively similar (with reversed trends) to those in the positive lepton number regime. However, as for ^{4}He, the presence of the threshold in $\bar{\nu}_e + p \rightarrow n + e^+$ serves to lessen the overall quantitative impact on $\mid \delta\mathrm{D/H} \mid$ of spectral distortions from given values of (negative) $\mathcal{L}_e$, δm^2 and lepton number distribution factor. This is shown in Figures 2.10 and 2.11.

The light element abundance yield alterations resulting from lepton numbers and spectral distortions can depend on δm^2, L_{ν_e}, L_{ν_μ}, L_{ν_τ}, and resonance sweep physics in complicated ways. In Figures 2.12 and 2.13 we show δ^4He and δD/H, respectively, for the full resonance sweep solution and for $\delta m^2 = 3\,\mathrm{eV}^2$ for many values of the lepton number distribution factor $(L_{\nu_\mu} + L_{\nu_\tau})/2L_{\nu_e} = 1$, 1.5, 2, 2.5, 3, up to 10. We see that there is a fair increase in δ^4He and δD/H with increasing values of this factor until it approaches ≈ 5. In broad brush, this trend comes about because larger values of this factor mean relatively lower ν_e degeneracy and resonance sweep to higher ν_e energy (*e.g.*, larger ϵ_{max}). Both of these consequences tend to increase ^{4}He and D/H yields.

Likewise, larger δm^2 values generally imply an earlier onset of resonance sweep and spectral distortion development. This, in turn, means a bigger effect on n/p, as the rates for the neutron-to-proton interconversion processes in Eqs. (3.2), (3.3), and (3.4) are faster at earlier epochs where temperature and, hence, average lepton energies are higher. These trends are evident in Figures 2.14 and 2.15 where con-

tours of δ^4He and δD/H, respectively, are shown as functions of δm^2 and (positive) $\mathcal{L}_e = 2L_{\nu_e} + L_{\nu_\mu} + L_{\nu_\tau}$ for the full resonance sweep solution and for lepton number distribution factor 3. There is little dependence of abundance yield deviation on δm^2 in either figure at low values of $\mathcal{L}_e$. However, for a given δm^2, increasing $\mathcal{L}_e$ tends to delay resonance sweep and the development of spectral distortions. This can be offset with larger δm^2. As a consequence, for larger values of $\mathcal{L}_e$ we see a significant δm^2 dependence in both δ^4He and δD/H.

The results shown in Figures 2.14 and 2.15 may help to indicate where we might expect active neutrino inelastic scattering to partially erase or modify the spectral distortions we calculate in the coherent neutrino propagation limit. The earlier the onset of resonance sweep, the more significant inelastic neutrino scattering will be. This regime will generally be where the δm^2 dependence in abundance deviations is weakest, *i.e.*, for parameters in the upper left hand corners of Figures 2.14 and 2.15, where lepton numbers are small and δm^2 is large.

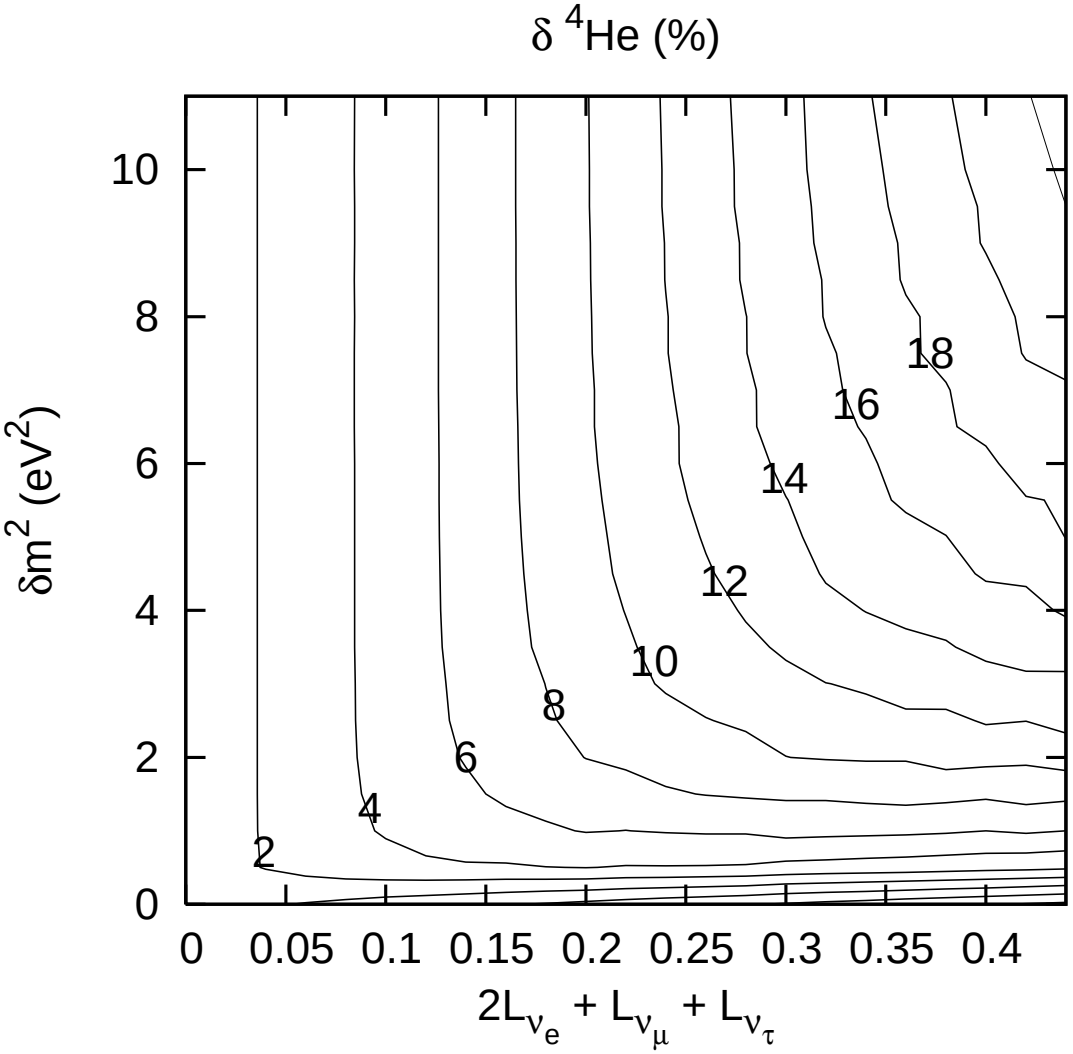

Figure 2.14: Contours of percent change in ^{4}He yield relative to standard BBN for ranges of $\delta m^2 = 0 - 11\,\mathrm{eV}^2$ and potential lepton number $0 - 0.44$, all for lepton number distribution factor 3 and the full resonance sweep scenario.

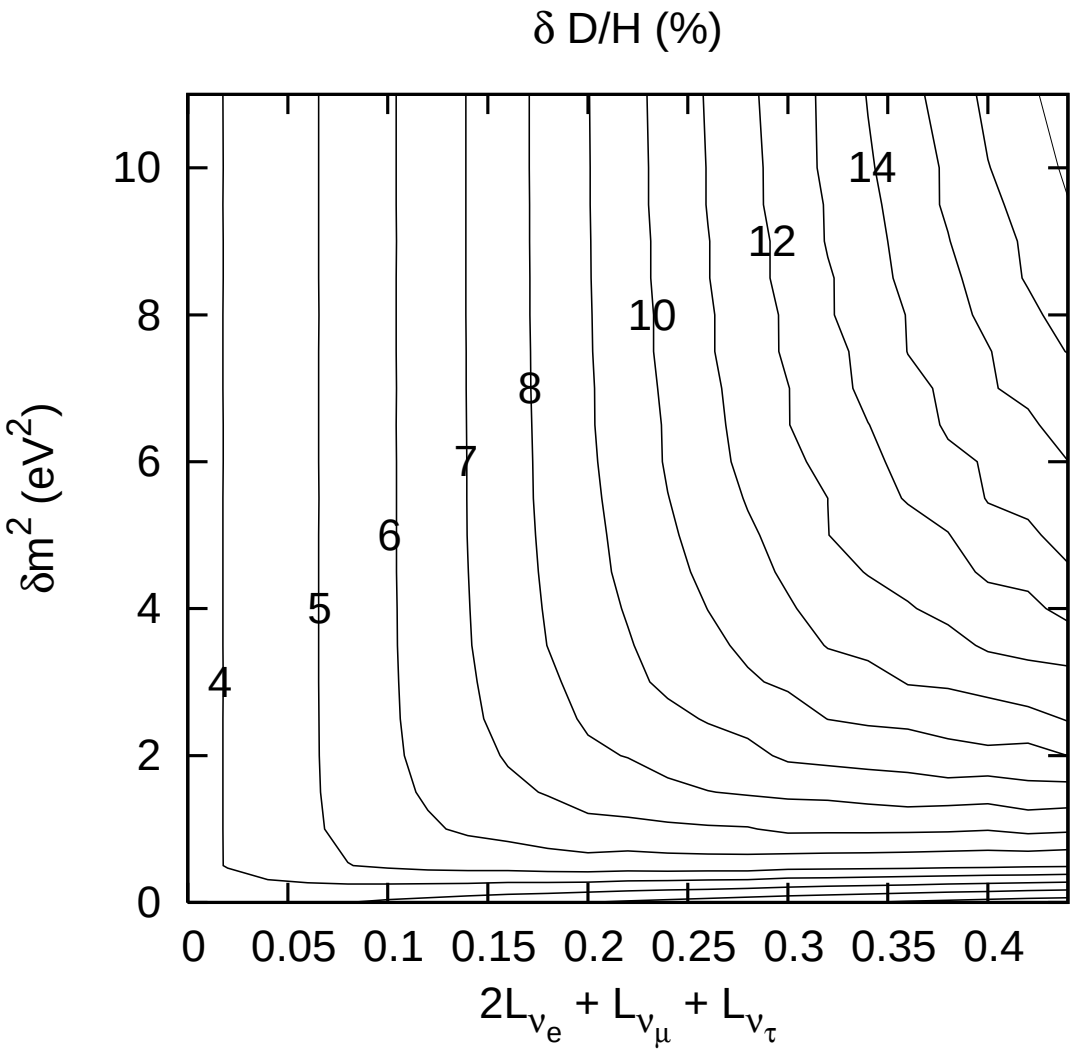

Figure 2.15: Same as Fig. 2.14 but now for the primordial deuterium abundance yield.

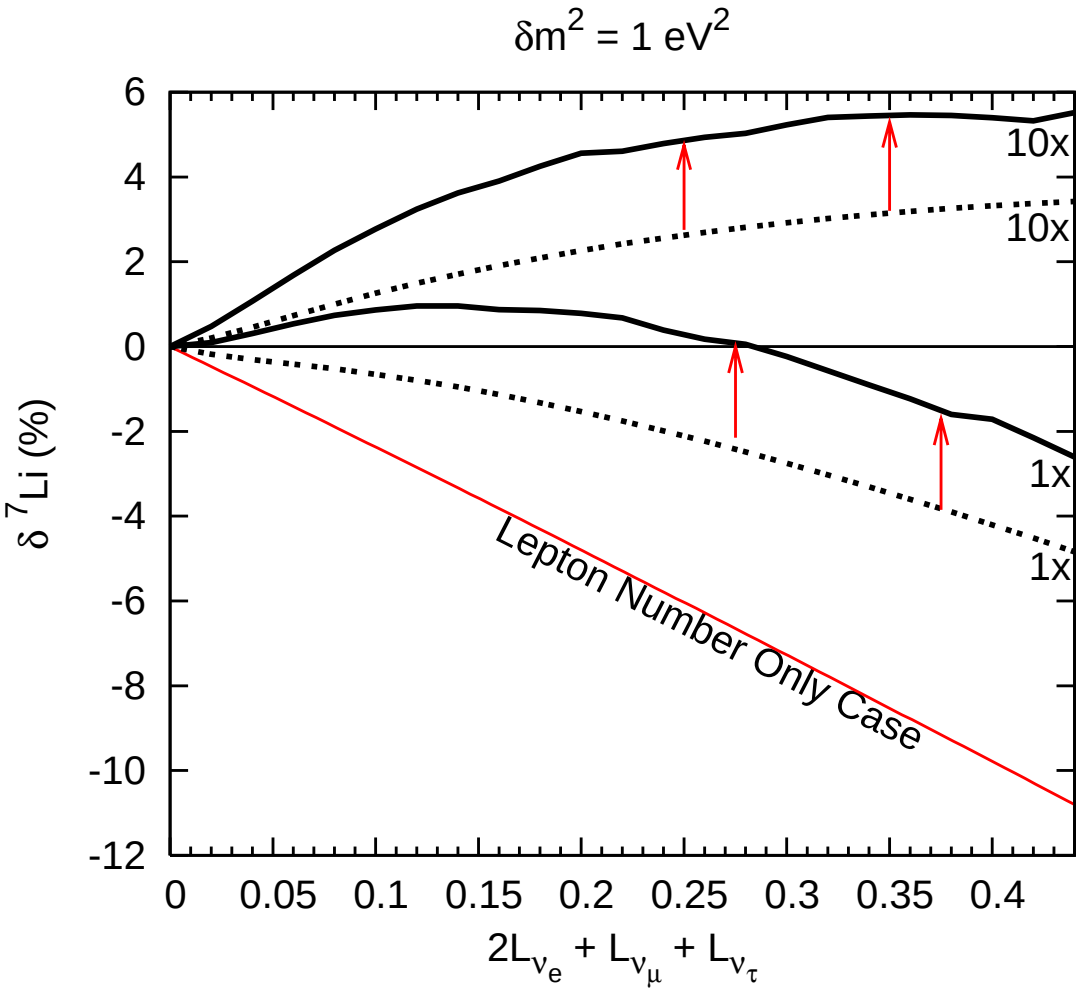

Figure 2.16: Same as Fig. 2.4 but now for percent change in ^{7}Li abundance.

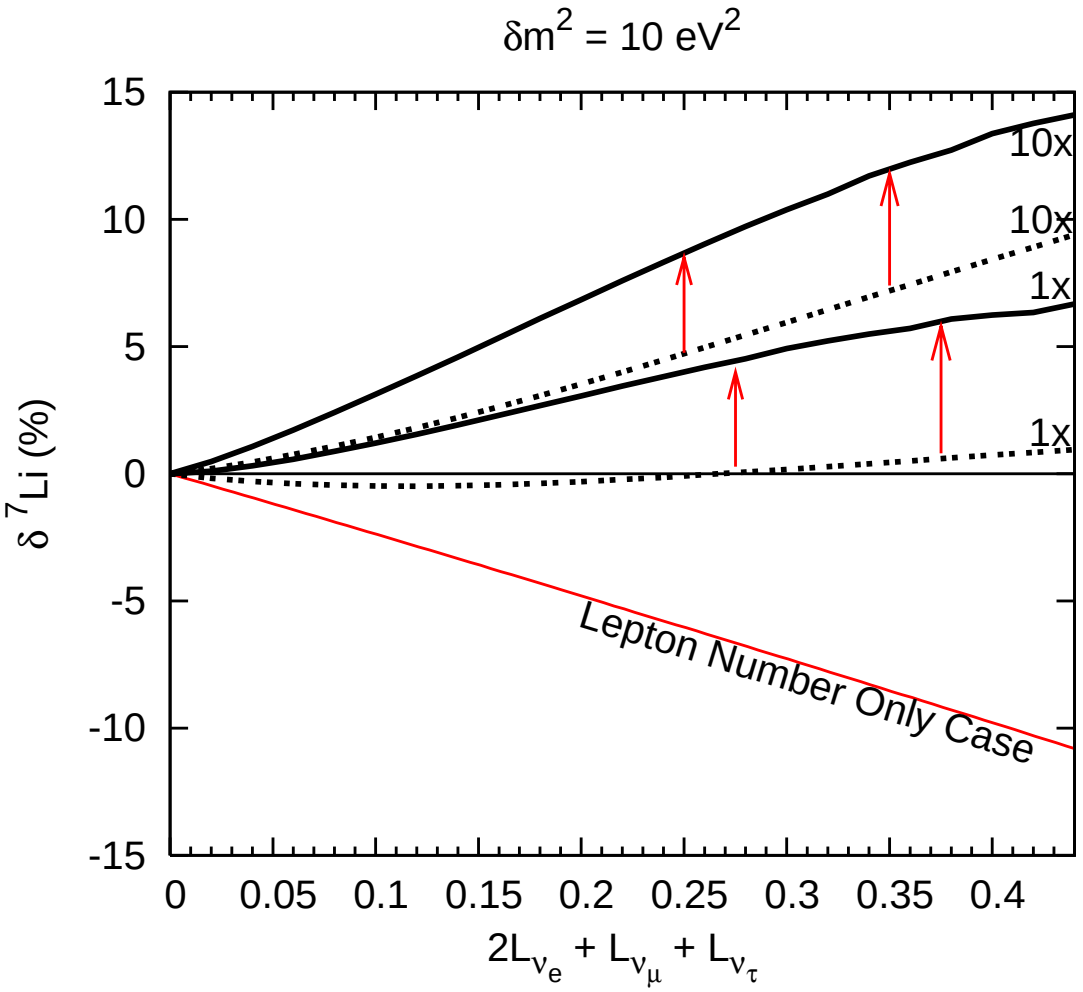

Figure 2.17: Same as Fig. 2.16 but now for $\delta m^2 = 10\,\mathrm{eV}^2$.

Finally, the deviation in ^{7}Li abundance (^{7}Li/H) yield, δ^7Li, relative to the standard BBN zero lepton number, no new neutrino physics case, is shown as a function of (positive) potential lepton number $\mathcal{L}_e$ in Figures 2.16 ($\delta m^2 = 1\,\mathrm{eV}^2$) and 2.17 ($\delta m^2 = 10\,\mathrm{eV}^2$) for several cases. The general trends in δ^7Li are similar to those for δ^4He. In the lepton number only case with no sterile neutrinos, increasing $\mathcal{L}_e$ and, hence, decreasing n/p suppresses the ^{7}Li yield. ^{7}Li is produced at this η principally as ^{7}Be through $^3\mathrm{He}(\alpha,\gamma)^7\mathrm{Be}$. However, there is a small contribution to ^{7}Li from direct production via $^3\mathrm{H}(\alpha,\gamma)^7\mathrm{Li}$ and the tritium, ^{3}H, abundance during BBN tracks the n/p ratio. Though δ^7Li can be large for several of the cases shown in these figures, it is at this time not a good candidate for lepton number or sterile neutrino constraint. This is because there remains considerable controversy surrounding both the observationally-determined primordial ^{7}Li abundance and the astration/production history of ^{7}Li in stars and in the interstellar medium. At the value of the baryon-to-photon ratio η adopted here, the calculated BBN ^{7}Li/H yield is a factor ~ 3 higher than the ^{7}Li/H abundance inferred from the Spite plateau in hot, old halo stars [48].

2.5 Discussion and Conclusions

We have for the first time self consistently and simultaneously coupled the full BBN nuclear reaction network with medium-enhanced active-sterile neutrino flavor transformation. One conclusion from our work is straightforward: the existence of light sterile neutrinos ν_s which mix with active neutrinos ν_e, ν_μ, ν_τ could alter significantly the relationship between primordial lepton numbers and the BBN light element (^{2}H, ^{4}He, ^{7}Li) abundance yields. Our work also shows that precision predictions of primordial nucleosynthesis yields for given neutrino properties and lepton numbers likely will require accurate treatment of the evolution of neutrino spectral distortion. Depending on neutrino mixing parameters, this may require a full 4×4 quantum kinetic equation neutrino flavor transformation scheme.

However, the calculations we have performed here allow us to point out some

intriguing trends that eventually may provide a means for constraining lepton numbers and/or sterile neutrino properties. In particular, though we find that positive (negative) potential lepton number causes the BBN ^{4}He, ^{2}H, and ^{7}Li abundance yields to be suppressed (increased) relative to the standard BBN zero-lepton-number case, these trends are counteracted and even *reversed* when sterile neutrinos exist and medium-enhanced $\nu_e \rightleftharpoons \nu_s$ ($\bar{\nu}_e \rightleftharpoons \bar{\nu}_s$) takes place.

An underlying theme of our work is that the BBN paradigm, especially as it concerns constraints on neutrino physics, may be changing. We now know to fair precision the baryon density from the CMB acoustic peak amplitude ratios. The uncertainty in baryon-to-photon ratio η likely will improve with future observations. This trend will culminate in the near term in the Planck mission, which is projected to reduce the uncertainty in η to $\leq 1\%$. The near elimination of uncertainty in this quantity and the neutron lifetime will leave the leptonic sector as the principle source of uncertainty in conventional, thermal BBN. This is an intriguing development which comes hard on the heels of new experimental/observational revelations of neutrino mass-squared differences, flavor mixing parameters, and CMB- and large scale structure- derived bounds on light neutrino mass contributions to closure.

The active neutrino mixing parameters in particular allow ^{4}He-derived constraints on electron lepton number L_{ν_e} [27] to be extended to L_{ν_μ} and L_{ν_τ} [44, 45, 46]. Certainly, improvements in precision in the observationally-inferred helium abundance Y_p will translate directly into improved constraints on lepton number [27]. This is obvious in Figures 2.4, 2.5, 2.6, 2.7, for the value of $\mathcal{L}_e = 4L_{\nu_e}$ at which the "Lepton Number Only Case" line crosses the limits of the horizontal band (^{4}He mass fraction 23%). This occurs for $L_{\nu_e} = \mathcal{L}_e/4 \approx 0.045$, corresponding to ν_e degeneracy parameter $\eta_{\nu_e} \approx 0.07$. This is, of course, a crude upper limit, corresponding to our adopted range for the primordial helium abundance.

If the uncertainty in the observationally-inferred deuterium abundance D/H could be improved significantly, it could become competitive with ^{4}He as a probe of lepton number and new neutrino physics. This is not the case currently. The

statistical uncertainty in D/H is between 15% and 30%, as derived from the isotope-shifted hydrogen absorption lines observed in Lyman Limit and Damped Lyman Alpha absorption systems along lines of sight to high redshift QSO's [4, 17]. As Figures 2.8, 2.9, 2.10, and 2.11 show, we would need to get the error in D/H down to $\leq 5\%$ to enable deuterium to provide constraints on, or signatures of, *e.g.*, sterile neutrinos.

This is problematic in the short term, but not an inconceivable eventuality in the longer term. The current deuterium abundance stems from of order a half dozen QSO absorption systems. With the projected increase in the number of 8m class telescopes and extensions of surveys to the southern hemisphere, we might expect to increase the number of "clean" (*i.e.*, no interloper cloud) Lyman-α absorption systems by a factor of 2 or so. This likely will not be good enough. However, the advent of 30m class telescopes could give many more QSO lines of sight and this might provide for much higher precision deuterium abundance determinations. This could be useful for probes of primordial baryon inhomogeneity or the star formation and chemical evolution history of the early universe. However, in this paper we point out that it also could be useful for constraints on new neutrino physics, especially as regards lepton numbers plus sterile neutrinos.

If, for example, we knew *a priori* the sign of the primordial lepton number, then there may be a signature for sterile neutrinos or at least a means for better constraining their properties. A positive lepton number would be expected to give a suppression of ^{2}H and ^{4}He relative to the zero-lepton-number, standard BBN predictions based on the CMB-derived baryon density. However, a light sterile neutrino could reverse this and give an *increase* in these abundances over the standard case. In broad brush, it works in an opposite sense for a negative lepton number, though the effect is less dramatic on account of the threshold in $\bar{\nu}_e + p \rightarrow n + e^+$.

Likewise, if experimental evidence exists for active-sterile neutrino mixing, then the sign of the deviation of ^{2}H, ^{4}He, or ^{7}Li from the standard zero-lepton number BBN case may afford a direct measure of the sign and magnitude of the potential

lepton number. At the least, measurements and reasoning along these lines may allow for significantly better constraints on lepton numbers in this case.

There is another possibility. Suppose that active-sterile mixing properties are measured in the lab and precise primordial light-element abundances are obtained from observation. Further suppose that the effects (abundance deviations from standard BBN) pointed out here are *not* seen. This could indicate that there is another mechanism, other than large ($|L_{\nu_\alpha}| > 10^{-3}$) lepton number [9, 29, 31], operating to suppress active neutrino scattering-induced de-coherence production [49, 50, 51, 52, 53, 30] of seas of ν_s and $\bar{\nu}_s$. We know that some mechanism must suppress this process because otherwise there would be a conflict with CMB- and large scale structure-derived bounds on light neutrino mass contribution to closure (see for example Ref. [9]). Two alternative means for sterile neutrino production suppression have been suggested: a low re-heat temperature for inflation [54]; and an alteration of neutrino mass/mixing properties (*i.e.*, no mass or mixing) at early epochs.

In any case, the linkage between the light elements and new neutrino physics which we have pointed out here increases the leverage of new developments in both observational cosmology and terrestrial neutrino oscillation experiments.

2.6 Acknowledgments

We would like to acknowledge discussions with Huaiyu Duan, David Kirkman, Max Pettini, Michael Smith, Nao Suzuki, and David Tytler. The work of G.M.F., C.T.K., and C.J.S. was supported in part by NSF grant PHY-04-00359 and a UC/LANL CARE grant at UCSD; C.T.K. acknowledges financial support from the ARCS Foundation, Inc.; K.N.A. was supported by Los Alamos National Laboratory (under DOE contract W-7405-ENG-36) and also acknowledges the UC/LANL CARE grant.

Chapter 2, in full, is a reprint of the material as it appears in Physical Review D 2006. Smith, Christel J.; Fuller, George M.; Kishimoto, Chad T.;Abazajian,

Kevork N.; Phys. Rev. D, 2006. The dissertation author was the primary investigator and author of this paper.

Bibliography

[1] SDSS Collaboration, M. Tegmark *et al.*, Phys. Rev. D **69**, 103501 (2004).

[2] D. N. Spergel *et al.*, Astrophys. J. Suppl. **148**, 175 (2003).

[3] D. N. Spergel *et al.*, astro-ph/0603449.

[4] D. Kirkman, D. Tytler, N. Suzuki, J. M. O'Meara, and D. Lubin, Astrophys. J. Suppl. **149**, 1 (2003).

[5] J. M. O'Meara, D. Tytler, D. Kirkman, N. Suzuki, J. X. Prochaska, D. Lubin and A. M. Wolfe, Astrophys. J. **552**, 718 (2001).

[6] S. Burles, K. M. Nollett and M. S. Turner, Astrophys. J. **552**, L1 (2001).

[7] R. H. Cyburt, B. D. Fields and K. A. Olive, Phys. Lett. B **567**, 227 (2003).

[8] C. Y. Cardall and G. M. Fuller., Astrophys. J. **472**, 435 (1996).

[9] K. Abazajian, N. F. Bell, G. M. Fuller and Y. Y. Y. Wong, Phys. Rev. D **72**, 063004 (2005).

[10] C. T. Kishimoto, G. M. Fuller and C. J. Smith, Phys. Rev. Lett. **97**, 141301 (2006), [astro-ph/0607403].

[11] K. A. Olive and E. D. Skillman, Astrophys. J. **617**, 29 (2004).

[12] K. A. Olive, G. Steigman and E. D. Skillman, Astrophys. J. **483**, 788 (1997).

[13] Y. I. Izotov and T. X. Thuan, Astrophys. J. **602**, 200 (2004).

[14] R. H. Cyburt, B. D. Fields, K. A. Olive and E. Skillman, Astropart. Phys. **23**, 313 (2005).

[15] G. Steigman, astro-ph/0501591.

[16] G. Steigman, Int. J. Mod. Phys. E **15**, 1 (2006).

[17] M. Pettini, in *Astrophysics in the Far Ultraviolet: Five Years of Discovery with FUSE*, edited by G. Sonneborn, H. W. Moos and B.-G. Andersson, ASP Conf. Ser. No. 348, p. 19, Provo, 2006, ASP.

[18] K. Eitel, New J. Phys. **2**, 1 (2000).

[19] MiniBooNE Collaboration, G. McGregor, in *Particle Physics and Cosmology: Third Tropical Workshop on Particle Physics and Cosmology - Neutrinos, Branes, and Cosmology*, edited by J. F. Nieves and C. N. Leung, AIP Conf. Proc. No. 655, p. 58, New York, 2003, AIP.

[20] U. Seljak, A. Slosar and P. McDonald, astro-ph/0604335.

[21] S. Hannestad, J. Cosmol. Astropart. Phys **0305**, 004 (2003).

[22] A. Pierce and H. Murayama, Phys. Lett. B **581**, 218 (2004).

[23] K. N. Abazajian, Astropart. Phys. **19**, 303 (2003).

[24] P. Di Bari, Phys. Rev. D **65**, 043509 (2002).

[25] P. Di Bari, Phys. Rev. D **67**, 127301 (2003).

[26] V. Barger, J. P. Kneller, P. Langacker, D. Marfatia and G. Steigman, Phys. Lett. B **569**, 123 (2003).

[27] J. P. Kneller, R. J. Scherrer, G. Steigman and T. P. Walker, Phys. Rev. D **64**, 123506 (2001).

[28] S. Dodelson, A. Melchiorri and A. Slosar, Phys. Rev. Lett. **97**, 041301 (2006).

[29] R. Foot and R. R. Volkas, Phys. Rev. Lett. **75**, 4350 (1995).

[30] R. Foot and R. R. Volkas, Phys. Rev. D **55**, 5147 (1997).

[31] Y.-Z. Chu and M. Cirelli, Phys. Rev. **D74**, 085015 (2006), [astro-ph/0608206].

[32] M. S. Smith, L. H. Kawano and R. A. Malaney, Astrophys. J. Suppl. **85**, 219 (1993).

[33] X. Shi and G. M. Fuller, Phys. Rev. Lett. **83**, 3120 (1999).

[34] S. P. Mikheyev and A. Y. Smirnov, Yad. Fiz. **42**, 1441 (1985).

[35] L. Wolfenstein, Phys. Rev. D **17**, 2369 (1978).

[36] R. V. Wagoner, W. A. Fowler and F. Hoyle, Astrophys. J. **148**, 3 (1967).

[37] L. Kawano, NASA STI/Recon Technical Report N **92**, 25163 (1992).

[38] L. Kawano, FERMILAB-PUB-88/34-A.

[39] W.-M. Yao *et al.*, J. Phys. G **33**, 1 (2006).

[40] A. Serebrov *et al.*, Phys. Lett. B **605**, 72 (2005).

[41] J. R. Bond, C. Contaldi, A. Lewis and D. Pogosyan, Int. J. Theor. Phys. **43**, 599 (2004).

[42] R. E. Lopez and M. S. Turner, Phys. Rev. D **59**, 103502 (1999).

[43] P. J. Kernan and L. M. Krauss, Phys. Rev. Lett. **72**, 3309 (1994).

[44] K. N. Abazajian, J. F. Beacom and N. F. Bell, Phys. Rev. D **66**, 013008 (2002).

[45] Y. Y. Y. Wong, Phys. Rev. D **66**, 025015 (2002).

[46] A. D. Dolgov, S. H. Hansen, S. Pastor, S. T. Petcov, G. G. Raffelt and D. V. Semikoz, Nucl. Phys. B **632**, 363 (2002).

[47] M. J. Savage, R. A. Malaney and G. M. Fuller, Astrophys. J. **368**, 1 (1991).

[48] F. Spite and M. Spite, Astron. Astrophys. **115**, 357 (1982).

[49] R. R. Volkas and Y. Y. Y. Wong, Phys. Rev. D **62**, 093024 (2000).

[50] K. S. M. Lee, R. R. Volkas and Y. Y. Y. Wong, Phys. Rev. D **62**, 093025 (2000).

[51] A. D. Dolgov, Yad. Fiz. **33**, 1309 (1981).

[52] B. H. J. McKellar and M. J. Thomson, Phys. Rev. D **49**, 2710 (1994).

[53] P. Di Bari, P. Lipari and M. Lusignoli, Int. J. Mod. Phys. A **15**, 2289 (2000).

[54] G. Gelmini, S. Palomares-Ruiz and S. Pascoli, Phys. Rev. Lett. **93**, 081302 (2004).

Chapter 3

Big Bang Nucleosynthesis with Independent Neutrino Distribution Functions

3.1 Introduction

There is a new paradigm in Big Bang Nucleosynthesis (BBN) studies which promises enhanced probes of the early universe and a window into new physics. In the past, BBN predictions have been used to place constraints on the baryon number at three minutes after the Big Bang. This was done by comparing the observationally-inferred primordial light element abundances to abundances predicted by BBN calculations over a wide range of baryon-to-photon ratio values. With the high precision results of the Wilkinson Microwave Anisotropy Probe (WMAP), however, the baryon-to-photon ratio, η, is now independently determined – at 300,000 years after the Big Bang – from observations of the cosmic microwave background (CMB) relative acoustic peak amplitudes [1, 2, 3]. Currently, the WMAP Three Year Mean value for the baryon-to-photon ratio is $\eta = (6.11 \pm .22) \times 10^{-10}$. Future missions (*e.g.*, Planck[4]) promise considerably higher precision determinations of η. In addition, current CMB measurements

can provide loose constraints on primordial helium[5] while forecasts for Planck precision data may constrain Y_p with error bars of 5%[6, 5].

Since the baryon-to-photon ratio is known independently, and to excellent precision albeit at much later times, BBN calculations can now be used to probe or constrain new physics or heretofore poorly determined parameters. For example, we can use BBN predictions to constrain not only the lepton numbers but also the physics behind these lepton numbers . The existence of a nonzero electron lepton number follows from charge neutrality and the observed proton content of the universe. The contributions of neutrinos and antineutrinos to the electron, muon, and tau (e, μ, τ) lepton numbers are not known, since we do not directly observe these relic particles. The neutrino contribution to the lepton number for a given flavor, $\alpha = \mathrm{e}, \mu, \tau$, is defined analogously to the baryon-to-photon ratio, $\eta \equiv (n_b - n_{\bar{b}})/n_\gamma$, as

$$L_{\nu_\alpha} \equiv \frac{n_{\nu_\alpha} - n_{\bar{\nu}_\alpha}}{n_\gamma}, \tag{3.1}$$

where $n_\gamma = (2\zeta(3)/\pi^2)T_\gamma^3$ is the proper photon number density at temperature T_γ, and n_{ν_α} and $n_{\bar{\nu}_\alpha}$ are the neutrino and antineutrino number densities. Observational bounds on the lepton numbers[7, 8, 9, 10, 11, 12, 13, 14, 15] remain large compared to the values of these that could significantly affect BBN when there is new leptonic sector physics (*e.g.*, sterile neutrinos)[7].

The neutrino lepton numbers influence BBN and the resulting primordial element abundances in a number of ways[16]. The energy density in the neutrino sector contributes to the total energy density of the universe, which determines the expansion rate. The expansion rate is crucial to the outcome of BBN because it determines the weak freeze-out temperature which in turn effectively sets the neutron-to-proton ratio and, therefore, the primordial abundances of ^{4}He and the other light elements.

Not only is the total number of neutrinos important to the outcome of BBN, but the neutrino distribution functions are key components of the phase space integrals in the weak reaction rates in BBN. The weak reactions of greatest interest are those

that interconvert neutrons and protons:

$$\nu_e + n \rightleftharpoons p + e^-, \tag{3.2}$$

$$\bar{\nu}_e + p \rightleftharpoons n + e^+, \tag{3.3}$$

$$n \rightleftharpoons p + e^- + \bar{\nu}_e. \tag{3.4}$$

Since the rates for the weak reactions are strongly energy dependent, the energy distributions of the neutrinos and antineutrinos can figure prominently in both the forward and reverse rates in the processes in Eqs. (3.2), (3.3), and (3.4). In standard BBN scenarios the neutrino distribution functions are assumed to be thermally-shaped Fermi-Dirac distributions. However, it is possible that non-thermal neutrino distribution functions arise after the neutrinos decouple from the background plasma around $T \approx 3\,\mathrm{MeV}$ and during times crucial to BBN.

There are many possible mechanisms that could alter the neutrino spectra. Altered neutrino energy spectra, in turn, could change the resulting primordial element abundances from what one would expect given a particular lepton number. Neutrino energy spectrum-altering scenarios include, but are not limited to, active-active neutrino oscillations[12, 10, 7, 11], active-sterile neutrino oscillations[7, 8, 17, 18, 19, 20], particle decay into the neutrino sea[21], or CP-violation in neutrino oscillations[22]. Moreover, active-sterile neutrino flavor mixing and other mechanisms for creating sterile neutrino dark matter before neutrino decoupling are a focus of current research[23, 24, 25, 26, 27, 28, 29, 24, 30, 31, 32, 33, 34, 35, 36], as is the constraint of these scenarios via x-ray observations and large-scale structure considerations[37, 38, 39, 40, 41, 42, 43, 44, 45, 46, 47, 48, 49, 50, 51, 52]. Though these models may not directly affect BBN through the spectral distortion of ν_e and $\bar{\nu}_e$ energy distribution functions discussed here, they nevertheless may affect the overall values of lepton number, entropy, and energy density which are relevant to BBN. In the end, the existence of sterile neutrino states changes the meaning and utility of lepton number[53, 54]. To use BBN predictions to probe or constrain any such scenario requires an approach that self-consistently includes neutrino and antineutrino energy spectra of arbitrary shape.

We have performed detailed calculations of primordial nucleosynthesis in which we include neutrino and antineutrino spectral distortion. Our results are surprising. We find that even modest distortions of the neutrino and/or antineutrino spectral shapes from Fermi-Dirac black body forms can result in significant modification of the net neutron-proton interconversion rates and, hence, alteration of the light element abundances.

To study the effects of neutrino spectral distortion, we have modified the original Kawano/Wagoner BBN code described in Ref. [55] to calculate the primordial element abundances self-consistently with arbitrarily-specified non-thermal and/or time-dependent neutrino distribution functions. This paper is structured as follows: Section II describes the calculation of weak charge-changing reaction rates in the early universe and our prescription for employing non-thermal neutrino and antineutrino energy distribution functions; Section III discusses our new BBN code; Section IV will present example results for non-thermal neutrino distribution functions resulting from various physical scenarios; and Section V gives conclusions.

3.2 BBN and the Weak Reaction Rates

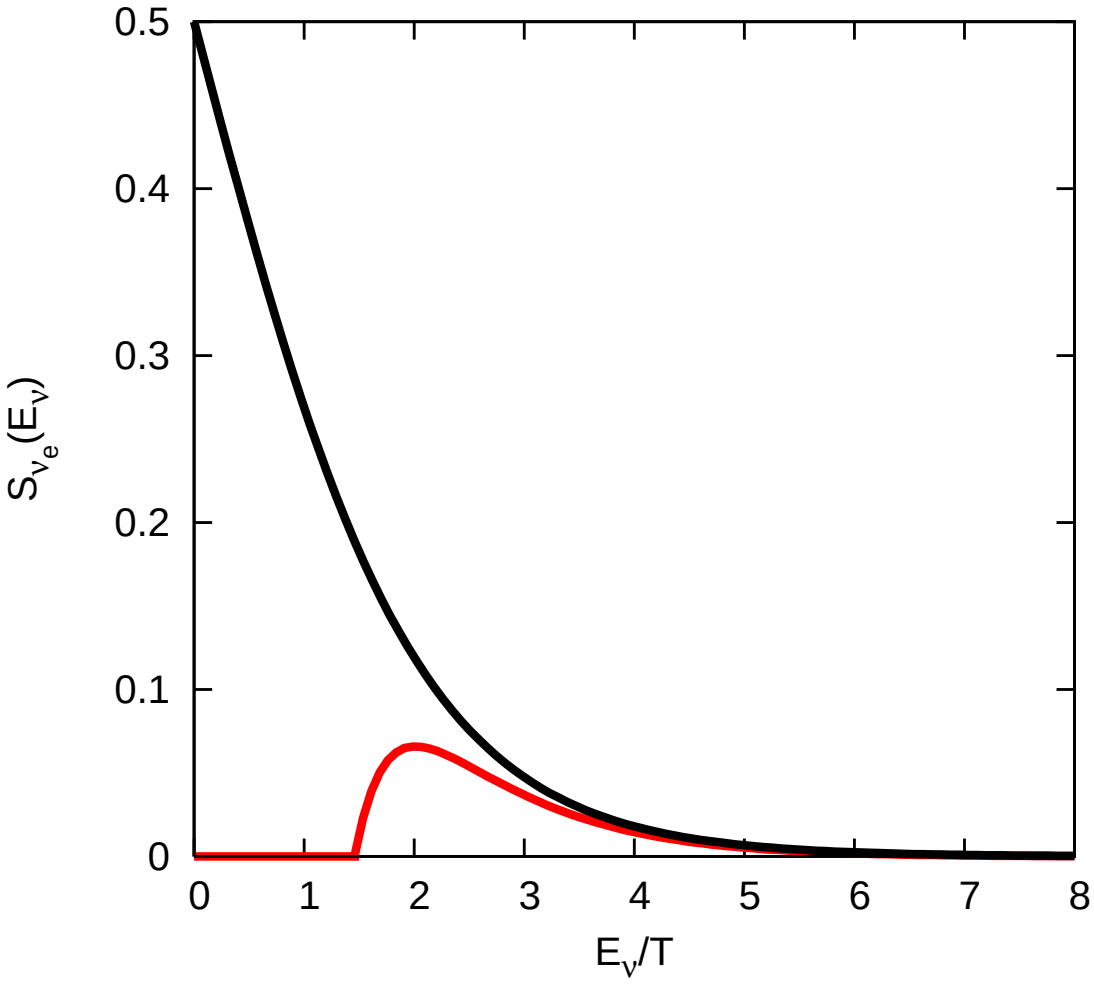

Figure 3.1: Example neutrino occupation probabilities. The upper dark (black) curve is the standard Fermi-Dirac thermally-distrubuted neutrino occupation probability and the lower light (red) curve is an example non-thermal neutrino occupation probability which can result from active-sterile neutrino transformation.

At early times and high temperatures, $t \sim 1$ sec and $T \gtrsim 1$ MeV, the primordial element abundances are given by nuclear statistical equilibrium (NSE). In NSE the rates for the processes that create a particular nucleus are equal to the rates that destroy it, so that the abundance for each element is given by the Saha equation.

As the universe expands and cools, reaction rates slow down to the point where they will not be fast enough to maintain NSE and the neutron and proton abundances, and subsequently the abundances of ^{4}He and the other light nuclei, "freeze-out". For example, the ^{4}He abundance falls below its equilibrium NSE track at $T \approx 0.6$ MeV, essentially as a consequence of the small NSE deuterium abundance. BBN can be looked at crudely as a series of freeze-outs from NSE, but with considerable post-equilibrium nuclear processing.

Because the entropy per baryon is high, alpha particles form copiously during BBN. Nearly all the neutrons in the universe at the epoch where α's form end up in alpha particles.

A key factor in the outcome of BBN is the value of the neutron-to-proton ratio. Like the nuclear abundances in NSE, at high enough temperatures ($T >$ 3 MeV) the *weak* neutron-proton interconversion rates are fast enough to maintain chemical equilibrium and the neutron-to-proton ratio can be determined from a Saha equation when the neutrinos have thermally-shaped distribution functions (as we will describe later).

For general conditions the neutron-to-proton ratio is determined by the weak reaction processes shown in Eqs. (3.2-3.4). The rates for these weak reactions are given in Eqs. (4.9-4.14) below. The forward rate for the reaction in Eq. (3.2) is given by $\lambda_{\nu_e n}$, Eq. (4.12), and the corresponding reverse rate is given by $\lambda_{e^- p}$, Eq. (4.9). Likewise, the forward and reverse rates for the process in Eq. (3.3) are $\lambda_{\bar{\nu}_e p}$ and $\lambda_{e^+ n}$ respectively. Eq. (4.13) gives the rate for free neutron decay denoted by $\lambda_{\mathrm{n-decay}}$, while the reverse three-body reaction rate is denoted by $\lambda_{pe^-\bar{\nu}_e}$ given in Eq. (4.14). These rates are detailed below[7, 56, 57, 58, 59, 60]:

$$\lambda_{e^-p} \approx \frac{\ln 2}{\langle ft\rangle (m_e c^2)^5} \int_0^\infty F\left[Z, E_\nu + Q_{np}\right] E_\nu^2 \left(E_\nu + Q_{np}\right) \times \left(\left(E_\nu + Q_{np}\right)^2 - m_e c^2\right)^{1/2} \left[S_{e^-}\right] \left[1 - S_{\nu_e}\right] dE_\nu, \tag{3.5}$$

$$\lambda_{\bar{\nu}_e p} \approx \frac{\ln 2}{\langle ft\rangle (m_e c^2)^5} \int_{Q_{np}+m_e c^2}^\infty E_\nu^2 \left(E_\nu - Q_{np}\right) \times \left(\left(E_\nu - Q_{np}\right)^2 - m_e c^2\right)^{1/2} \left[S_{\bar{\nu}_e}\right] \left[1 - S_{e^+}\right] dE_\nu, \tag{3.6}$$

$$\lambda_{e^+n} \approx \frac{\ln 2}{\langle ft\rangle (m_e c^2)^5} \int_{Q_{np}+m_e c^2}^\infty E_\nu^2 \left(E_\nu - Q_{np}\right) \times \left(\left(E_\nu - Q_{np}\right)^2 - m_e c^2\right)^{1/2} \left[S_{e^+}\right] \left[1 - S_{\bar{\nu}_e}\right] dE_\nu, \tag{3.7}$$

$$\lambda_{\nu_e n} \approx \frac{\ln 2}{\langle ft\rangle (m_e c^2)^5} \int_0^\infty F\left[Z, E_\nu + Q_{np}\right] E_\nu^2 \left(E_\nu + Q_{np}\right) \times \left(\left(E_\nu + Q_{np}\right)^2 - m_e c^2\right)^{1/2} \left[S_{\nu_e}\right] \left[1 - S_{e^-}\right] dE_\nu, \tag{3.8}$$

$$\lambda_{\mathrm{n-decay}} \approx \frac{\ln 2}{\langle ft\rangle (m_e c^2)^5} \int_0^{Q_{np}-m_e c^2} F\left[Z, Q_{np} - E_\nu\right] E_\nu^2 \left(Q_{np} - E_\nu\right) \times \left(\left(Q_{np} - E_\nu\right)^2 - m_e c^2\right)^{1/2} \left[1 - S_{\bar{\nu}_e}\right] \left[1 - S_{e^-}\right] dE_\nu, \tag{3.9}$$

$$\lambda_{pe^-\bar{\nu}_e} \approx \frac{\ln 2}{\langle ft\rangle (m_e c^2)^5} \int_0^{Q_{np}-m_e c^2} F\left[Z, Q_{np} - E_\nu\right] E_\nu^2 \left(Q_{np} - E_\nu\right) \times \left(\left(Q_{np} - E_\nu\right)^2 - m_e c^2\right)^{1/2} \left[S_{\bar{\nu}_e}\right] \left[S_{e^-}\right] dE_\nu, \tag{3.10}$$

where E_e and E_ν are the appropriate electron/positron and neutrino/antineutrino energies. In these expressions the neutron-proton mass difference is $Q_{np} \approx 1.293$

MeV. Here $\ln 2/\langle ft\rangle$ is proportional to the effective weak coupling applying to free nucleons with $\langle ft\rangle$ the effective ft-value defined in Ref.[57]. The weak matrix element is $\ln 2/\langle ft\rangle \propto G_F^2(1+3g_A^2)$, where G_F is the Fermi constant and g_A is the ratio of axial to vector coupling for the free nucleons. In the BBN calculation the value for $\ln 2/\langle ft\rangle$ is normalized by the free neutron decay lifetime at zero-temperature. Here $F\,[Z, E_e]$ is the relativistic coulomb correction factor (or Fermi factor)[57],

$$F(\pm Z, w) \approx 2(1+s)(2pR)^{2(s-1)} e^{\pi\eta} \left| \frac{\Gamma(s+i\eta)}{\Gamma(2s+1)} \right|. \tag{3.11}$$

In this expression the upper signs are for electron emission and capture, the lower signs are for positron emission and capture, $s = [1-(\alpha Z)^2]^{1/2}$, Z is the appropriate nuclear charge (which is $Z = 1$ for the proton), α is the fine structure constant, $\eta = \pm Zw/p$, and R is the nuclear radius in electron Compton wavelengths. $R \approx 2.908 \times 10^{-3} A^{1/3} - 2.437 A^{-1/3}$ where A is the nuclear mass number and $\omega \equiv (p^2 + m_e^2)^{1/2}$ with m_e the electron rest mass. This expression appears in the phase space integrand of the weak rates which require a Coulomb factor in either the initial or final state [61, 56, 62].

$S_{e^{-/+}}$ and $S_{\nu_e/\bar{\nu}_e}$ are the phase space occupation probabilities for electrons or positrons and neutrinos or antineutrinos, respectively. For example, the $[1 - S_{\nu_e}]$ factor in $\lambda_{e^- p}$ is the Pauli phase space blocking factor for processes which create a neutrino. In the limit that the neutrinos have *thermally-shaped* Fermi-Dirac distribution functions, these phase space occupation probabilities become two parameter functions:

$$S_{\nu_e} = \frac{1}{e^{E_\nu/T_\nu - \eta_{\nu_e}} + 1}, \tag{3.12}$$

$$S_{\bar{\nu}_e} = \frac{1}{e^{E_\nu/T_\nu - \eta_{\bar{\nu}_e}} + 1}. \tag{3.13}$$

The two parameters, T_ν and η_{ν_e}, correspond to neutrino temperature and degeneracy parameter (the ratio of chemical potential to temperature), respectively. For example, a thermally-shaped neutrino phase space occupation probability function is graphed in Fig. 3.1 as the upper black curve.

The total weak neutron destruction rate is $\lambda_n = \lambda_{\nu_e n} + \lambda_{e^+ n} + \lambda_{n-\text{decay}}$ and the corresponding total weak proton destruction rate is $\lambda_p = \lambda_{\bar{\nu}_e p} + \lambda_{e^- p} + \lambda_{\bar{\nu}_e e^- p}$. It is convenient to define

$$\Lambda_{\text{tot}} = \lambda_n + \lambda_p. \tag{3.14}$$

With this definition, the rate of change of the net electron number per baryon, Y_e, with Friedmann-Lemaître-Robertson-Walker (FLRW) time-like coordinate t in the early universe will be

$$\frac{dY_e}{dt} = \lambda_n - Y_e \, \Lambda_{\text{tot}}. \tag{3.15}$$

At early times where temperatures are high, the forward and reverse rates of these reactions are fast compared to the expansion rate of the universe. In this regime the neutron-to-proton ratio is just

$$\frac{n}{p} = \frac{\lambda_{\bar{\nu}_e p} + \lambda_{e^- p} + \lambda_{p e^- \bar{\nu}_e}}{\lambda_{\nu_e n} + \lambda_{e^+ n} + \lambda_{n \text{ decay}}}. \tag{3.16}$$

This can be approximated as

$$\frac{n}{p} \approx \frac{\lambda_{\bar{\nu}_e p} + \lambda_{e^- p}}{\lambda_{\nu_e n} + \lambda_{e^+ n}} \tag{3.17}$$

because neutron decay and the reverse three-body reaction are negligible by comparison at high temperatures. When the neutrino distribution functions have thermally-shaped Fermi-Dirac forms, the neutron-to-proton ratio is given by

$$\frac{n}{p} \approx \frac{(\lambda_{e^- p}/\lambda_{e^+ n}) + e^{-\eta_{\nu_e} + \eta_e - \xi}}{(\lambda_{e^- p}/\lambda_{e^+ n})\, e^{\eta_{\nu_e} - \eta_e + \xi} + 1}, \tag{3.18}$$

where $\eta_{\nu_e} = \mu_{\nu_e}/T$ is the electron neutrino degeneracy parameter, $\eta_e = \mu_e/T$ is the electron degeneracy parameter, and ξ is the neutron-proton mass difference divided by temperature, $\xi = (m_n - m_p)/T$[7]. This equation is generally true whenever the lepton distribution functions have Fermi-Dirac forms and identical temperature parameters T and whenever we can neglect neutron decay and its reverse process. Of course, at lower temperatures the neutrino and electron-photon plasma temperatures will differ and free neutron decay will be important.

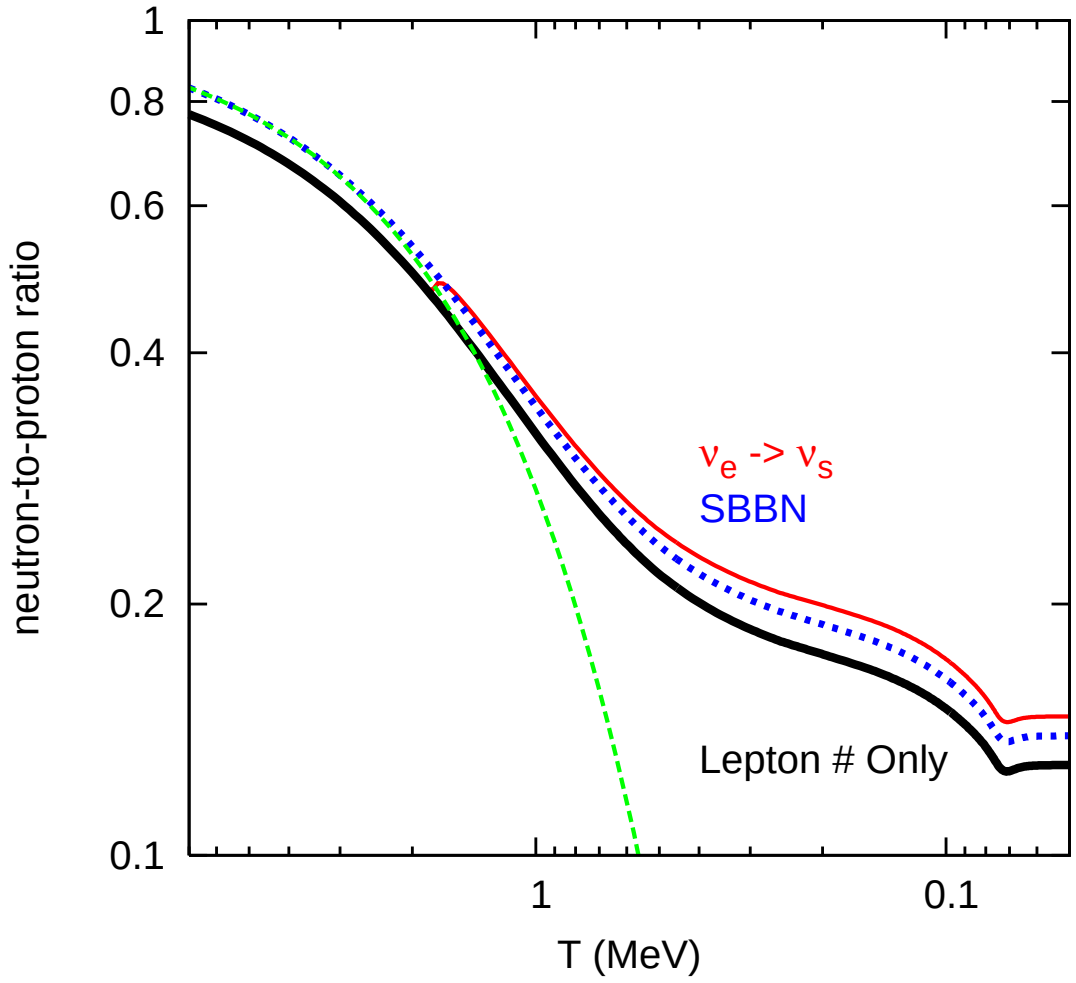

Figure 3.2: The neutron to proton ratio, n/p, as a function of temperature for three nucleosynthesis scenarios. The lower solid curve is for BBN with degenerate neutrinos and no neutrino transformation, where $L_{\nu_e} = L_{\nu_\tau} = L_{\nu_\mu} = 0.05$. The upper solid curve is the n/p ratio with the same lepton numbers as above but now including a particular active-sterile neutrino transformation scenario. The dotted cure is the n/p ratio for standard BBN (no lepton numbers or neutrino oscillation). The dashed line is the n/p equilibrium prediction for standard BBN (no lepton numbers or sterile neutrinos) with enforced weak chemical equilibrium.

If the weak reactions occur rapidly enough to maintain chemical equilibrium, then the Saha equation, $\mu_{\nu_e} + \mu_n = \mu_{e^-} + \mu_p$, can be used to predict the neutron-to-proton ratio. Interestingly, both the Saha equation and the steady state rate equilibrium condition in Eq. (4.7), with the full lepton capture rates of Eqs. (4.9-4.14), can be written as[7]

$$\frac{n}{p} \approx e^{(\mu_e - \mu_{\nu_e} - \delta m_{np})/T}. \tag{3.19}$$

This equilibrium neutron-to-proton ratio is shown in Fig. 3.2 as the dashed (green) line for zero electron and neutron chemical potentials, $\mu_e = \mu_{\nu_e} = 0$.

As the universe cools, the weak reaction rates become slow compared to the expansion rate of the universe and the neutron-to-proton ratio falls out of equilibrium. This is called “weak freeze-out" and occurs over a range of temperatures. Fig. 3.2 shows the actual neutron-to-proton ratio evolving as a function of temperature for the standard BBN scenario (thermal neutrino distribution functions and zero chemical potentials $\mu_e = \mu_{\nu_e} = 0$). At high temperatures, the actual neutron-to-proton ratio follows the equilibrium value and then around 1 MeV, the weak freeze-out commences. This happens because the weak rates have a stronger dependence on temperature than does the expansion rate of the universe. The lepton capture/decay rates given in Eqs. (4.9-4.14) scale very roughly as T^5 (see Ref.[60] for the detailed temperature dependence), while the expansion rate of the universe is $\propto T^2$. As a result, the neutron-proton weak interconversion rates eventually will fall below the expansion rate.

Although the weak rates become relatively slow, they still have a significant effect on the neutron-to-proton ratio, even for temperatures well below $T = 0.8$ MeV. In fact, free neutron decay continues to lower the n/p ratio until there are virtually no more free neutrons or until the neutrons are sequestered in alpha particles, where they are effectively shielded from the weak interaction. This is illustrated in Fig. 3.2 where the dotted (blue) line continues to decrease until $T \approx .08$ MeV (when the neutrons have been captured during rapid alpha particle formation). It is important to correctly calculate the weak reactions in order to

appropriately track the n/p ratio. This ratio sets the scale, in varying degrees, for all the primordial element abundances[55, 16].

3.3 New BBN Code

A nucleosynthesis code was written by Robert V. Wagoner in 1969[63, 64] to track and time evolve the nuclear abundances and the neutron-to-proton ratio in an expanding cooling universe. It was later updated and revised by Lawrence Kawano in 1988[65].

This code time-evolves three main quantities, the electron fraction, Y_e, the baryon-to-photon ratio, η, and the temperature, along with the primordial element abundances. It follows 48 nuclides using a reaction network composed of 168 nuclear reactions, whose rates have primarily been based on, and in some cases extrapolated from, laboratory cross sections. The main numerical technique is a 2nd order Runga-Kutta routine.

The code also tracks the neutron-to-proton ratio by calculating the weak reaction rates using the standard thermally-shaped Fermi-Dirac neutrino distribution functions, setting S_{ν_e} and $S_{\bar{\nu}_e}$ as given in Eq. (4.15) and Eq. (4.16).

In their approach, electron energy is used as the integration variable, instead of neutrino energy as given in Eqs. (4.9-4.14) above. To save computational time, they calculate only the sum of each of the forward $n \rightarrow p$ rates and the reverse $p \rightarrow n$ rates:

$$\lambda_n = \lambda_{\nu_e+n\rightarrow p+e^-} + \lambda_{n+e^+\rightarrow p+\bar{\nu}_e} + \lambda_{n\rightarrow p+e^-+\bar{\nu}_e} \tag{3.20}$$

$$\lambda_p = \lambda_{p+e^-\rightarrow \nu_e+n} + \lambda_{\bar{\nu}_e+p\rightarrow n+e^+} + \lambda_{p+e^-+\bar{\nu}_e\rightarrow n}. \tag{3.21}$$

With an algebraic trick, this simplifies the calculation by condensing the six phase space integrals (for each weak reaction rate) into two integrals:

$$\lambda_n \approx \frac{\ln 2}{\langle ft \rangle (m_e c^2)^5} \int_{m_e c^2}^{\infty} E_e \left(E_e^2 - \left(m_e c^2 \right)^2 \right)^{1/2} \tag{3.22}$$
$$\times \left[\frac{(E_e + Q_{np})^2}{(e^{E_e/T} + 1)\,(e^{-(E_e+Q_{np})/T_\nu - \eta_{\nu_e}} + 1)} + \frac{(E_e - Q_{np})^2}{(e^{-E_e/T} + 1)\,(e^{(E_e-Q_{np})/T_\nu - \eta_{\nu_e}} + 1)} \right] dE_e$$

$$\lambda_p \approx \frac{\ln 2}{\langle ft \rangle (m_e c^2)^5} \int_{m_e c^2}^{\infty} E_e \left(E_e^2 - \left(m_e c^2 \right)^2 \right)^{1/2} \tag{3.23}$$
$$\times \left[\frac{(E_e + Q_{np})^2}{(e^{E_e/T} + 1)\,(e^{(E_e+Q_{np})/T_\nu + \eta_{\nu_e}} + 1)} + \frac{(Q_{np} - E_e)^2}{(e^{E_e/T} + 1)\,(e^{(Q_{np}-E_e)/T_\nu + \eta_{\nu_e}} + 1)} \right] dE_e.$$

This algebraic trick requires the approximation of thermally-shaped Fermi-Dirac neutrino and antineutrino distribution functions. This summed rate cannot properly treat the Coulomb correction, $F[Z, E_e]$, which should be included in the phase space integral of reaction rates which have an electron and proton in either the final or initial state.

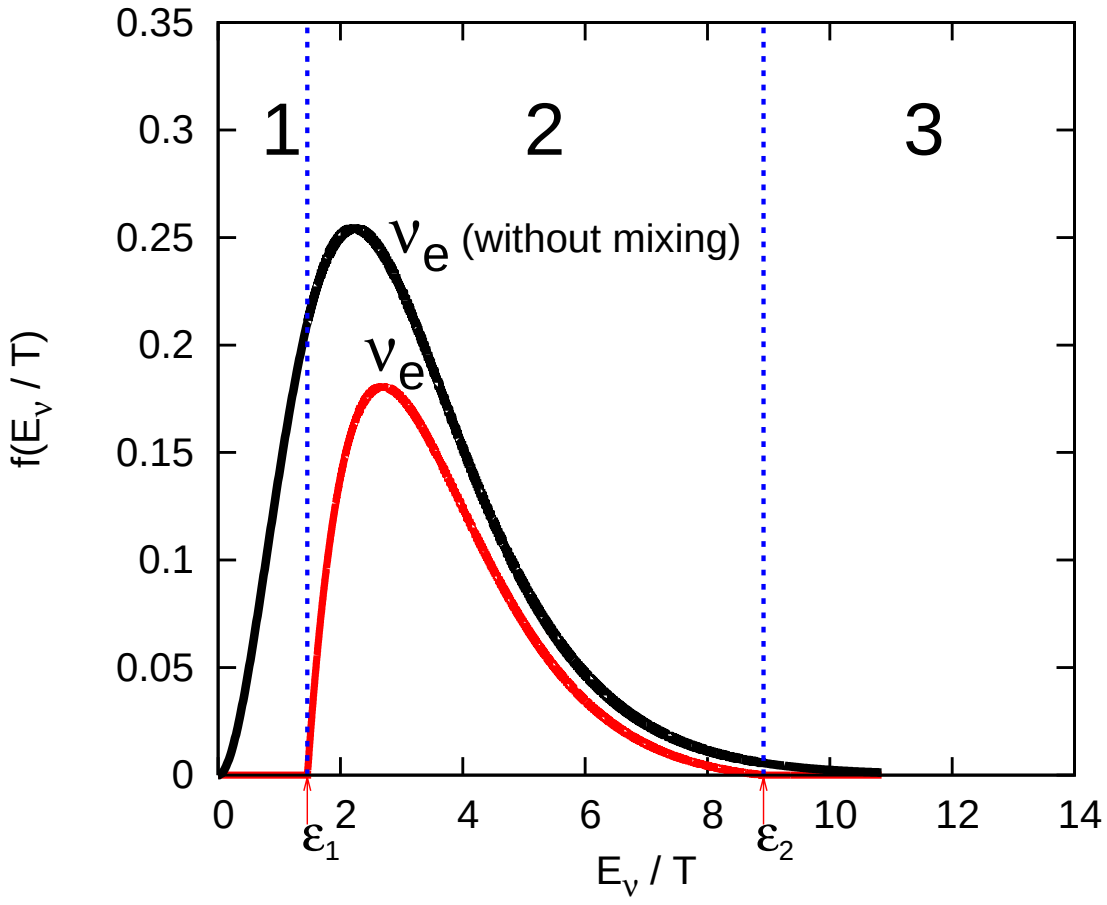

Figure 3.3: Two example electron neutrino distribution functions, where the upper black line is the standard thermal spectrum and the lower red line is a spectrum resulting from a particular scenario for active-sterile neutrino mixing. The vertical dashed lines show where a weak rate calculation employing the lower distribution function would be broken up to be integrated piecewise in our new version of the code.

We have modified the Kawano/Wagoner BBN code so that it can accommodate and integrate any arbitrary neutrino and/or antineutrino distribution function with any specified time dependence. The majority of our changes lie in the weak reaction rate calculation.

We first separated the summed neutron destruction and production rates, λ_n and λ_p. Individual calculation of the weak reaction rates has been implemented in the Kawano/Wagoner code by Refs. [66, 67, 68] to examine neutrino spectral distortion from massive neutrino decay and neutrino interaction with the hotter electrons and positrons in the plasma of the early universe. This has also been done in independent BBN codes by Refs[62, 69] to analyze corrections to the weak reaction rates such as the coulomb and radiative corrections.

Calculating each reaction rate individually enabled us to use non-thermal distribution functions and to change the neutrino and antineutrino distribution functions independently. Then, we removed a series approximation for λ_n and λ_p which is applied when the lepton numbers are zero. This approximation results in an erroneous $\approx 0.5\%$ increase in the neutron-to-proton ratio[70, 65]. Furthermore, we added the capability to separate a weak rate calculation into an arbitrary number of neutrino energy bins. This is useful for calculating a reaction rate where the neutrino energy spectrum is comprised of different functions over different energy ranges.

For example, in Fig. 3.3, we have shown two electron neutrino distribution functions. The upper curve is just the standard thermally-shaped Fermi-Dirac distribution function,

$$f_{\nu_\alpha}(E_\nu) = \frac{1}{T_{\nu_\alpha}^3 F_2\left(\eta_{\nu_\alpha}\right)} \frac{{E_\nu}^2}{e^{E_\nu/T_{\nu_\alpha} - \eta_{\nu_\alpha}} + 1}, \tag{3.24}$$

which is consistent with the occupation probability derived from Eq. (4.15). Here the relativistic Fermi integral of order two is $F_2\left(\eta\right) = \int_0^\infty \frac{x^2 dx}{e^{x-\eta}+1}$. The lower curve is a distribution function resulting from a particular active-sterile neutrino oscillation scheme described in Refs. [8, 17]. In this scheme, electron neutrinos have been completely converted into steriles at low and high energies (1 and 3), but some

active neutrinos remain in the center (2) energy band. To calculate a rate using this non-thermal distribution function, we break up the rate into three parts. The first part integrates from zero to ϵ_1 using the neutrino distribution function $f(E_\nu/T) = 0$. The second part integrates from ϵ_1 to ϵ_2 using the modified function shown in 2. The third part integrates from ϵ_2 to ∞ and again use $f(E_\nu/T) = 0$. Finally, the total rate is calculated by summing all three pieces.

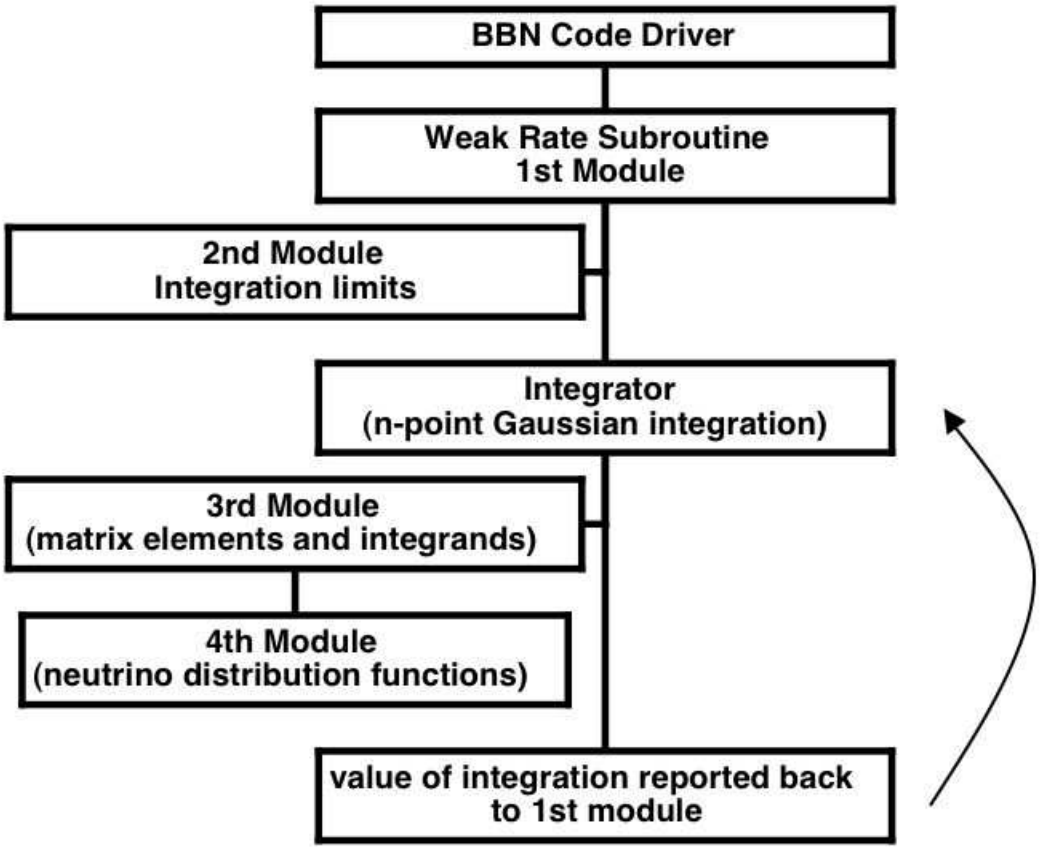

Figure 3.4: Flow chart for our modified BBN calculation.

To perform these non-thermal piece-wise calculations in the BBN code, we completely replaced the original weak rate calculation with a series of four modules. These modules allow the user to define the distribution functions, break up the integration into specifiable pieces and define the energy ranges for each piece, and set any desired time/temperature dependence of the distribution functions. A flow chart of the weak rate calculations is shown in Fig. 3.4. At each time step, the BBN code calls the weak rate calculation subroutine, Module 1 in Fig. 3.4, to time-evolve the neutron to proton ratio and, subsequently, all the nuclear abundances.

Module 1 acts as the central line of communication in that it calls the other modules and reports back the value of the weak rates at every time step in the BBN code. In this module, the user can first define how many pieces to split the rate integration into for reactions involving either neutrinos or antineutrinos or both. For example, if the user wanted to use the lower non-thermal neutrino distribution function in Fig. 3.3 and a thermal antineutrino distribution function, the user can specify that the rate integrations involving neutrinos should be integrated in three parts and that rates involving antineutrinos should be integrated with one energy bin.

Next, Module 1 calls Module 2 to retrieve the integration limits for each piece, *i.e.*, where the user wants each energy bin to begin and end. In Module 2, the user can define these integration limits and couple them to any time dependences desired. Module 1 makes an array with these limits so they can be accessed later in the integration. This procedure can be extended to an arbitrary number of energy bins for any neutrino type.

The first module calculates all six weak reaction rates by utilizing two main loops. These loop over the number of energy bins. One loop calculates the two reaction rates that include neutrinos and the other loop calculates the four remaining weak reaction rates that include antineutrinos. The number of iterations for each loop is determined by the number of energy bins. Each loop iteration integrates the weak reaction rates over the range of energy and neutrino distribution function specified for that energy bin. At the end of the iteration, each rate is summed.

For every loop cycle, the first module calls the integrator which inputs the function to be integrated and the limits of the energy bins (from Module 2). The matrix elements and integrands for the six weak reaction rates, as shown in Eqs. (4.9-4.14), are retrieved from Module 3. Here, the electron occupation probability is set as $S_e = 1/(e^{E_e/T} + 1)$ and the neutrino and antineutrino occupation probabilities are called from Module 4.

The sole purpose of Module 4 is to house the neutrino and antineutrino occupation probabilities. This makes it easy for a user to modify the neutrino distribution functions – by inputting analytic functions for S_{ν_e} and $S_{\bar{\nu}_e}$ – without having to modify any other portion of the weak rate calculation. The user can also define different functions or populations for each integration energy bin. After each energy bin is integrated, the total rate is summed and the values for the six weak reaction rates are returned to the main BBN code driver.

Our modified Kawano/Wagoner BBN code – which can now accommodate and integrate any arbitrary neutrino and/or antineutrino distribution function with any specified time dependence – will be available to the community at bigbangonline.org [71].

3.4 Example Code Results

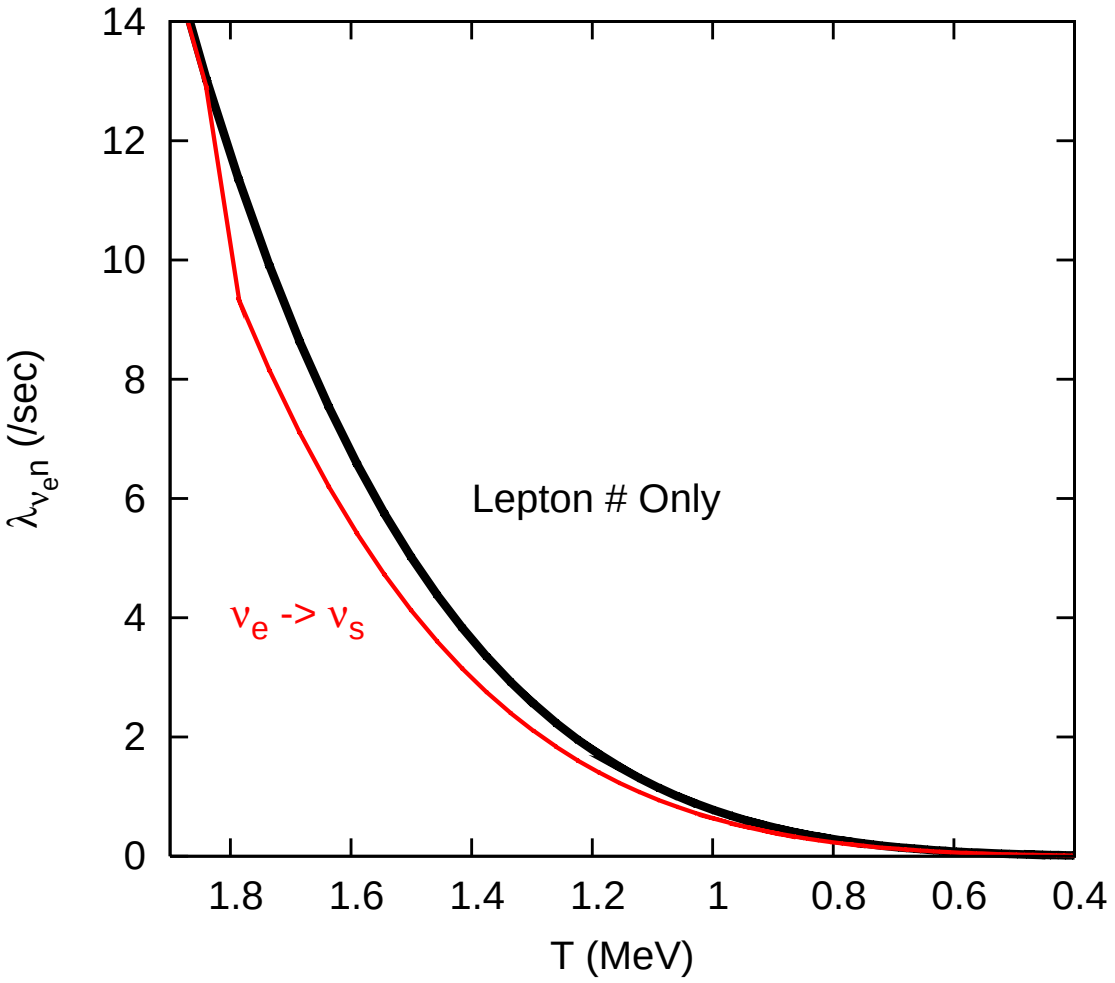

Figure 3.5: The rate of electron neutrino capture on a neutron as a function of temperature. The upper curve is $\lambda_{\nu_e \mathrm{n}}$ in the lepton number only case for lepton numbers of $L_{\nu_e} = L_{\nu_\tau} = L_{\nu_\mu} = 0.05$. The lower curve is the rate when there is active-sterile neutrino transformation along with the same lepton numbers as above.

We have utilized this code to study nucleosynthesis abundance yields in the presence of a light-mass sterile neutrino over a range of lepton numbers[8, 17]. The lower red line in Fig. 3.1 shows a final non-thermal neutrino occupation probability function that can result from active-sterile neutrino transformation. In this particular scenario, we started with normal thermal electron neutrino and antineutrino distribution functions and an assumed initial lepton number. The lepton numbers that we have taken are within the range which is allowed by conventional BBN (primordial ^{4}He) considerations. But, of course, the point is that a sterile neutrino that mixes with an active neutrino can result in non-thermal neutrino and/or antineutrino energy spectra which produce BBN abundance yields that can be quite different than in the standard scenario. This, in turn, could provide new, more appropriate constraints on lepton numbers or on active-sterile neutrino mass and mixing parameter space or on both.

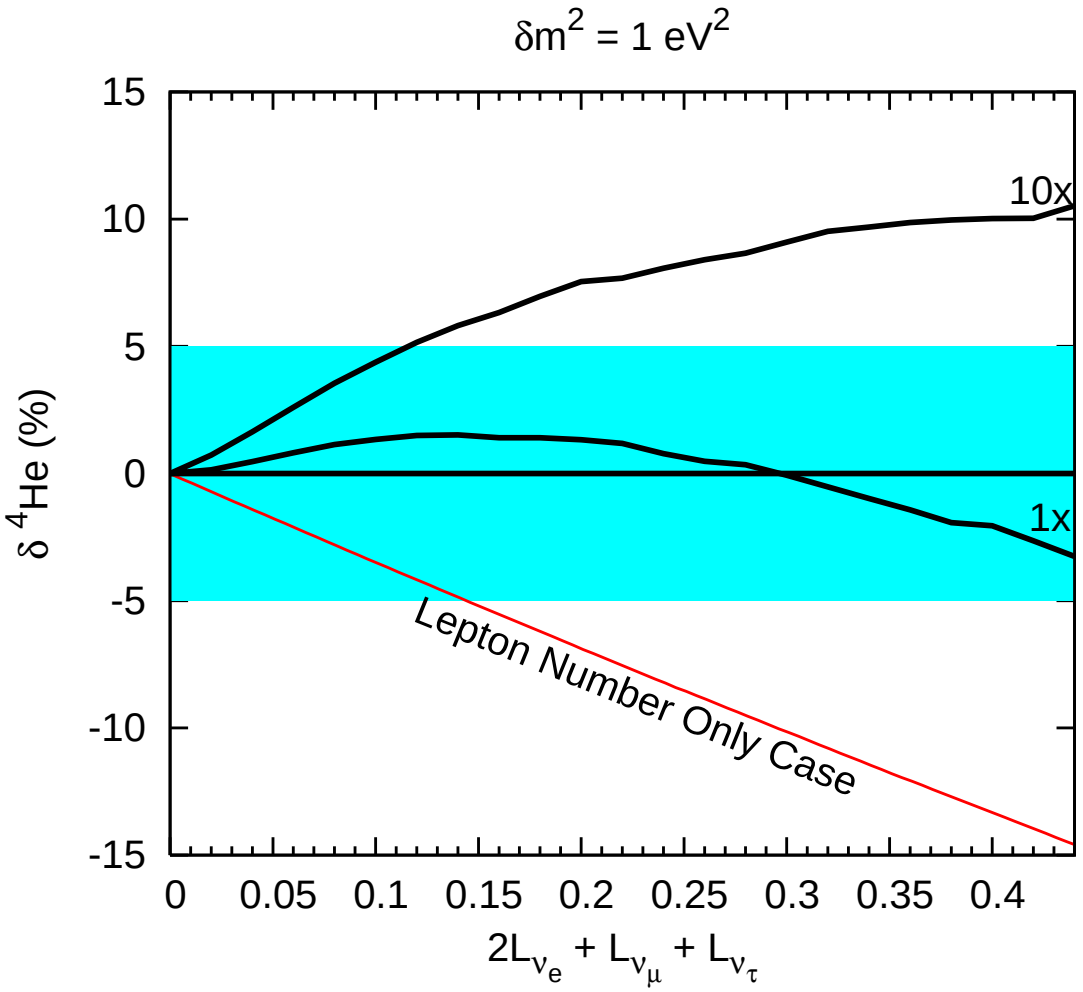

Figure 3.6: Percent change in ^{4}He from the standard BBN predicted value as a function of potential lepton number $\mathcal{L} = 2L_{\nu_e} + L_{\nu_\mu} + L_{\nu_\tau}$. The low light line is the case with lepton numbers only and standard thermally-shaped Fermi-Dirac neutrino distribution functions. The upper dark lines are for cases with non-thermal neutrino distrubution functions resulting from active-sterile neutrino transformation in addition to lepton numbers. The 1x factor corresponds to $L_{\nu_e} = L_{\nu_\mu} = L_{\nu_\tau}$ and the 10x factor is for $L_{\nu_\mu} = L_{\nu_\tau} = 10L_{\nu_e}$. The horizontal band corresponds to the allowed ^{4}He mass fraction from observational bounds. This is for active-sterile mass squared difference $\delta m^2 = m^2_{\nu_s} - m^2_{\nu_e}$ =1 eV^2.

The presence of a significant net lepton number can delay significant sterile neutrino production until after the weak decoupling temperature. With a positive net lepton number, a Mikheyev-Smirnov-Wolfenstein (MSW) resonance occurs first for low neutrino energies. This resonance subsequently sweeps to higher neutrino energies as the universe expands and cools. At first, this resonance sweep process occurs adiabatically, efficiently converting all active neutrinos into sterile neutrinos. This continues until the rate of active-sterile conversion becomes too fast to maintain adiabaticity. At this point, production becomes inefficient. However, at high enough resonance energies transformations can occur adiabatically again.

Accurately following such a scenario requires all the modifications in our new code. Without being able to include a dynamically changing neutrino distribution function, for example, we could not calculate correctly the neutron-to-proton interconversion rates. In fact, in the example scenario presented here, not only are there non-thermal neutrino distribution functions to handle, but these change on time scales which are important to BBN. In Fig. 3.5, we show the rate for electron neutrino capture on a neutron, the forward process in Eq. 3.2, as a function of temperature. The top curve is the rate when there is no active-sterile neutrino oscillation. The lower curve shows the decreased rate when there is active-sterile mixing and the final neutrino distribution function is that of Fig. 3.1. By reducing the number of electron neutrinos available for capture on neutrons, the capture rate is decreased. Additionally, the altered neutrino distribution function also results in a modestly increased reverse rate (electron capture on protons). The depleted electron neutrino distribution function in this scenario has the effect of increasing the electron capture rate because of the smaller neutrino phase space blocking factor.

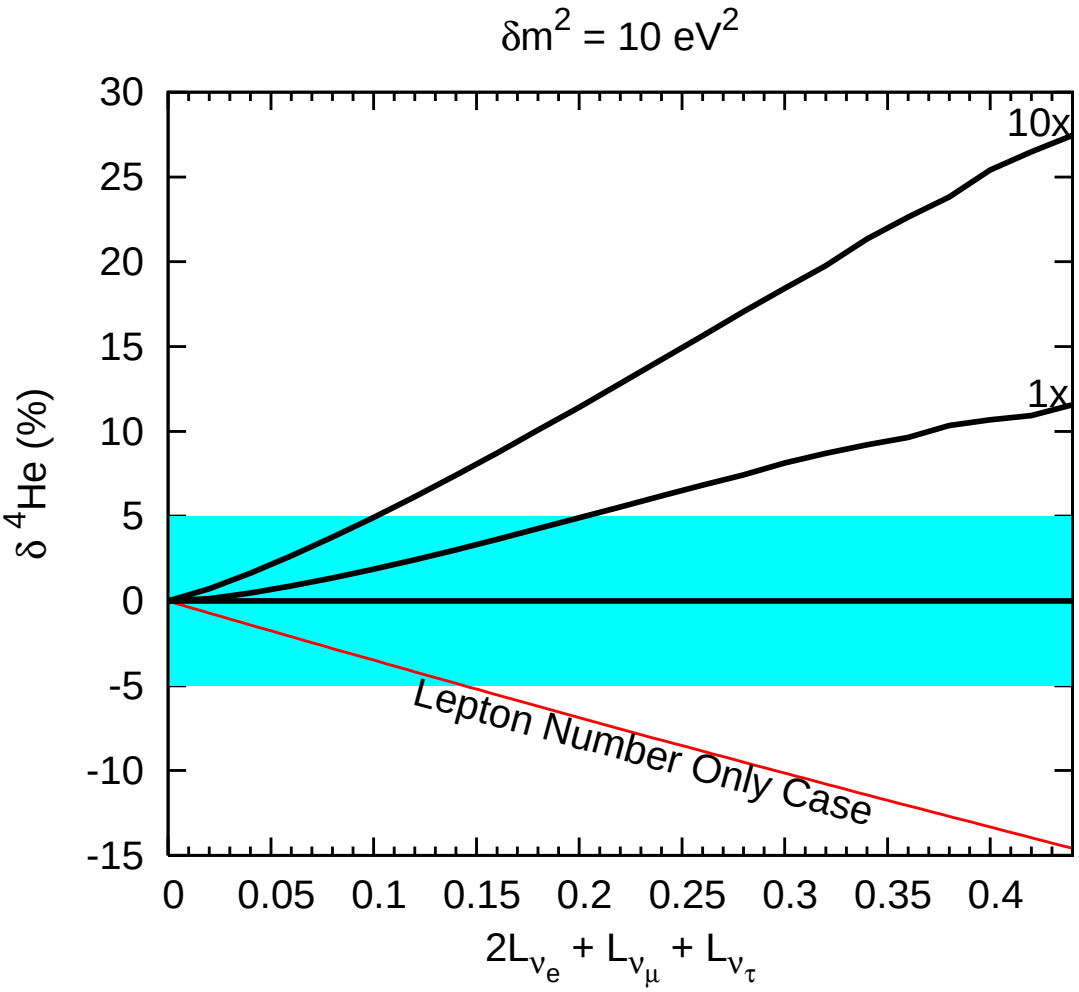

Figure 3.7: The same as Fig. 6 but now for $\delta m^2 = 10$ eV^2.

The final integrated effect in this scenario can be gauged by the changes in the light element abundances. This can be seen in Fig. 3.6 and Fig. 3.7 where we plot the percent change in the prediction of primordial ^{4}He from the standard BBN prediction (zero lepton numbers and thermally-shaped neutrino distribution functions) as a function of potential lepton number $\mathcal{L} = 2L_{\nu_e} + L_{\nu_\mu} + L_{\nu_\tau}$. In our calculation, for illustrative purposes, we adopt neutron lifetime $\tau_n = 887.8$ s and baryon-to-photon ratio $\eta = 6.11 \times 10^{-10}$. This yields a standard BBN prediction for the ^{4}He mass fraction $Y_p = 0.2429$. For the lepton number only case (neutrino chemical potentials with no spectral distortion), the positive electron neutrino chemical potential enhances neutron destruction and therefore less ^{4}He is produced. The upper black contours show the percent change in predicted ^{4}He, but now with lepton numbers and neutrino spectral distortion resulting from active-sterile transformation. This shows that the presence of neutrino spectral distortion can nullify and even reverse the effect of a lepton number. The 1x factor corresponds to equal lepton numbers ($L_{\nu_e} = L_{\nu_\mu} = L_{\nu_\tau}$) and the 10x factor corresponds to $10L_{\nu_e} = L_{\nu_\mu} = L_{\nu_\tau}$.

For example, with lepton numbers of $L_{\nu_e} = L_{\nu_\mu} = L_{\nu_\tau} = 0.05$, which corresponds to electron, mu, and tau neutrino degeneracy parameters of, $\eta_{\nu_e} = \eta_{\nu_\mu} = \eta_{\nu_\tau} \approx 0.073$ (*i.e.,* near the conventional BBN upper limits on these quantities), we see a 4.9% increase of ^{4}He over the standard (no neutrino mixing and no lepton numbers) BBN value and a 12.7% increase over the ^{4}He calculation with only lepton numbers included but no active-sterile neutrino oscillation effects. With this example scenario we find an increase in D/H (deuterium abundance relative to hydrogen) of 2.8% over the standard BBN calculation and an increase of 6.9% from the lepton number only calculation.

The increase in helium for these adopted parameters is likely unacceptable, exceeding observational bounds[72, 73, 74]. Likewise, if the observationally-determined value of D/H can be increased in precision sufficiently (to better than $\pm 5\%$ [17]), it may be possible that D/H could compete with helium as an avenue for constraint of new neutrino physics. Ultimately, allowing for dynamically-altered neutrino

and antineutrino distribution functions could add a new dimension to the way in which BBN and light element abundances might constrain new physics in the weak sector.

We have also used our new code to apply a relativistic version of the Coulomb correction into the appropriate weak rate integrands[61]. This has never been done before in the Wagoner/Kawano BBN code.

3.5 Conclusion

We have developed an approach to Big Bang Nucleosynthesis (BBN) calculations where we can treat arbitrarily-specified energy distributions for all neutrino types, including ν_e and $\bar{\nu}_e$. We can also allow these distribution functions to be altered dynamically and follow all nuclear and weak reactions self-consistently with these alterations. This new approach can extend the usefulness of BBN predictions for exploring and constraining new physics in the neutrino and weak interaction sectors.

Examples of such new physics include active-sterile neutrino mixing and particle decays that have neutrinos in the final state. We have given an explicit example of the former scenario. In this example we have demonstrated how active-sterile neutrino oscillation physics can alter neutrino or antineutrino distribution functions on short time scales, alter the neutron-proton interconversion rates, and so modify BBN abundance yields over those of the standard scenario.

Our calculations hold out the promise that light element abundances could place the best constraints on primordial lepton numbers and active-sterile neutrino mixing parameters when the sterile neutrino mass is in the $\sim 1\,\mathrm{eV}$ range. Present laboratory experiments, like mini-BooNE, are sensitive to neutrino flavor mixing in the active-sterile channel at the $\sim 1\,\mathrm{eV}$ mass scale only when the appropriate effective 2×2 vacuum mixing angle satisfies $\sin^2 2\theta \gg 10^{-4}$. By contrast, in the presence of a net lepton number, BBN abundance yields might be significantly altered for active-sterile neutrino mixing parameters for $\sin^2 2\theta > 10^{-8}$. The greater

reach in vacuum mixing angle afforded by BBN considerations stems from: (1) the long (gravitational) expansion time scale of the early universe which dictates the MSW resonance sweep rate and sets the minimum mixing angle required for adiabatic and efficient conversion of the active neutrinos into sterile species; and (2) the significant sensitivity of the neutron-proton weak interconversion rates to alterations of the neutrino or antineutrino energy distribution functions. Our new calculations allow us to follow simultaneously and self-consistently both of these effects along with all relevant weak, electromagnetic, and strong nuclear reaction rates.

This new approach is incorporated into an update of the Kawano/Wagoner BBN code – which can now accommodate and integrate any arbitrary neutrino and/or antineutrino distribution function with any specified time dependence. We will soon make this code available to the community at bigbangonline.org.

3.6 Acknowledgments

We would like to acknowledge discussions with Chad Kishimoto and Kevork Abazajian. ORNL is managed by UT-Battelle, LLC, for the U.S. DOE under Contract No. DE-AC05-00OR22725. The work of G.M.F and C.J.S. was supported in part by NSF Grant No. PHY-06-53626 and a UC/LANL CARE grant at UCSD.

Chapter 3, in full, is a reprint of the material as it appears in Physical Review D 2009. Smith, Christel J.; Fuller, George M.; Smith, Michael S., Phys. Rev. D, 2009. The dissertation author was the primary investigator and author of this paper.

Bibliography

[1] SDSS Collaboration, M. Tegmark *et al.*, Phys. Rev. D **69**, 103501 (2004).

[2] D. N. Spergel *et al.*, Astrophys. J. Suppl. **148**, 175 (2003).

[3] D. N. Spergel *et al.*, astro-ph/0603449.

[4] J. R. Bond, C. Contaldi, A. Lewis and D. Pogosyan, Int. J. Theor. Phys. **43**, 599 (2004).

[5] K. Ichikawa, T. Sekiguchi and T. Takahashi, Phys. Rev. **D78**, 043509 (2008), [0712.4327].

[6] R. Trotta and S. H. Hansen, Phys. Rev. **D69**, 023509 (2004), [astro-ph/0306588].

[7] K. Abazajian, N. F. Bell, G. M. Fuller and Y. Y. Y. Wong, Phys. Rev. D **72**, 063004 (2005).

[8] C. T. Kishimoto, G. M. Fuller and C. J. Smith, Phys. Rev. Lett. **97**, 141301 (2006), [astro-ph/0607403].

[9] J. P. Kneller, R. J. Scherrer, G. Steigman and T. P. Walker, Phys. Rev. D **64**, 123506 (2001).

[10] K. N. Abazajian, J. F. Beacom and N. F. Bell, Phys. Rev. D **66**, 013008 (2002).

[11] Y. Y. Y. Wong, Phys. Rev. D **66**, 025015 (2002).

[12] A. D. Dolgov, S. H. Hansen, S. Pastor, S. T. Petcov, G. G. Raffelt and D. V. Semikoz, Nucl. Phys. B **632**, 363 (2002).

[13] V. Simha and G. Steigman, JCAP **0808**, 011 (2008), [hep-ph/0806.0179].

[14] A. Cuoco *et al.*, Int. J. Mod. Phys. **A19**, 4431 (2004), [astro-ph/0307213].

[15] P. D. Serpico and G. G. Raffelt, Phys. Rev. **D71**, 127301 (2005), [astro-ph/0506162].

[16] R. V. Wagoner, W. A. Fowler and F. Hoyle, Astrophys. J. **148**, 3 (1967).

[17] C. J. Smith, G. M. Fuller, C. T. Kishimoto and K. N. Abazajian, Phys. Rev. **D74**, 085008 (2006), [astro-ph/0608377].

[18] Y.-Z. Chu and M. Cirelli, Phys. Rev. **D74**, 085015 (2006), [astro-ph/0608206].

[19] R. Foot and R. R. Volkas, Phys. Rev. Lett. **75**, 4350 (1995).

[20] R. Foot and R. R. Volkas, Phys. Rev. D **55**, 5147 (1997).

[21] A. Cuoco, J. Lesgourgues, G. Mangano and S. Pastor, Phys. Rev. **D71**, 123501 (2005), [astro-ph/0502465].

[22] M. Y. Khlopov and S. T. Petcov, Phys. Lett. **B99**, 117 (1981).

[23] A. Kusenko, S. Pascoli and D. Semikoz, JHEP **11**, 028 (2005), [hep-ph/0405198].

[24] K. Petraki and A. Kusenko, Phys. Rev. **D77**, 065014 (2008), [0711.4646].

[25] S. Dodelson and L. M. Widrow, Phys. Rev. Lett. **72**, 17 (1994), [hep-ph/9303287].

[26] K. Abazajian, G. M. Fuller and M. Patel, Phys. Rev. **D64**, 023501 (2001), [astro-ph/0101524].

[27] A. D. Dolgov and S. H. Hansen, Astropart. Phys. **16**, 339 (2002), [hep-ph/0009083].

[28] M. Shaposhnikov and I. Tkachev, Phys. Lett. **B639**, 414 (2006), [hep-ph/0604236].

[29] A. Kusenko, Phys. Rev. Lett. **97**, 241301 (2006), [hep-ph/0609081].

[30] K. Petraki, Phys. Rev. **D77**, 105004 (2008), [hep-ph/0801.3470].

[31] X.-D. Shi and G. M. Fuller, Phys. Rev. Lett. **83**, 3120 (1999), [astro-ph/9904041].

[32] C. B. Chiu, E. C. G. Sudarshan and B. Misra, Phys. Rev. **D16**, 520 (1977).

[33] D. Boyanovsky and C. M. Ho, Phys. Rev. **D76**, 085011 (2007), [hep-ph/0705.0703].

[34] D. Boyanovsky and C. M. Ho, JHEP **07**, 030 (2007), [hep-ph/0612092].

[35] D. Boyanovsky, Phys. Rev. **D77**, 023528 (2008), [astro-ph/0711.0470].

[36] K. N. Abazajian and G. M. Fuller, Phys. Rev. **D66**, 023526 (2002), [astro-ph/0204293].

[37] K. Abazajian, G. M. Fuller and W. H. Tucker, Astrophys. J. **562**, 593 (2001), [astro-ph/0106002].

[38] K. Abazajian and S. M. Koushiappas, Phys. Rev. **D74**, 023527 (2006), [astro-ph/0605271].

[39] A. Boyarsky, A. Neronov, O. Ruchayskiy, M. Shaposhnikov and I. Tkachev, Phys. Rev. Lett. **97**, 261302 (2006), [astro-ph/0603660].

[40] A. Boyarsky, A. Neronov, O. Ruchayskiy and M. Shaposhnikov, Mon. Not. Roy. Astron. Soc. **370**, 213 (2006), [astro-ph/0512509].

[41] H. Yuksel, J. F. Beacom and C. R. Watson, Phys. Rev. Lett. **101**, 121301 (2008), [astro-ph/0706.4084].

[42] C. R. Watson, J. F. Beacom, H. Yuksel and T. P. Walker, Phys. Rev. **D74**, 033009 (2006), [astro-ph/0605424].

[43] M. Viel, J. Lesgourgues, M. G. Haehnelt, S. Matarrese and A. Riotto, Phys. Rev. **D71**, 063534 (2005), [astro-ph/0501562].

[44] K. Abazajian, Phys. Rev. **D73**, 063513 (2006), [astro-ph/0512631].

[45] U. Seljak, A. Makarov, P. McDonald and H. Trac, Phys. Rev. Lett. **97**, 191303 (2006), [astro-ph/0602430].

[46] A. Boyarsky, J. Nevalainen and O. Ruchayskiy, Astron. Astrophys. **471**, 51 (2007), [astro-ph/0610961].

[47] A. Boyarsky, J. W. den Herder, A. Neronov and O. Ruchayskiy, Astropart. Phys. **28**, 303 (2007), [astro-ph/0612219].

[48] A. Boyarsky, D. Malyshev, A. Neronov and O. Ruchayskiy, 0710.4922.

[49] A. Boyarsky, D. Iakubovskyi, O. Ruchayskiy and V. Savchenko, Mon. Not. Roy. Astron. Soc. **387**, 1361 (2008), [0709.2301].

[50] A. Boyarsky, O. Ruchayskiy and D. Iakubovskyi, 0808.3902.

[51] M. Viel, J. Lesgourgues, M. G. Haehnelt, S. Matarrese and A. Riotto, Phys. Rev. Lett. **97**, 071301 (2006), [astro-ph/0605706].

[52] A. Boyarsky, J. Lesgourgues, O. Ruchayskiy and M. Viel, 0812.0010.

[53] R. Foot, M. J. Thomson and R. R. Volkas, Phys. Rev. **D53**, R5349 (1996), [hep-ph/9509327].

[54] X.-D. Shi, Phys. Rev. **D54**, 2753 (1996), [astro-ph/9602135].

[55] M. S. Smith, L. H. Kawano and R. A. Malaney, Astrophys. J. Suppl. **85**, 219 (1993).

[56] D. A. Dicus *et al.*, Phys. Rev. **D26**, 2694 (1982).

[57] G. M. Fuller, W. A. Fowler and M. J. Newman, Astrophys. J. Suppl. **42**, 447 (1980).

[58] G. M. Fuller, W. A. Fowler and M. J. Newman, Astrophys. J. **252**, 715 (1982).

[59] G. M. Fuller, W. A. Fowler and M. J. Newman, Astrophys. J. Suppl. **48**, 279 (1982).

[60] G. M. Fuller, W. A. Fowler and M. J. Newman, **293**, 1 (1985).

[61] C. J. Smith and G. M. Fuller, In preparation (2008).

[62] R. E. Lopez and M. S. Turner, Phys. Rev. **D59**, 103502 (1999), [astro-ph/9807279].

[63] R. V. Wagoner, Astrophys. J. **179**, 343 (1973).

[64] R. V. Wagoner, Ann. Rev. Astron. Astrophys. **7**, 553 (1969).

[65] L. Kawano, FERMILAB-PUB-88/34-A.

[66] A. D. Dolgov, S. H. Hansen and D. V. Semikoz, Nucl. Phys. **B503**, 426 (1997), [hep-ph/9703315].

[67] A. D. Dolgov, S. H. Hansen and D. V. Semikoz, Nucl. Phys. **B524**, 621 (1998), [hep-ph/9712284].

[68] A. D. Dolgov, S. H. Hansen, S. Pastor and D. V. Semikoz, Nucl. Phys. **B548**, 385 (1999), [hep-ph/9809598].

[69] S. Esposito, G. Mangano, G. Miele and O. Pisanti, Nucl. Phys. **B540**, 3 (1999), [astro-ph/9808196].

[70] L. Kawano, NASA STI/Recon Technical Report N **92**, 25163 (1992).

[71] M. S. Smith, Big bang online, http://bigbangonline.org.

[72] K. A. Olive and E. D. Skillman, Astrophys. J. **617**, 29 (2004).

[73] K. A. Olive, G. Steigman and E. D. Skillman, Astrophys. J. **483**, 788 (1997).

[74] Y. I. Izotov and T. X. Thuan, Astrophys. J. **602**, 200 (2004).

Chapter 4

Big Bang Nucleosynthesis Weak Rate Corrections

4.1 Introduction

The study of Big Bang Nucleosynthesis (BBN) has been and is a powerful tool for testing cosmological models and constraining the fundamental parameters of the universe. Since primordial nucleosynthesis occurs relatively soon after the Big Bang ($\sim 1\,\mathrm{s}$), BBN provides one of the best windows into the physics of the early universe.

Before the launch of the Wilkinson Microwave Anisotropy Probe (WMAP), BBN predictions along with direct observation of the primordial element abundances were used to constrain the baryon-to-photon ratio, η. The independent high precision determination of η from the ratio of the acoustic peak amplitudes in the cosmic microwave background (CMB) from WMAP [1, 2, 3] allows us now to use BBN to constrain other unknowns in the early universe and physics beyond the Standard Model.

The CMB measurement of η increases in precision with accumulating WMAP data and the future Planck mission promises even higher precision, with a projected $\sim 1\%$ accuracy in η [3, 4]. The measurement of primordial deuterium also shows

promise for higher accuracy determination as more QSO lines of sight become available [5, 6] . This fuels the motivation to further refine the calculation of predicted primordial element abundances. For this reason we have analyzed the effect of adding the full relativistic Coulomb wave correction factor (relativistic Coulomb barrier factor) to the weak reaction rates in the BBN calculation.

Among many issues, a key piece of physics that sets the stage for primordial element nucleosynthesis is the evolution of the neutron-to-proton ratio, n/p. The n/p ratio is critical in determining the synthesis of the primordial elements because it sets the number of neutrons available to build nuclei.

The neutron-to-proton ratio is effectively determined by the competition between the charge-changing weak interaction rates and the expansion rate of the universe. Listed below are the weak reactions which interconvert neutrons and protons:

$$\nu_e + n \rightleftharpoons p + e^-, \tag{4.1}$$

$$\bar{\nu}_e + p \rightleftharpoons n + e^+, \tag{4.2}$$

$$n \rightleftharpoons p + e^- + \bar{\nu}_e. \tag{4.3}$$

The corresponding rates for these weak reactions are denoted by $\lambda_{\nu_e n}$ and $\lambda_{e^- p}$, $\lambda_{\bar{\nu}_e p}$ and $\lambda_{e^+ n}$, $\lambda_{n_{\rm decay}}$ and $\lambda_{p e^- \bar{\nu}_e}$ for the forward and reverse reactions in Eq. (4.1), Eq. (4.2), and Eq. (4.3), respectively. Defining $\Lambda_n = \lambda_{\nu_e n} + \lambda_{e^+ n} + \lambda_{n_{\rm decay}}$ and $\Lambda_{\rm tot} = \Lambda_n + \lambda_{\bar{\nu}_e} + \lambda_{e^- p} + \lambda_{p e^- \bar{\nu}_e}$, and defining the neutron-to-proton ratio to be n/p, we can show that in the early universe

$$\frac{d}{dt}\left(\frac{n}{p}\right) = (1 + n/p)^2 \left(\frac{\Lambda_{\rm tot}}{1 + n/p} - \Lambda_n\right), \tag{4.4}$$

where t is the Freidmann-Lemaitre-Robertson-Walker timelike coordinate [7]. Note that the net number of electrons minus positrons per baryon is $Y_e \equiv (n_{e^-} - n_{e^+})/n_b = (1 + n/p)^{-1}$. At high temperatures, $T \gg 1$ MeV, the weak reaction rates are fast compared to the expansion rate of the universe, steady state equilibrium ($\frac{d}{dt}(n/p) = 0$) is a good approximation, and the neutron-to-proton ratio is

given by [7, 8]

$$\frac{n}{p} = \frac{\lambda_{\bar{\nu}_e p} + \lambda_{e^- p} + \lambda_{p e^- \bar{\nu}_e}}{\lambda_{\nu_e n} + \lambda_{e^+ n} + \lambda_{n \text{ decay}}}. \tag{4.5}$$

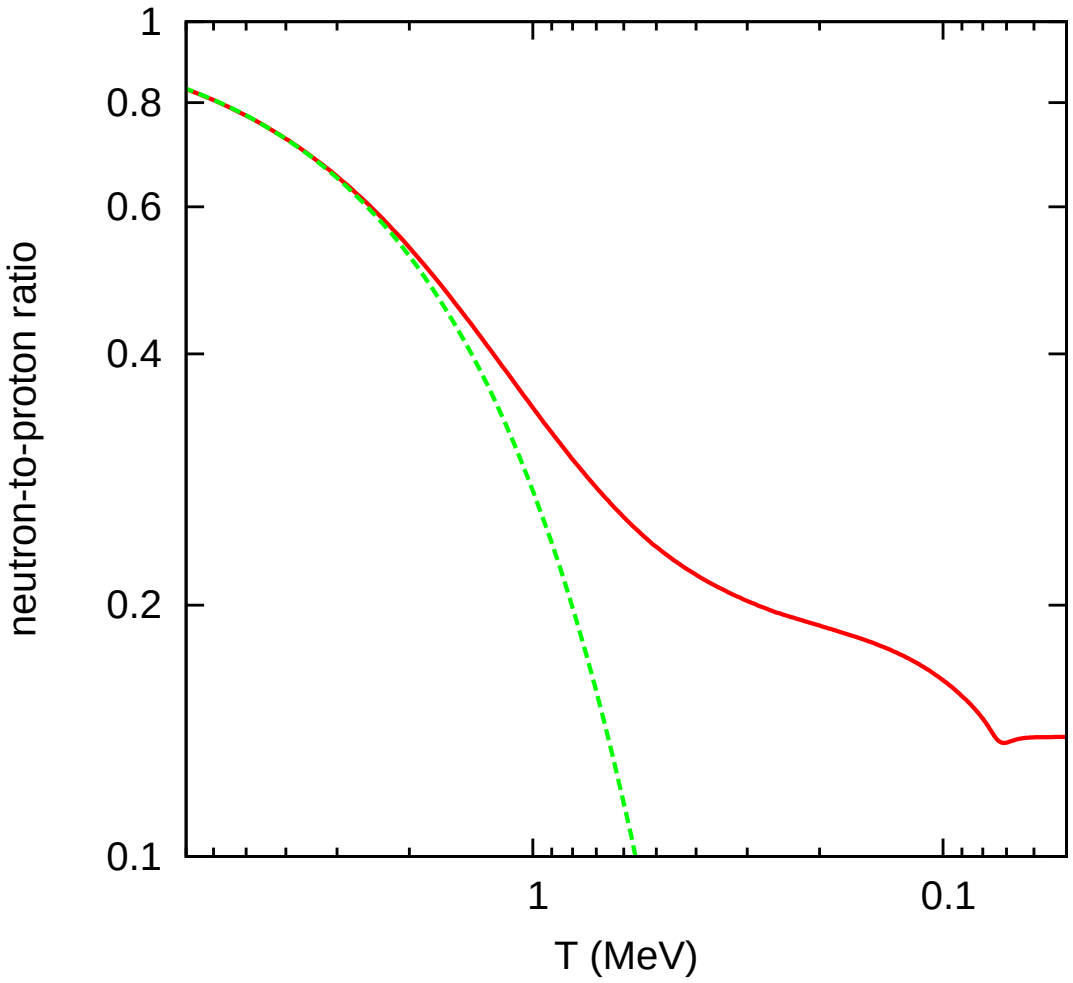

Figure 4.1: Neutron-to-proton ratio as a function of temperature. The full standard BBN zero lepton number case is given by the solid line. The dashed line is the neutron-to-proton ratio as calculated with an enforced assumption of steady state equilibrium, *i.e.*, Eq. (4.8).

The relatively slow rates at high temperatures for both free neutron decay and the corresponding reverse three body reaction allow the steady state equilibrium neutron-to-proton ratio to be approximated as

$$\frac{n}{p} \approx \frac{\lambda_{\bar{\nu}_e p} + \lambda_{e^- p}}{\lambda_{\nu_e n} + \lambda_{e^+ n}}. \tag{4.6}$$

If the neutrinos have thermal, Fermi-Dirac energy distribution functions, this can be written by

$$\frac{n}{p} \approx \frac{(\lambda_{e^- p}/\lambda_{e^+ n}) + e^{-\eta_{\nu_e} + \eta_e - \xi}}{(\lambda_{e^- p}/\lambda_{e^+ n})\, e^{\eta_{\nu_e} - \eta_e + \xi} + 1}, \tag{4.7}$$

where $\eta_{\nu_e} = \mu_{\nu_e}/T$ is the electron neutrino degeneracy parameter, $\eta_e = \mu_e/T$ is the electron degeneracy parameter, with μ_{ν_e} and μ_e the electron neutrino and electron chemical potentials, respectively, and ξ is the neutron-proton mass difference divided by temperature, $\xi = \delta m_{np}/T$ with $\delta m_{np} = m_n c^2 - m_p c^2 \approx 1.293\,\mathrm{MeV}$, where we take the Boltzmann constant to be $k_\mathrm{B} = 1$ [7].

At high temperatures the weak reactions can be fast enough to maintain chemical equilibrium. In chemical equilibrium, the chemical potentials satisfy the Saha equation, $\mu_{\nu_e} + \mu_n = \mu_{e^-} + \mu_p$. When chemical equilibrium is maintained the neutron-to-proton ratio will be

$$\frac{n}{p} \approx e^{(\mu_e - \mu_{\nu_e} - \delta m_{np})/T}. \tag{4.8}$$

This result can be obtained directly from the ratio of the appropriate Fermi-Dirac distribution functions or, alternatively and equivalently so long as all reactants have a Fermi-Dirac form for their energy spectra, from evaluation of the rates in Eq. (4.7) [7].

As the universe cools and expands, the rates of the weak reactions become slow compared to the expansion rate of the universe. At this point chemical equilibrium can no longer be maintained and a period known as the "weak freeze out" occurs as the neutron-to-proton ratio pulls away from its equilibrium value. For a faster expansion rate of the universe the weak reaction rates become comparatively slow earlier and the neutron-to-proton ratio falls out of equilibrium at higher temperatures, yielding a relatively larger n/p value. Likewise, for a slower expansion rate,

the weak reactions can maintain chemical equilibrium longer and the neutron-to-proton ratio consequently would be lower. The expansion rate of the universe is set by the local total energy density through the Freidman equation.

Figure 4.1 shows the neutron-to-proton ratio as a function of temperature for a standard Big Bang scenario with zero lepton numbers, *i.e.*, $\mu_{\nu_e} = \mu_{\bar{\nu}_e} = \mu_e = 0$. This figure shows both the actual n/p ratio and the approximation to this with an enforced chemical equilibrium condition. Obviously, these agree for high temperature but diverge once the weak reaction rates become slow compared to the expansion rate of the universe. Note that the actual n/p ratio becomes constant once nearly all free neutrons are incorporated into alpha particles at $T < 100$ keV. This figure shows the n/p ratio only for free neutrons and neutrons bound within alpha particles, and neglects the neutrons bound in ^{2}H, ^{3}H, ^{3}He, and nuclei heavier than ^{4}He, accounting for the small divit in the upper curve near T =80 keV.

Primordial element abundance yields are calculated by a BBN code that time evolves the temperature and expansion rate of the universe along with the nuclear and weak reactions rates. We have used a modified version of the Kawano/Wagoner BBN code [9, 10, 11, 12] in order investigate the effect of integrating the relativistic Coulomb barrier factor in the appropriate weak reaction rates. In section II we discuss the calculation of the weak reaction rates. In section III we discuss the relativistic Coulomb correction employed here and Coulomb correction prescriptions studied previously. In section IV we present results and give a discussion and in section V we give conclusions.

4.2 The Weak Reaction Rates

We calculate the individual weak interaction rates with the following phase space factor forms and with a common matrix element which is proportional to the inverse of an effective ft-value $\langle ft \rangle$ [7, 13, 14, 15, 16, 17, 8]:

$$\lambda_{e^-p} \approx \frac{\ln 2}{\langle ft \rangle (m_e c^2)^5} \int_{\delta m_{np}}^{\infty} F\left[Z, E_e\right] (E_e - \delta m_{np})^2 E_e \left(E_e^2 - m_e c^2\right)^{1/2} \left[S_{e^-}\right] \left[1 - S_{\nu_e}\right] dE_e, \tag{4.9}$$

$$\lambda_{\bar{\nu}_e p} \approx \frac{\ln 2}{\langle ft \rangle (m_e c^2)^5} \int_{m_e c^2}^{\infty} (E_e + \delta m_{np})^2 E_e (E_e^2 - m_e c^2)^{1/2} \left[S_{\bar{\nu}_e}\right] \left[1 - S_{e^+}\right] dE_e, \tag{4.10}$$

$$\lambda_{e^+ n} \approx \frac{\ln 2}{\langle ft \rangle (m_e c^2)^5} \int_{m_e c^2}^{\infty} (E_e + \delta m_{np})^2 E_e (E_e^2 - m_e c^2)^{1/2} \left[S_{e^+}\right] \left[1 - S_{\bar{\nu}_e}\right] dE_e, \tag{4.11}$$

$$\lambda_{\nu_e n} \approx \frac{\ln 2}{\langle ft \rangle (m_e c^2)^5} \int_{\delta m_{np}}^{\infty} F\left[Z, E_e\right] (E_e - \delta m_{np})^2 E_e (E_e^2 - m_e c^2)^{1/2} \left[S_{\nu_e}\right] \left[1 - S_{e^-}\right] dE_e, \tag{4.12}$$

$$\begin{aligned} \lambda_{n_{\text{decay}}} \quad \approx \quad & \frac{\ln 2}{\langle ft \rangle (m_e c^2)^5} \int_{m_e c^2}^{\delta m_{np}} F\left[Z, E_e\right] (\delta m_{np} - E_e)^2 E_e \left(E_e^2 - m_e c^2\right)^{1/2} \\ & \left[1 - S_{\bar{\nu}_e}\right] \left[1 - S_{e^-}\right] dE_e, \end{aligned} \tag{4.13}$$

$$\lambda_{p e^- \bar{\nu}_e} \approx \frac{\ln 2}{\langle ft \rangle (m_e c^2)^5} \int_{m_e c^2}^{\delta m_{np}} F\left[Z, E_e\right] (\delta m_{np} - E_e)^2 E_e \left(E_e^2 - m_e c^2\right)^{1/2} \left[S_{\bar{\nu}_e}\right] \left[S_{e^-}\right] dE_e, \tag{4.14}$$

where E_e is the total electron or positron energy as appropriate, $m_e c^2$ is the electron rest mass, and $F\left[Z, E_e\right]$ is the Coulomb correction Fermi factor which will be discussed in detail below. Note that the nuclear charge relevant here is $Z = 1$. $S_{e^{-/+}}$ and $S_{\nu_e/\bar{\nu}_e}$ are the phase space occupation probabilities for electrons/positrons and neutrinos/antineutrinos, respectively. For neutrinos and electrons with energy distributions with the expected thermal form, the occupation probabilities are

$$S_{\nu_e} = \frac{1}{e^{E_\nu / T_\nu - \eta_{\nu_e}} + 1}, \tag{4.15}$$

$$S_{\bar{\nu}_e} = \frac{1}{e^{E_\nu/T_\nu - \eta_{\bar{\nu}_e}} + 1}, \tag{4.16}$$

$$S_e = \frac{1}{e^{E_e/T} + 1}, \tag{4.17}$$

where T_ν is the neutrino temperature parameter, η_ν is the neutrino degeneracy parameter (the ratio of chemical potential to temperature), and E_ν is the appropriate neutrino or antineutrino energy.

We take

$$\frac{\ln 2}{\langle ft \rangle} = \frac{c\,(m_e c^2)^5}{\hbar c} \cdot \delta \cdot \frac{G_F^2 |C_V|^2 \,(1 + 3|C_A/C_V|^2)}{2\pi^3}, \tag{4.18}$$

where $G_F \approx 1.166 \times 10^{-11}\,\mathrm{MeV}^{-2}$ is the Fermi constant, C_V and C_A are the vector and axial vector coupling constants, respectively, and we have taken the absolute squares of the Fermi and Gamow-Teller matrix elements for the free nucleons to be $|M_F|^2 = 1$ and $|M_{GT}|^2 = 3$, respectively. Here δ is a factor which includes both Coulomb and other ("radiative correction") effects which amount to a few percent change in the effective ft-value, $\langle ft \rangle$.

Of course, C_V and C_A are coupling constants that are renormalized by the particular strong interaction environment characterizing free neutrons and protons. (Absent strong interactions $C_V = C_A = 1$.) Given that these are *a priori* unknowns, as is δ, we follow the standard procedure [12]: we take the free neutron decay rate as the product of Eq. (4.18) and the phase space factor in Eq. (4.13) (with $S_{\bar{\nu}_e} = S_{e^-} = 0$) and we then set this equal to the inverse of the laboratory-measured free neutron lifetime, τ_n. The world-average of the laboratory measurements is $\tau_n = 887.7$ seconds [18].

Note that changing the prescription for the Coulomb correction factor $F[Z, E_e]$ in Eq. (4.13) will have the effect of renormalizing the effective free nucleon weak interaction matrix elements (*i.e.*, renormalizing $\langle ft \rangle$) for a given τ_n. As we will see below, this renormalization will be the dominant component of the Coulomb correction alteration in, *e.g.*, the ^{4}He BBN yield.

The rates for all the individual weak reactions are shown as functions of temperature in Fig. 4.2. At high temperatures the forward and reverse rates of the

lepton capture reactions in Eq. (4.1) and Eq. (4.2) dominate the neutron-proton inter-conversion process. Note that the rates for the forward process in Eq. (4.2) and the reverse process in Eq. (4.1) are affected by the threshold, $\delta m_{np} + m_e c^2$. At lower temperatures this threshold makes these rates relatively slower than the rates for the lepton capture channels without this threshold, *i.e.*, the forward process in Eq. (4.1) and the reverse process in Eq. (4.2).

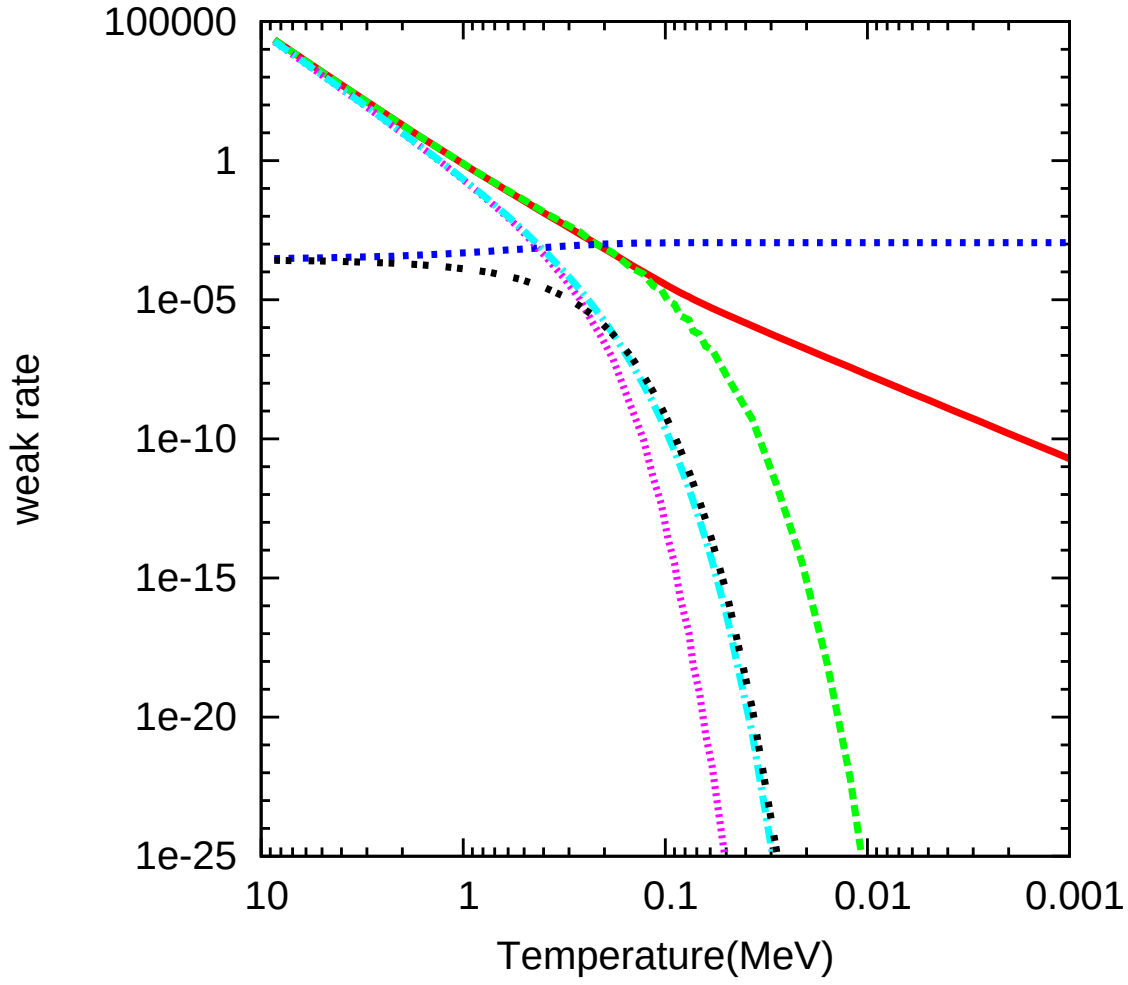

Figure 4.2: All six weak reaction rates as a function of temperature. The solid (red) line is for $\lambda_{\nu_e n}$, the dashed (green) line is for $\lambda_{e^+ n}$, the dotted (blue) line is for $\lambda_{n_{\rm decay}}$, the small-dashed(pink) line is for $\lambda_{p\bar{\nu}_e}$, the dotted-dashed (cyan) line is for $\lambda_{e^- p}$, and the black dotted-spaced line is for $\lambda_{pe^-\bar{\nu}_e}$. All lepton chemical potentials are set to zero here.

This figure shows that at a lower temperature ($T \ll \delta m_{np}$) the electron capture rate λ_{e^-p} and the three-body rate $\lambda_{pe^-\bar{\nu}_e}$ track each other closely, differing by a factor of order unity. This is readily explained as follows. First note that the integrands in the phase space factors in Eq. (4.9) and Eq. (4.14) are identical. Although the former phase space factor is proportional to $1 - S_{\nu_e}$ and the latter to $S_{\bar{\nu}_e}$, when the ν_e and $\bar{\nu}_e$ energies in these distributions are expressed in terms of electron energy, $E_{\nu_e} = E_e - \delta m_{np}$ and $E_{\bar{\nu}_e} = \delta m_{np} - E_e$, respectively, we see that $1 - S_{\nu_e} = S_{\bar{\nu}_e}$. Second, though the limits of integration for these phase space factors differ, we note that when $T \ll \delta m_{np}$ the upper limits are effectively the same. Only the lower limit is different in the two cases, $\approx 1.3\,\mathrm{MeV}$ in the former and $\approx 0.511\,\mathrm{MeV}$ in the latter.

As the temperature decreases, free neutron decay becomes the dominant weak reaction. This remains the case through the epoch when strong and electromagnetic nuclear reactions freeze out of equilibrium ("nucleosynthesis"), when nearly all free neutrons are incorporated into alpha particles.

4.3 Coulomb Correction to the Weak Interaction Rates

For weak interaction processes that have an electron and a proton in either the initial or final state, the Coulomb interaction must be taken into account. In fact, the phase space factors presented above are derived by using plane wave functions for the entrance and exit channel leptons, but then "correcting" where Coulomb waves should be used instead by multiplying the appropriate phase space integrals by the Fermi factor $F(Z, E_e)$.

The Coulomb potential is attractive in the e^-/p channel. This has the effect of *increasing* the electron probability amplitude at the nucleus (proton) and, in turn, this will always *increase* the affected phase space factors. In other words, the phase space factors in the expressions for the rates for both the forward and

reverse processes in Eq. (4.1) and Eq. (4.3) will be increased over a case where only plane waves are used.

4.3.1 Previous Corrections to the BBN Weak Reaction Rates

The Coulomb correction to the weak rates in BBN was first employed by Wagoner [19] in an early version of the BBN code. Wagoner took a representative value of the correction from around the time of weak freeze out, when the weak rates have the largest effect on the n/p ratio, and used this to scale the neutron lifetime, τ_n. This had the effect of increasing the effective neutron lifetime over what had been chosen for τ_n by about 2%. This effectively slowed down all weak interaction rates by 2% because the weak rates are all normalized by the neutron lifetime. Wagoner's correction over-estimated the Fermi factor, giving an erroneous increase in helium mass-fraction, Y_p, of about 0.5%. This over production was largely a result of "correcting" weak reactions that should not have been corrected, *e.g.*, $n + e^+ \rightleftharpoons p + \bar{\nu}_e$. Wagoner did not include any radiative corrections.

Dicus *et. al* [13] were the first to add an energy dependent Coulomb correction to the BBN calculation, along with the zero-temperature radiative corrections and finite-temperature radiative corrections. They approximated the Coulomb correction using the non-relativistic form for the Fermi factor

$$F_+(\beta) \simeq \frac{2\pi\alpha/\beta}{1 - e^{-2\pi\alpha/\beta}}. \tag{4.19}$$

where $\beta = v/c$ is the electron velocity. It was pointed out in Ref. [20] that Ref. [13], like Wagoner, Coulomb-corrected the rates that should not have had a Fermi factor in their phase space integrands.

Ref. [13] derived the zero-temperature radiative corrections for a point nucleon, finding that all the weak rate integrands should be multiplied by

$$1 + \frac{\alpha}{2\pi} C(\beta, y), \tag{4.20}$$

where β is again the electron velocity and y and ϵ are the neutrino energy and electron energy divided by the electron mass, respectively, and

$$\begin{aligned} C(\beta, y) \;\cong\; & 40 + 4(U-1)(y/3\epsilon - 3/2 + \ln 2y) \\ & + U(2(1+\beta^2) + y^2/6\epsilon^2 - 4\beta U] \\ & - 4[2 + 11\beta + 25\beta^2 + 25\beta^3 + 30\beta^4 \\ & + 20\beta^5 + 8\beta^6)/(1+\beta)^6. \end{aligned} \tag{4.21}$$

Here U is defined to be

$$U \equiv \beta^{-1} \tanh^{-1} \beta. \tag{4.22}$$

The corrections in Ref. [13] resulted in a $\sim 0.4\%$ reduction in Y_p from a calculation with the Coulomb effect alone, plus a $\sim 0.2\%$ increase stemming from the zero-temperature radiative corrections.

Ref. [21] and Ref. [22] appropriately applied the Coulomb correction to only those rates which require one. Ref. [21] used the Fermi factor approximated at order α, while Ref. [22] used a non-relativistic version of the Fermi factor in Eq. (4.19). They also applied the zero-temperature radiative corrections defined above as well as several other corrections.

4.3.2 New Coulomb Correction and Modifications to the BBN code

In this work we employ a version of the Coulomb correction which can better take into account the potentially relativistic kinematics of initial or final state electrons. We use the Coulomb correction that is discussed in Ref.s [14, 23, 24]:

$$G(\pm Z, E_e) \equiv x\, F(\pm Z, E_e), \tag{4.23}$$

and we define $x \equiv (E_e^2 - (m_e c^2)^2)^{1/2}/E_e$, the ratio of charged lepton (electron here) momentum to energy. In Eq. (4.23), $F(\pm Z, E_e)$ is the Fermi factor (or relativistic

Coulomb barrier factor) approximated here as

$$F(\pm Z, E_e) \approx 2(1+s)(2pR)^{2(s-1)} e^{\pi\omega} \left| \frac{\Gamma(s+i\omega)}{\Gamma(2s+1)} \right|. \tag{4.24}$$

In this expression, the upper signs are for electron emission and capture, the lower signs are for positron emission and capture in the general case for a nucleus of electric charge Z (in our case $Z = 1$), $s = [1 - (\alpha Z)^2]^{1/2}$, α is the fine structure constant, $\omega = \pm Z/x$ ("+" for the e^- in our cases), and R is the nuclear radius in electron Compton wavelengths, $R = 2.908 \times 10^{-3} A^{1/3} - 2.437 A^{-1/3}$ where A is the nuclear mass number and A=1 in our case. This is the most accurate Coulomb correction that has been employed in a BBN calculation.

In order to properly apply these features of the correction, we used a version of the Kawano/Wagoner code where the weak reaction rates have been entirely rewritten. We will only briefly describe this code here. A detailed description can be found in Ref. [8].

The original Kawano/Wagoner code calculates the weak rates with a total lumped sum of the $n \to p$ and $p \to n$ rates:

$$\lambda_n = \lambda_{\nu_e + n \to p + e^-} + \lambda_{n + e^+ \to p + \bar{\nu}_e} + \lambda_{n \to p + e^- + \bar{\nu}_e} \tag{4.25}$$

$$\lambda_p = \lambda_{p + e^- \to \nu_e + n} + \lambda_{\bar{\nu}_e + p \to n + e^+} + \lambda_{p + e^- + \bar{\nu}_e \to n}. \tag{4.26}$$

In our version, we have separated these summed rates to calculate all 6 weak reaction rates individually. Another key feature of the code is that each rate is modularized, so that any neutrino and antineutrino distribution function and time dependence thereof can be applied.

Because of this modularization we were able to apply a Coulomb correction to only those rates that require one. In other words, we were also able to include an appropriate relativistic Fermi factor in the integrand of those weak rates.

Additionally, this is the first time this version of the correction has been applied to the full reaction network in the Kawano/Wagoner code. This allowed us to study the effect of the correction on all of the light element abundances. We were also

able to study the effect of the correction on nucleosynthesis in the presence of neutrino degeneracy (a lepton number).

4.4 Results and Discussion

We have applied the Coulomb correction described above along with zero temperature radiative corrections in the full Kawano/Wagoner BBN code. The integrated effect of these corrections can be seen by the changes in the light element abundances.

The Coulomb correction described above affects BBN abundance yields in a subtle, but interesting way which gives insight into the weak interaction's role in setting the neutron abundance in the early universe. First, as outlined in the last sections, the key effect of calculating the weak rates with Coulomb waves instead of plane waves is to increase the electron's probability amplitude at the proton. This means that the rates corresponding to $e^- + p \rightarrow n + \nu_e$, $\nu_e + n \rightarrow p + e^-$, $n \rightarrow p + e^- + \bar{\nu}_e$, and $p + e^- + \bar{\nu}_e \rightarrow n$ will all *increase* over plane-wave calculated rates.

This is true, but in the BBN calculation the net effect of adding a Coulomb or radiative correction which *increases* the phases space factor for free, vacuum neutron decay is to *reduce* the weak matrix element (*increase* $\langle ft \rangle$) common to all of the rates of the forward and reverse processes in Eq. (4.1), Eq. (4.2), and Eq. (4.3). This is because for a given vacuum ($S_e = S_{\bar{\nu}_e} = 0$) neutron lifetime, τ_n, we set $\lambda_{n_{\rm decay}}|_{\rm vacuum} = \tau^{-1}$, and an increased phase space factor then implies an increased value for $\langle ft \rangle$.

Therefore, the chief effect of a Coulomb correction-mediated increase in phase space factors is a decrease in the overall strength of the weak interaction. In turn, a weaker weak interaction would cause a higher temperature for freeze-out from chemical equilibrium and a concomitant increase in the neutron-to-proton ratio emerging from the weak freeze out process. Since, to first approximation, all neutrons will eventually be incorporated into alpha particles, the phase space

factor-enhancing Coulomb correction should give rise to an *increase* in the primordial mass fraction Y_p.

In broad brush this is indeed what the BBN calculations show. Our modularized code, which allows us to track the individual weak rates, affords us a deeper insight into what is happening. Though all rates are renormalized downward by the Coulomb correction, the rates for the particular processes with a Fermi factor in their phase space integrals (Eq.s (4.9), (4.12), (4.13), and (4.14)) are decreased less. In other words, they are increased relative to the rates in Eq. (4.10) and Eq. (4.11), $\lambda_{\bar{\nu}_e p}$ and $\lambda_{e^+ n}$, respectively.

Nevertheless, neutron decay has more leverage over the eventual n/p ratio than do the lepton capture processes. At higher temperatures where the n/p ratio is well approximated as the ratio of the sum of the neutron production rates to the sum of the neutron destruction rates, Eq. (4.6), note that the small and comparable fractional relative increases in $\lambda_{e^- p}$ and $\lambda_{\nu_e n}$ tend to compensate each other to first order. This is because $\lambda_{e^- p}$ is in the numerator and $\lambda_{\nu_e n}$ is in the denominator in Eq. (4.6). As a consequence, changes in n/p stemming from lepton capture processes are second order in the Coulomb corrections.

Table I presents a comparison of BBN calculations of the ^{4}He mass fraction, Y_p, and the deuterium abundance relative to hydrogen, D/H, all performed with our code. Shown in this table are a "Baseline," standard ($\mu_{\nu_e} = \mu_e = 0$) BBN case with no Coulomb corrections (*i.e.*, $F(Z, E_e) = 1$), and cases where the same calculations were done but where the Coulomb corrections of Wagoner Ref. [19], Esposito *et al.* Ref. [21], and Lopez and Turner Ref. [25], were used. This table also shows results from the same BBN calculation but using our new relativistic Coulomb correction for cases with and without a radiative correction. Consistent with the arguments given above, we see that the Coulomb correction prescriptions in all of these cases give a $\sim 1\%$ increase in Y_p. All of the various versions of the Coulomb correction are consistent with each other. The relativistic Fermi factor used in this work results in a modest 0.04% increase in Y_p over the result in Ref. [21].

Table 4.1: ^{4}He mass fraction Y_p and deuterium abundance D/H as calculated with our code for various implementations of Coulomb and radiative corrections as indicated. The Baseline table entries are the uncorrected values; table entries designated by Wagoner, Esposito, and Lopez and Turner were computed using the correction prescriptions in Ref. [19], [21], and [25], respectively, but with our code and with the current world-average neutron lifetime.

	Y_p	D/H	$\Delta Y_p/Y_p$
Baseline	0.239	2.522×10^{-5}	
Wagoner	0.2427	2.543×10^{-5}	1.16%
Esposito	0.2416	2.537×10^{-5}	1.09%
Lopez and Turner	0.2416	2.537×10^{-5}	1.09%
New Correction	0.2417	2.543×10^{-5}	1.13%
New Correction with Zero-Temperature Radiative Corrections	0.2422	2.542×10^{-5}	1.34%

The modular nature of the weak rates in our BBN code allows us to examine the effects of the Coulomb correction for scenarios in which the lepton numbers residing in the ν_e and $\bar{\nu}_e$ seas are nonzero. This is the first such study of the Coulomb and radiative correction effects in a case with nonzero values for μ_{ν_e} and $\mu_{\bar{\nu}_e}$. (Here we take $\mu_{\nu_e} + \mu_{\bar{\nu}_e} = 0$, reflecting assumed neutrino chemical equilibrium at high temperatures.) We define the lepton number residing in these neutrino seas to be

$$L_{\nu_e} = \frac{n_{\nu_e} - n_{\bar{\nu}_e}}{n_\gamma}, \tag{4.27}$$

where n_{ν_e} and $n_{\bar{\nu}_e}$ are the ν_e and $\bar{\nu}_e$ proper number densities, respectively, and $n_\gamma = (2\xi(3)/\pi^2)T_\gamma^3$ is the corresponding photon number density with $\xi(3) \approx 1.20206$ the Riemann-Zeta function of argument 3. The primordial helium abundance plus observationally-and experimentally-determined neutrino flavor oscillation data restrict $|L_{\nu_e}| < 0.1$ [26, 27, 28, 29]. This upper limit conceivably could rise to ≈ 0.2 if allowance is made for additional contributions to the energy density in the early universe [29, 30]. Models which attempt to reconcile light-mass sterile neutrinos with BBN and large scale structure plus cosmic microwave background-derived overall neutrino mass closure constraints usually invoke lepton numbers. But the lepton numbers invoked in these schemes can increase the ^{4}He-based upper limit on $|L_{\nu_e}|$ [31, 32]. Sterile neutrino dark matter scenarios [33, 34, 35, 36, 37, 38, 39, 34, 40, 41, 42, 43, 44, 45, 46, 47] also can invoke significant lepton numbers. We therefore consider a range $0 \leq L_{\nu_e} \leq 0.3$ as an interesting example.

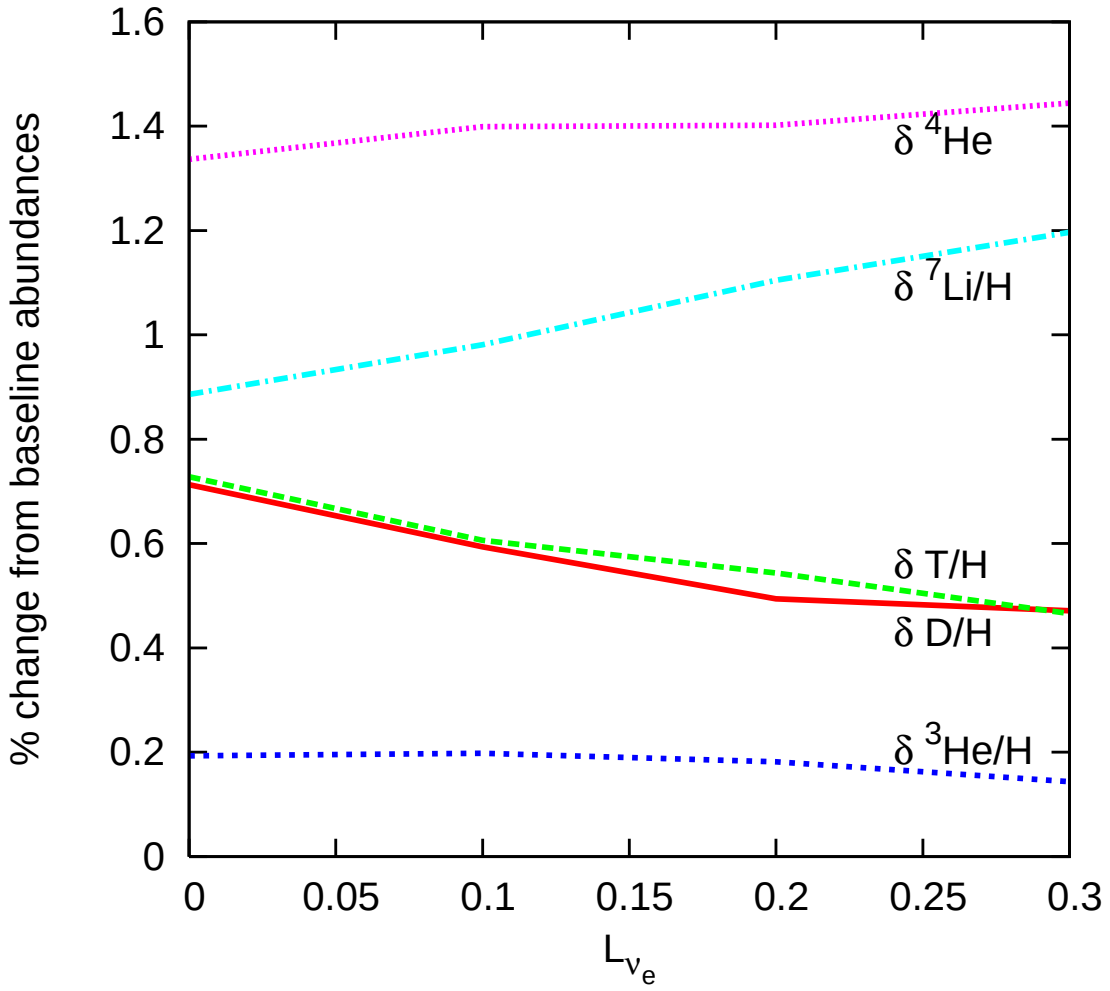

Figure 4.3: Percent change in nuclear abundances from the Baseline values as a function of electron lepton number from when the Coulomb and zero-temperature radiative corrections are included.

Unlike the neutrino degeneracy parameter, L_{ν_e} is not a co-moving invariant. The ratio of the neutrino temperature parameter, T_ν, in S_{ν_e} and $S_{\bar{\nu}_e}$ to the temperature of the plasma, T_γ, evolves in time. This ratio starts out as unity for $T \gg 1$ MeV and, as electrons and positrons annihilate and transfer their entropy preferentially to the photons and plasma, eventually asymptotes to $(4/11)^{1/3}$ at low temperatures. The lepton numbers and the neutrino degeneracy parameters are related by

$$L_{\nu_\alpha} = \left(\frac{\pi^2}{12\zeta\left(3\right)}\right)\left(\frac{T_\nu}{T_\gamma}\right)^3 \left[\eta_{\nu_\alpha} + \eta_{\nu_\alpha}^3/\pi^2\right], \tag{4.28}$$

and at small lepton number $\eta_{\nu_e} \approx 1.46 L_{\nu_e}$. Here we consider only positive values of L_{ν_e}, *i.e.*, cases with a preponderance of ν_e's over $\bar{\nu}_e$'s, as these are the most interesting with respect to ^{4}He.

An effect of nonzero μ_{ν_e} and $\mu_{\bar{\nu}_e}$ will be to change the energy weighting in the phase space integrands in Eq. (4.9), Eq. (4.12), Eq. (4.13), and Eq. (4.14). We might then expect a concomitant alteration in the effect of the Coulomb correction over the zero lepton number cases for λ_{e^-p}, $\lambda_{\nu_e n}, \lambda_{n_{\rm decay}}$, and $\lambda_{pe^-\bar{\nu}_e}$, respectively. In Fig. 4.3 we show the relative change in BBN abundance yields for ^{4}He, ^{7}Li, ^{3}H, ^{2}H, and ^{3}He, over the Baseline (no Coulomb or radiative corrections) case as a function of L_{ν_e}. In the figure the percent change in the ^{4}He mass fraction is designated by δ^4He, while the percent change in the abundances for deuterium, tritium, and ^{3}He are given by δD/H, δT/H, and δ^3He/H, respectively. First, we note that the overall sense of the Coulomb correction is to increase Y_p and all of the nuclear abundances yields over the Baseline case for the lepton number range examined.

A higher L_{ν_e} and the accompanying higher number density n_{ν_e} and lower number density $n_{\bar{\nu}_e}$, will have the effect of increasing $\lambda_{\nu_e n}$ and $\lambda_{n_{\rm decay}}$ and decreasing λ_{e^-p} and $\lambda_{pe^-\bar{\nu}_e}$ over the zero lepton number case. This is simply a result of an enhancement or reduction in final state blocking or entrance channel lepton number density as appropriate. Figure 3 shows that while the ^{4}He and ^{3}He Coulomb correction abundance yield enhancements are essentially flat with increasing L_{ν_e},

the abundance yield enhancement for ^{7}Li increases while the corresponding enhancements for ^{3}H and ^{2}H decrease with increasing L_{ν_e}. The trends with L_{ν_e} of ^{7}Li/H, ^{3}H/H, and ^{2}H/H, versus those for the ^{3,4}He yields reflect the different times at which these species are formed and the sensitivity of the relevant reaction production mechanisms to the local neutron abundance and temperature.

4.5 Conclusion

We have for the first time implemented a relativistic version of the Coulomb correction in the full reaction network of the Kawano/Wagoner BBN code. We have used this code to study BBN abundance yields for a range of neutrino chemical potentials. We find that the fully relativistic Coulomb correction essentially agrees with previous non-relativistic prescriptions, giving only a 0.04% increase in the ^{4}He yield over that in Esposito *et al.* [21]. Our calculations show interesting trends in the light element abundance yields with increasing electron lepton number. The modularization of the individual weak interaction processes in our code has allowed us to gain insights into how the rates for these processes are altered by the Coulomb and radiative corrections and how these alterations affect the neutron-to-proton n/p ratio in the early universe during the BBN epoch. In particular, we point out that the lepton capture processes produce changes in the n/p ratio which are only second order in the small Coulomb corrections.

As the accuracy of measurements of the CMB and the primordial abundances of the light elements increase, BBN will give even better constraints on physics in the early universe. Currently, the increase in precision gained from including this relativistic version of the correction is probably unnecessary. However, in the future as the measurements for the main parameters affecting BBN, such as the baryon-to-photon ratio and the neutron lifetime, increase in precision, it may be beneficial to include this version of the correction.

4.6 Acknowledgments

We would like to acknowledge helpful discussions with Kevork Abazajian, Chad Kishimoto, and Michael Smith. This work was supported in part by NSF Grant No. PHY-06-53626.

Chapter 4, in full, is in preparation for submission to Physical Review D. Smith, Christel J.; Fuller, George M. The dissertation author was the primary investigator and author of this paper.

Bibliography

[1] SDSS Collaboration, M. Tegmark *et al.*, Phys. Rev. D **69**, 103501 (2004).

[2] D. N. Spergel *et al.*, Astrophys. J. Suppl. **148**, 175 (2003).

[3] D. N. Spergel *et al.*, astro-ph/0603449.

[4] J. R. Bond, C. Contaldi, A. Lewis and D. Pogosyan, Int. J. Theor. Phys. **43**, 599 (2004).

[5] D. Kirkman, D. Tytler, N. Suzuki, J. M. O'Meara, and D. Lubin, Astrophys. J. Suppl. **149**, 1 (2003).

[6] J. M. O'Meara, D. Tytler, D. Kirkman, N. Suzuki, J. X. Prochaska, D. Lubin and A. M. Wolfe, Astrophys. J. **552**, 718 (2001).

[7] K. Abazajian, N. F. Bell, G. M. Fuller and Y. Y. Y. Wong, Phys. Rev. D **72**, 063004 (2005).

[8] C. J. Smith, G. M. Fuller and M. S. Smith, Physical Review D (Particles, Fields, Gravitation, and Cosmology) **79**, 105001 (2009).

[9] L. Kawano, NASA STI/Recon Technical Report N **92**, 25163 (1992).

[10] L. Kawano, FERMILAB-PUB-88/34-A.

[11] R. V. Wagoner, Ann. Rev. Astron. Astrophys. **7**, 553 (1969).

[12] R. V. Wagoner, W. A. Fowler and F. Hoyle, Astrophys. J. **148**, 3 (1967).

[13] D. A. Dicus *et al.*, Phys. Rev. **D26**, 2694 (1982).

[14] G. M. Fuller, W. A. Fowler and M. J. Newman, Astrophys. J. Suppl. **42**, 447 (1980).

[15] G. M. Fuller, W. A. Fowler and M. J. Newman, Astrophys. J. **252**, 715 (1982).

[16] G. M. Fuller, W. A. Fowler and M. J. Newman, Astrophys. J. Suppl. **48**, 279 (1982).

[17] G. M. Fuller, W. A. Fowler and M. J. Newman, **293**, 1 (1985).

[18] W.-M. Yao *et al.*, J. Phys. G **33**, 1 (2006).

[19] R. V. Wagoner, Astrophys. J. **179**, 343 (1973).

[20] P. J. Kernan and L. M. Krauss, Phys. Rev. Lett. **72**, 3309 (1994).

[21] S. Esposito, G. Mangano, G. Miele and O. Pisanti, Nucl. Phys. **B540**, 3 (1999), [astro-ph/9808196].

[22] R. E. Lopez and M. S. Turner, Phys. Rev. D **59**, 103502 (1999).

[23] N. B. Gove and M. J. Martin, Nuclear Data Tables **10**, 205 (1971).

[24] A. deShalit and H. Feshbach, *Theoretical Nuclear Physics, Volume I: Nuclear Structure*, 1 ed. (John Wiley and Sons, Inc., 1974).

[25] R. E. Lopez and M. S. Turner, Phys. Rev. **D59**, 103502 (1999), [astro-ph/9807279].

[26] K. N. Abazajian, J. F. Beacom and N. F. Bell, Phys. Rev. D **66**, 013008 (2002).

[27] Y. Y. Y. Wong, Phys. Rev. D **66**, 025015 (2002).

[28] A. D. Dolgov, S. H. Hansen, S. Pastor, S. T. Petcov, G. G. Raffelt and D. V. Semikoz, Nucl. Phys. B **632**, 363 (2002).

[29] J. P. Kneller, R. J. Scherrer, G. Steigman and T. P. Walker, Phys. Rev. D **64**, 123506 (2001).

[30] V. Barger, J. P. Kneller, P. Langacker, D. Marfatia and G. Steigman, Phys. Lett. B **569**, 123 (2003).

[31] C. J. Smith, G. M. Fuller, C. T. Kishimoto and K. N. Abazajian, Phys. Rev. **D74**, 085008 (2006), [astro-ph/0608377].

[32] Y.-Z. Chu and M. Cirelli, Phys. Rev. **D74**, 085015 (2006), [astro-ph/0608206].

[33] A. Kusenko, S. Pascoli and D. Semikoz, JHEP **11**, 028 (2005), [hep-ph/0405198].

[34] K. Petraki and A. Kusenko, Phys. Rev. **D77**, 065014 (2008), [0711.4646].

[35] S. Dodelson and L. M. Widrow, Phys. Rev. Lett. **72**, 17 (1994), [hep-ph/9303287].

[36] K. Abazajian, G. M. Fuller and M. Patel, Phys. Rev. **D64**, 023501 (2001), [astro-ph/0101524].

[37] A. D. Dolgov and S. H. Hansen, Astropart. Phys. **16**, 339 (2002), [hep-ph/0009083].

[38] M. Shaposhnikov and I. Tkachev, Phys. Lett. **B639**, 414 (2006), [hep-ph/0604236].

[39] A. Kusenko, Phys. Rev. Lett. **97**, 241301 (2006), [hep-ph/0609081].

[40] K. Petraki, Phys. Rev. **D77**, 105004 (2008), [hep-ph/0801.3470].

[41] X.-D. Shi and G. M. Fuller, Phys. Rev. Lett. **83**, 3120 (1999), [astro-ph/9904041].

[42] C. B. Chiu, E. C. G. Sudarshan and B. Misra, Phys. Rev. **D16**, 520 (1977).

[43] D. Boyanovsky and C. M. Ho, Phys. Rev. **D76**, 085011 (2007), [hep-ph/0705.0703].

[44] D. Boyanovsky and C. M. Ho, JHEP **07**, 030 (2007), [hep-ph/0612092].

[45] D. Boyanovsky, Phys. Rev. **D77**, 023528 (2008), [astro-ph/0711.0470].

[46] K. N. Abazajian and G. M. Fuller, Phys. Rev. **D66**, 023526 (2002), [astro-ph/0204293].

[47] C. T. Kishimoto and G. M. Fuller, Physical Review D (Particles, Fields, Gravitation, and Cosmology) **78**, 023524 (2008).

Appendix A

Coherent Active-Sterile Neutrino Flavor Transformation in the Early Universe

We solve the problem of coherent Mikheyev-Smirnov-Wolfenstein (MSW) resonant active-to-sterile neutrino flavor conversion driven by an initial lepton number in the early universe. We find incomplete destruction of lepton number in this process and a sterile neutrino energy distribution with a distinctive cusp and high energy tail. These features imply alteration of the non-zero lepton number primordial nucleosynthesis paradigm when there exist sterile neutrinos with rest masses $m_{\rm s} \sim 1\,{\rm eV}$. This could result in better light element probes of (constraints on) these particles.

Recent advances in observational cosmology and in experimental neutrino physics promise a well constrained picture for the evolution of the early universe. The existence of a light sterile neutrino (ν_s) presents an immediate problem: how do sterile neutrinos affect primordial seas of active neutrinos ν_α or $\bar{\nu}_\alpha$ ($\alpha = e, \mu, \tau$) and consequentially affect the standard big bang paradigm? In this letter we study the lepton number-driven transformation of active neutrinos to sterile neutrinos in the epoch of the early universe after weak decoupling, when neutrinos propagate

coherently. This process could leave both the active neutrinos and sterile neutrinos with distorted, non-thermal energy spectra [1]. A non-thermal ν_e or $\bar{\nu}_e$ spectrum could lead to significant modification in the relationship between lepton number and Big Bang Nucleosynthesis (BBN) ^{4}He abundance yield [1, 2]. Concomitantly, a distorted ν_s distribution function changes closure mass constraints on light sterile neutrinos [1, 3], allowing rest masses and vacuum mixing angles for these species in the range ($0.4\,\mathrm{eV} < m_\mathrm{s} < 5\,\mathrm{eV}$) suggested by the LSND experiment [4, 5] and currently being probed by the mini-BooNE experiment [6].

Active neutrinos propagating in the homogeneous early universe experience a potential stemming from forward scattering $V = 2\sqrt{2}\zeta(3)\pi^{-2}G_F T^3 \mathcal{L}_\alpha - r_\alpha G_F^2 E_\nu T^4$, where T is the photon/plasma temperature, E_ν is the neutrino energy, r_α is a numerical coefficient which depends on the number of relativistic charged lepton degrees of freedom and can be found in Refs. [1, 7], G_F is the Fermi constant, and $\zeta\,(3) \approx 1.20206$. Here the potential lepton number is $\mathcal{L}_\alpha \equiv 2L_{\nu_\alpha} + \sum_{\beta\neq\alpha} L_{\nu_\beta}$, where the individual lepton numbers are given in terms of the neutrino, antineutrino, and photon proper number densities by $L_{\nu_\alpha} \equiv (n_{\nu_\alpha} - n_{\bar{\nu}_\alpha})/n_\gamma$. Current observational bounds on these are $|L_{\nu_\alpha}| < 0.1$ [8, 9, 10], and could be slightly weaker if there are additional sources of energy density in the early universe [11, 12]. We have neglected contributions to V from neutrino-baryon/electron scattering since we consider relatively large lepton numbers with $\mathcal{L} \gg \eta$, where the baryon-to-photon ratio is $\eta \equiv n_\mathrm{b}/n_\gamma$ (see Refs. [1, 7]). The second term in V is negligible for the temperatures characteristic of the post weak decoupling era, $T < 3\,\mathrm{MeV}$.

The scattering-induced de-coherence production [13, 14, 15, 16, 17, 18] of seas of ν_s and $\bar{\nu}_s$, with rest mass $m_\mathrm{s} \sim 1\,\mathrm{eV}$, could be avoided if theses species are massless for $T > 3\,\mathrm{MeV}$, inflation has a low reheat temperature [19], or there exists a preexisting lepton number $|L_{\nu_\alpha}| > 10^{-3}$ [1, 20]. However, a lepton number could subsequently, after weak decoupling, drive [1] coherent medium-enhanced MSW [21, 22] resonant conversion $\nu_\alpha \rightarrow \nu_s$ or $\bar{\nu}_\alpha \rightarrow \bar{\nu}_s$, depending on the sign of the lepton number. (Resonant de-coherence production of sterile neutrinos with $m_\mathrm{s} \sim 1\,\mathrm{keV}$ with accompanying ν_s spectral distortion was considered in Refs.

[23, 7].) The MSW condition for the resonant scaled neutrino energy $\epsilon = E_\nu^{\rm res}/T$ is $\delta m^2 \cos 2\theta = 2\epsilon TV$, or

$$\epsilon\mathcal{L} = \left(\frac{\delta m^2 \cos 2\theta}{4\sqrt{2}\zeta(3)\pi^{-2}G_F}\right) T^{-4}, \tag{A.1}$$

where $\delta m^2 \equiv m_2^2 - m_1^2$ is the difference of the squares of the vacuum neutrino mass eigenvalues. For illustrative purposes, we consider 2×2 vacuum mixing with a one-parameter (vacuum mixing angle θ) unitary transformation between weak interaction eigenstates $|\nu_\alpha\rangle$, $|\nu_s\rangle$, and energy/mass eigenstates:

$$\begin{aligned} |\nu_\alpha\rangle &= \cos\theta|\nu_1\rangle + \sin\theta|\nu_2\rangle; \\ |\nu_s\rangle &= -\sin\theta|\nu_1\rangle + \cos\theta|\nu_2\rangle. \end{aligned} \tag{A.2}$$

As the universe expands, the temperature falls, causing the resonance to sweep from low to higher values of the scaled neutrino energy, ϵ. This resonance sweep converts active neutrinos into sterile neutrinos, reducing $\mathcal{L}$, which accelerates the resonance sweep rate.

The evolution of $\mathcal{L}$ is dictated by the resonance sweep rate and the dimensionless adiabaticity parameter. The adiabaticity parameter, γ, is proportional to the ratio of the width of the MSW resonance, $\delta t = |1/VdV/dt|^{-1}\tan 2\theta$, and the neutrino oscillation length at resonance, $L_{\rm osc} = 4\pi E_\nu/(\delta m^2 \sin 2\theta)$. Combining the expansion rate of the universe in the radiation dominated epoch with the conservation of co-moving entropy density and the forward scattering potential V, the adiabaticity parameter is

$$\begin{aligned} \gamma &\approx \frac{\sqrt{5}\zeta^{3/4}(3)}{2^{1/8}\pi^3}\frac{(\delta m^2)^{1/4} m_{pl} G_F^{3/4}}{g^{1/2}}\frac{\sin^2 2\theta}{\cos^{7/4} 2\theta}\mathcal{L}^{3/4}\epsilon^{-1/4} \\ &\quad \times \left|1 + \frac{\dot{g}/g}{3H} - \frac{\dot{\mathcal{L}}/\mathcal{L}}{3H}\right|^{-1}, \end{aligned} \tag{A.3}$$

where m_{pl} is the Planck mass, g is the total statistical weight for relativistic species in the early universe, and $H \approx (4\pi^3/45)^{1/2} g^{1/2} T^2/m_{pl}$ is the local Hubble expansion rate. If the onset of resonant flavor conversion occurs in the epoch between weak

decoupling and weak freeze out, then initially $\gamma \gg 1$ for the active-sterile mixing parameters of interest [1]. However, when the fractional time rate of change of $\mathcal{L}$ becomes larger than the expansion rate of the universe, the evolution of the system can be non-adiabatic with $\gamma < 1$.

Large values of γ result when many oscillation lengths fit within the resonance width. In this case there will be a small probability of jumping from the high mass eigenstate to the low mass eigenstate. In turn, this implies efficient flavor transformation at the MSW resonance. Alternatively, a small value of γ means that the resonance width is much smaller than an oscillation length, and the neutrino jumps between the two mass eigenstates, resulting in virtually no flavor transformation. To describe intermediate cases we use the Landau-Zener jump probability, $P_{\rm LZ} = \exp(-\pi\gamma/2)$ [24, 25], which gives the likelihood for a neutrino at resonance to make the jump between mass eigenstates. It is valid in the limit where the change in V across the resonance width δt can be regarded as linear. This is a good approximation in part because the resonance width is small compared to the causal horizon length for the values of θ and the conditions in the early universe considered here.

It follows that the evolution of the potential lepton number as the resonant scaled neutrino energy sweeps from 0 to ϵ is

$$\mathcal{L}(\epsilon) = \mathcal{L}^{\rm initial} - \frac{1}{2\zeta(3)}\left(\frac{T_\nu}{T}\right)^3 \int_0^\epsilon \frac{x^2(1-e^{-\pi\gamma(x)/2})}{e^{x-\eta_{\nu_\alpha}}+1}dx, \tag{A.4}$$

where T_ν is the temperature of the active neutrino distribution function with degeneracy parameter $\eta_{\nu_\alpha} \equiv \mu_{\nu_\alpha}/T_\nu$, and where μ_{ν_α} is the ν_α chemical potential.

The evolution of the active neutrino spectrum is dictated by three conspiring factors: the MSW resonance condition (Eq. A.1), the adiabaticity parameter (Eq. A.3), and the evolution of potential lepton numbers through active-sterile conversion (Eq. A.4). We solve Eqs. (A.1), (A.3) and (A.4) simultaneously and self-consistently to obtain γ and $\mathcal{L}$ as continuous functions across the entire range of ϵ.

Resonant conversion of active neutrinos to sterile neutrinos begins at $\epsilon \ll 1$.

The resonance sweeps to higher values of ϵ as the temperature of the universe drops. When $\dot{\mathcal{L}}/\mathcal{L} \ll H$, we have $\gamma \gg 1$, and adiabatic conversion of active neutrinos to sterile neutrinos ensues. However, this trend cannot continue. Note that the right hand side of equation (A.1) is a monotonically increasing function of time, while the left hand side is a peaked function if one assumes continued adiabatic conversion of neutrino flavors. At this peak, this assumption fails. Taking the time derivative of the resonance condition, Eq. (A.1), shows that the sweep rate is $\dot{\epsilon} \propto T^{-5}\dot{T}(d(\epsilon\mathcal{L})/d\epsilon)^{-1}$. At the peak, $d(\epsilon\mathcal{L})/d\epsilon = 0$, causing the sweep rate to diverge. Taking the time derivative of both sides of Eq. (A.4) and assuming that T_ν/T is constant, we conclude that $\dot{\mathcal{L}} \propto \dot{\epsilon}$. With this relation, it follows from equation (A.3) that the MSW resonance is no longer adiabatic. We define $\epsilon_{\rm max}$ as the particular value of ϵ at this peak, implicitly specified by

$$\frac{1}{2\zeta(3)}\frac{\epsilon_{\rm max}^3}{e^{\epsilon_{\rm max}-\eta_{\nu_\alpha}}+1} = \mathcal{L}^{\rm initial} - \frac{1}{2\zeta(3)}\left(\frac{T_\nu}{T}\right)^3 \int_0^{\epsilon_{\rm max}} \frac{x^2}{e^{x-\eta_{\nu_\alpha}}+1}dx. \tag{A.5}$$

Our complete continuous solution for γ shows that neutrino flavor evolution/ transformation is adiabatic for $\epsilon < \epsilon_{\rm max}$, but becomes (quickly) progressively less adiabatic for $\epsilon > \epsilon_{\rm max}$. For $\epsilon \geq \epsilon_{\rm max}$, our solution yields a large, but finite resonance sweep rate, and concomitant large fractional lepton number destruction rate, $\dot{\mathcal{L}}/\mathcal{L} \gg H$, leading to $\gamma \lesssim 1$. This behavior continues through the heart of the active neutrino distribution until the resonance sweep rate decreases to a point where $\gamma \gg 1$ again. This last transition back to adiabatic evolution occurs at $\epsilon \sim \mathcal{O}(10)$, approximately where $\mathcal{L}(\epsilon) = 1/(2\zeta(3))\epsilon^3/(e^{\epsilon-\eta_{\nu_\alpha}}+1)$. (Note that this is the same condition as for $\epsilon_{\rm max}$.) Resonance sweep continues to higher ϵ, adiabatically converting active neutrinos to sterile neutrinos.

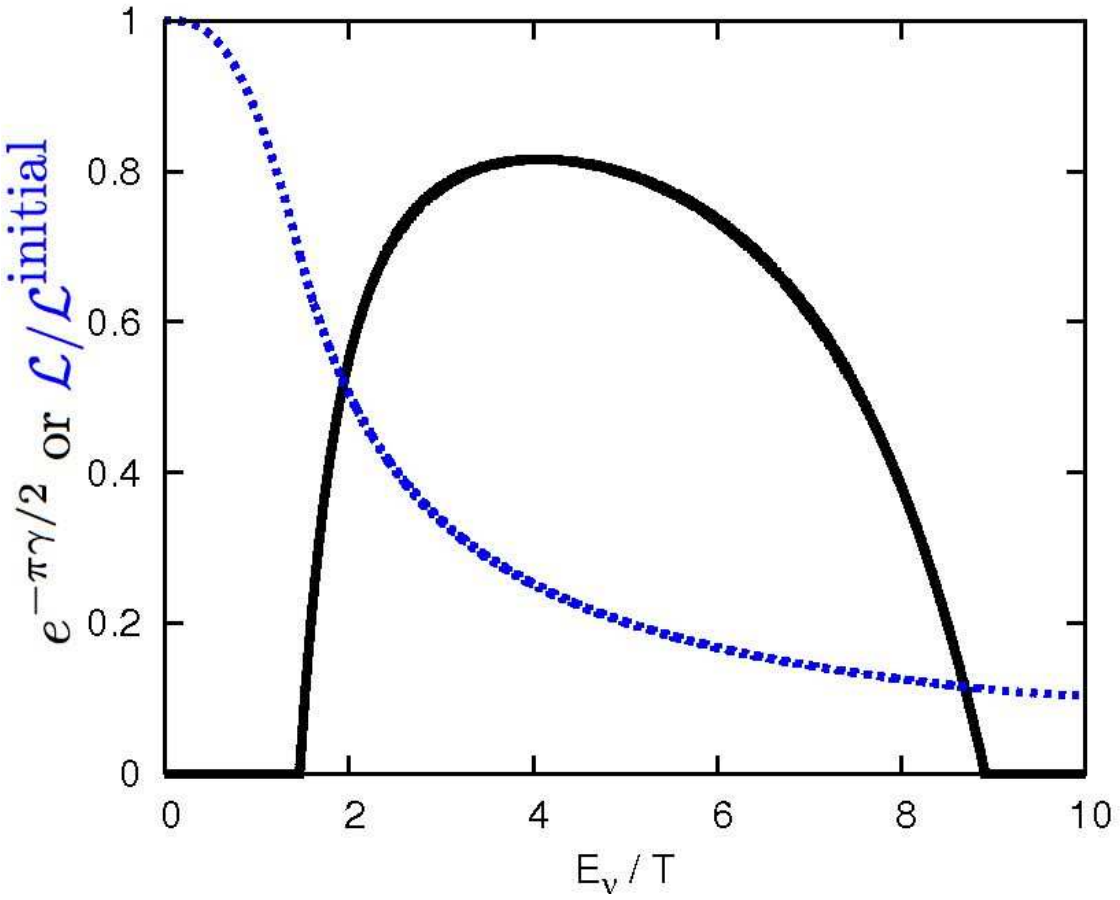

Figure A.1: Landau-Zener jump probability $e^{-\pi\gamma/2}$ (solid curve) and potential lepton number given as a fraction of its initial value (dashed curve) are shown as a function of MSW scaled resonance energy E_ν/T. Here we assume $\delta m^2 = 1\,\mathrm{eV}^2$, $\sin^2 2\theta = 10^{-3}$, and initial individual lepton numbers $L_{\nu_\mu} = L_{\nu_\tau} = 0.15$ and $L_{\nu_e} = 0.0343$.

The evolution of the Landau-Zener jump probability $e^{-\pi\gamma/2}$ and the history of the potential lepton number as a fraction of its initial value are both shown in Figure A.1 for the particular case where $\delta m^2 = 1\,\mathrm{eV}^2$, $\sin^2 2\theta = 10^{-3}$, and where we assume initial lepton numbers near their conventional upper limits, $L_{\nu_\mu} = L_{\nu_\tau} = 0.15$ and $L_{\nu_e} = 0.0343$. For this particular case $\epsilon_{\max} = 1.46$, and Figure A.1 shows the rather abrupt (but continuous) change to non-adiabatic evolution for $\epsilon \approx \epsilon_{\max}$. In this example, the final transition back to adiabatic evolution occurs at $\epsilon \approx 8.9$. Altogether, more than 90% of the initial potential lepton number is destroyed for this case. We find that the fractional depletion of potential lepton number is $\sim 90\%$ across a wide range of initial values of this parameter. This, in turn, suggests that this new solution will result in little change in existing closure mass constraints on light sterile neutrinos [1].

Figure A.2 shows the original ν_e Fermi-Dirac ($f(E_\nu/T) = 1/[T_\nu^3 F_2(\eta_\nu)]E_\nu^2/(e^{E_\nu/T_\nu - \eta_\nu}+1)$, where $F_2(\eta_\nu) \equiv \int_0^\infty x^2/(e^{x-\eta_\nu}+1)dx$) and final ν_e and the ν_s energy distribution functions resulting from $\nu_e \rightarrow \nu_s$ resonance sweep for the example parameters of Fig. A.1. Forced, adiabatic resonance sweep to $\epsilon_{\mathrm{c.o.}}$ would result in complete depletion of the initial potential lepton number. $\epsilon_{\max}$ and $\epsilon_{\mathrm{c.o.}}$ are shown for this case in Fig. A.2. Forced, adiabatic resonance sweep would result in a final ν_e spectrum identical to the initial one except cut-off (hence, "c.o."), with zero population, for $E_\nu/T \leq \epsilon_{\mathrm{c.o.}}$. The ν_s distribution in this case would be simply the complement. By contrast, with the full resonance sweep solution presented here we see that the actual final ν_e spectrum has a population deficit relative to the original distribution, even for $E_\nu/T > \epsilon_{\mathrm{c.o.}}$. Likewise, the actual final ν_s spectrum will now have a tail extending to higher E_ν/T. Including simultaneous active-sterile and active-active neutrino flavor transformation in a full 4×4 scheme will modify this result, but we can expect some general features of our solution to remain. In particular, although neutrino flavor evolution will start out adiabatic, the transition to non-adiabatic evolution could be altered by, *e.g.*, active-active neutrino mixing partially "filling-in" depleted ν_e population [1].

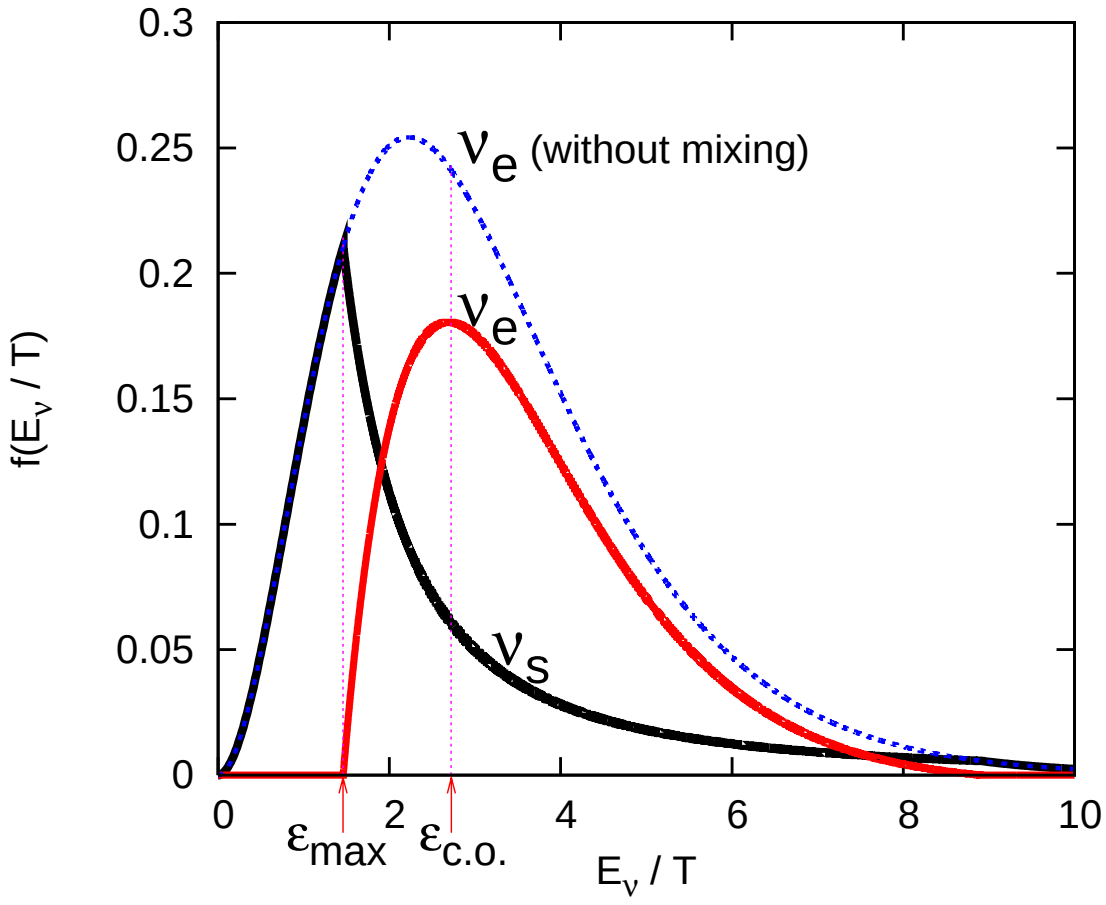

Figure A.2: Shown are the original ν_e distribution function (dashed curve), the final ν_e distribution function (lighter solid curve), and final ν_s distribution function (heavier solid curve) all as functions of scaled neutrino energy E_ν/T for a $\nu_e \to \nu_s$ resonant, coherent flavor conversion process with $\delta m^2 = 1\,\mathrm{eV}^2$, $\sin^2 2\theta = 10^{-3}$, and individual lepton numbers as in Fig. A.1. Vertical dotted lines indicate ϵ_{max} and $\epsilon_{\mathrm{c.o.}}$.

The BBN ^{4}He yield can depend sensitively on the shape of the ν_e energy distribution function [26, 27, 1]. This is because the neutron-to-proton ratio n/p is a crucial determinant of the ^{4}He abundance and, in turn, this ratio is set by the competition among the charged current weak neutron/proton interconversion processes:

$$\begin{aligned} \nu_e + n &\rightleftharpoons p + e^-; \\ \bar{\nu}_e + p &\rightleftharpoons n + e^+; \\ n &\rightleftharpoons p + e^- + \bar{\nu}_e. \end{aligned} \tag{A.6}$$

The net rate for the forward direction in the first of these processes will be reduced if ν_e-population is removed via $\nu_e \rightarrow \nu_s$, resulting in a larger n/p and, hence, a larger ^{4}He yield. Likewise, a negative potential lepton number-driven $\bar{\nu}_e \rightarrow \bar{\nu}_s$ scenario could result in $\bar{\nu}_e$ spectral depletion which will result in a smaller n/p and, hence, less ^{4}He. Removing ν_e ($\bar{\nu}_e$) population at higher E_ν/T values in the energy distribution function accentuates these effects because the cross section for the ν_e ($\bar{\nu}_e$) capture process scales as E_ν^2 and because the Fermi-Dirac spectral peak, where neutrino populations are large, corresponds to values of neutrino energy satisfying $E_\nu/T > \epsilon_{\rm c.o.}$ for the potential lepton numbers $\mathcal{L}$ of interest here. As a consequence, our full resonance sweep scenario can result in significant alteration in ^{4}He yield over the forced, adiabatic scenario.

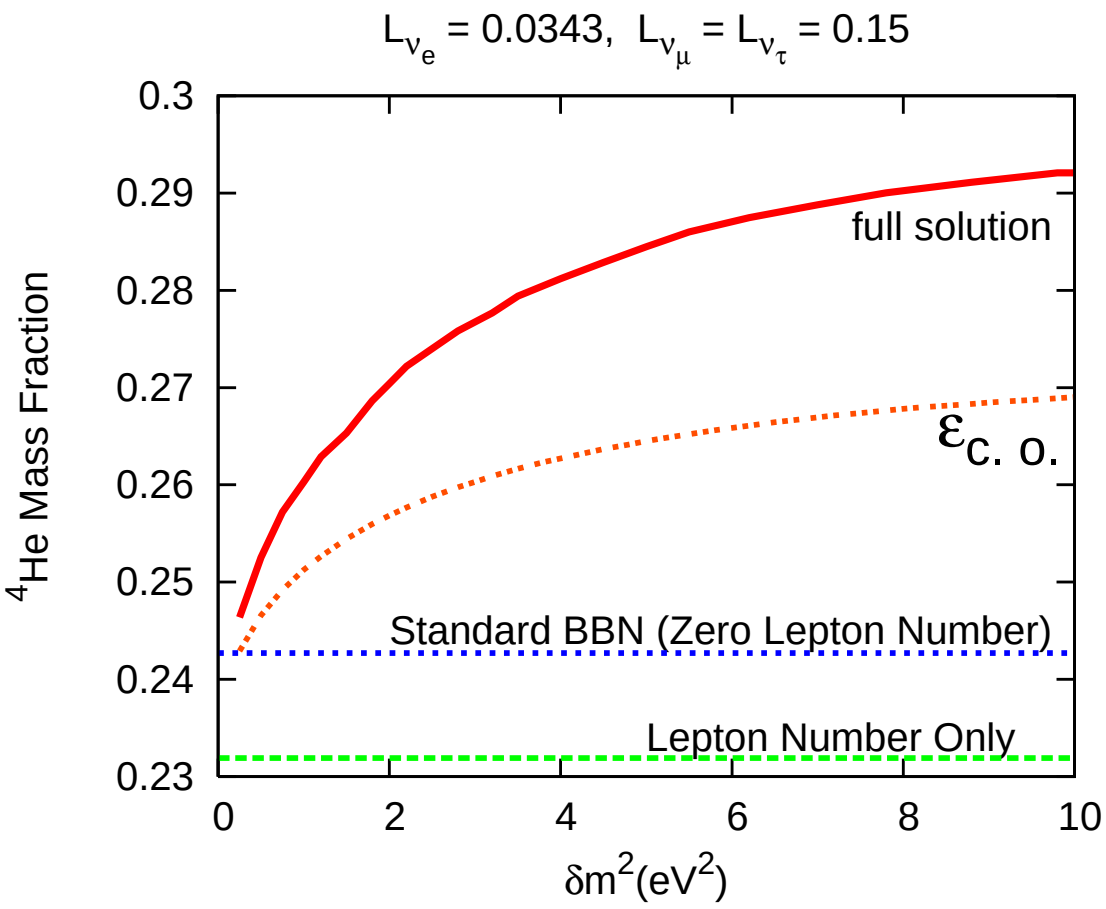

Figure A.3: Primordial nucleosynthesis (BBN) ^{4}He abundance yield as a function of δm^2 for the $\nu_e \rightarrow \nu_s$ channel and the indicated initial individual lepton numbers (same as in Fig. A.1). Standard BBN (zero lepton numbers, no sterile neutrinos) is the heavy dashed horizontal line. The case for BBN with the indicated lepton number, but no active-sterile mixing is the light dashed horizontal line. The case for forced, adiabatic resonance sweep to $\epsilon_{c.o.}$ is the light dotted line. The full non-adiabatic solution is given by the heavy solid line.

We have computed the BBN ^{4}He abundance yield with a version of the Kawano-Wagoner-Fowler-Hoyle code [28, 29] modified to allow for dynamic alteration/ distortion in the neutrino energy distribution functions. The results of these calculations for the initial lepton numbers adopted in the example of Fig. A.1 are shown in Figure A.3. The standard (zero lepton number, no sterile neutrinos) BBN ^{4}He abundance yield mass fraction is $\approx 24\%$ when we adopt neutron lifetime $\tau_n = 887.8\,\mathrm{s}$ and $\eta = 6.1102 \times 10^{-10}$. The adopted value of η corresponds to the central value of the cosmic microwave background radiation acoustic peak-determined WMAP 3-year data, $\eta = (6.11 \pm 0.22) \times 10^{-10}$ [30]. The observational error in η corresponds to a $\pm 0.03\%$ range in the calculated ^{4}He abundance yield.

Alternatively, the case with the example lepton numbers but with no active-sterile neutrino mixing gives a healthy ^{4}He yield suppression. However, once the spectral distortion is included the ^{4}He yield is larger than in standard BBN. Given that the observationally-inferred helium abundance is between $23\% - 26\%$ [31] (and possibly more precisely determined [32, 33]), we see that the dramatically larger ^{4}He yield in the cases with ν_e spectral distortion may allow for new constraints on a combination of lepton number and sterile neutrino masses. Our resonance sweep solution gives a larger ^{4}He yield than in previous models of active-sterile neutrino transformation which employ, *e.g.*, forced, adiabatic resonance sweep to $\epsilon_{\mathrm{c.o.}}$ [1]. This shows the sensitivity of BBN abundance yields to sterile neutrino-induced active neutrino spectral distortion. This effect eventually may allow light element probes/constraints on the sterile neutrino sector which complement those of mini-BooNE and may extend to sterile neutrino mass/mixing parameters currently inaccessible experimentally.

We would like to thank K. Abazajian, N. Bell, M. Smith, and especially M. Patel for insightful discussions. This work was supported in part by NSF Grant PHY-04-00359 at UCSD. C.T.K. would like to acknowledge a fellowship from the ARCS Foundation, Inc.

Appendix B, in full, is a reprint of the material as it appears in Physical Review Letters 2006. Kishimoto, Chad T.; Fuller, George M.; Smith, Christel J.,

Phys. Rev. Lett. 2006. The dissertation author was a contributing author and investigator.

Bibliography

[1] K. Abazajian, N. F. Bell, G. M. Fuller and Y. Y. Y. Wong, Phys. Rev. D **72**, 063004 (2005).

[2] G. Mangano *et al.*, Nucl. Phys. **B729**, 221 (2005), [hep-ph/0506164].

[3] S. Dodelson, A. Melchiorri and A. Slosar, Phys. Rev. Lett. **97**, 041301 (2006).

[4] K. Eitel, New J. Phys. **2**, 1 (2000).

[5] LSND, C. Athanassopoulos *et al.*, Phys. Rev. Lett. **75**, 2650 (1995), [nucl-ex/9504002].

[6] MiniBooNE Collaboration, G. McGregor, in *Particle Physics and Cosmology: Third Tropical Workshop on Particle Physics and Cosmology - Neutrinos, Branes, and Cosmology*, edited by J. F. Nieves and C. N. Leung, AIP Conf. Proc. No. 655, p. 58, New York, 2003, AIP.

[7] K. Abazajian, G. M. Fuller and M. Patel, Phys. Rev. **D64**, 023501 (2001), [astro-ph/0101524].

[8] A. D. Dolgov, S. H. Hansen, S. Pastor, S. T. Petcov, G. G. Raffelt and D. V. Semikoz, Nucl. Phys. B **632**, 363 (2002).

[9] K. N. Abazajian, J. F. Beacom and N. F. Bell, Phys. Rev. D **66**, 013008 (2002).

[10] Y. Y. Y. Wong, Phys. Rev. D **66**, 025015 (2002).

[11] V. Barger, J. P. Kneller, P. Langacker, D. Marfatia and G. Steigman, Phys. Lett. B **569**, 123 (2003).

[12] J. P. Kneller, R. J. Scherrer, G. Steigman and T. P. Walker, Phys. Rev. D **64**, 123506 (2001).

[13] A. D. Dolgov, Yad. Fiz. **33**, 1309 (1981).

[14] B. H. J. McKellar and M. J. Thomson, Phys. Rev. D **49**, 2710 (1994).

[15] R. Foot and R. R. Volkas, Phys. Rev. D **55**, 5147 (1997).

[16] P. Di Bari, P. Lipari and M. Lusignoli, Int. J. Mod. Phys. A **15**, 2289 (2000).

[17] R. R. Volkas and Y. Y. Y. Wong, Phys. Rev. D **62**, 093024 (2000).

[18] K. S. M. Lee, R. R. Volkas and Y. Y. Y. Wong, Phys. Rev. D **62**, 093025 (2000).

[19] G. Gelmini, S. Palomares-Ruiz and S. Pascoli, Phys. Rev. Lett. **93**, 081302 (2004).

[20] R. Foot and R. R. Volkas, Phys. Rev. Lett. **75**, 4350 (1995).

[21] S. P. Mikheyev and A. Y. Smirnov, Yad. Fiz. **42**, 1441 (1985).

[22] L. Wolfenstein, Phys. Rev. D **17**, 2369 (1978).

[23] X.-D. Shi and G. M. Fuller, Phys. Rev. Lett. **83**, 3120 (1999), [astro-ph/9904041].

[24] L. D. Landau, Phys. Z. Sowjetunion **2**, 46 (1932).

[25] C. Zener, Proc. R. Soc. London Ser. A **137**, 696 (1932).

[26] D. Kirilova, Astropart. Phys. **19**, 409 (2003).

[27] K. Abazajian, X. Shi and G. M. Fuller, astro-ph/9909320.

[28] L. Kawano, NASA STI/Recon Technical Report N **92**, 25163 (1992).

[29] R. V. Wagoner, W. A. Fowler and F. Hoyle, Astrophys. J. **148**, 3 (1967).

[30] D. N. Spergel *et al.*, astro-ph/0603449.

[31] K. A. Olive and E. D. Skillman, Astrophys. J. **617**, 29 (2004).

[32] K. A. Olive, G. Steigman and E. D. Skillman, Astrophys. J. **483**, 788 (1997).

[33] Y. I. Izotov and T. X. Thuan, Astrophys. J. **602**, 200 (2004).